



UNIVERSITÀ
DEGLI STUDI
DI PADOVA

Sede Amministrativa: Università degli Studi di Padova

DIPARTIMENTO DI Ingegneria INDUSTRIALE

CORSO DI DOTTORATO DI RICERCA IN INGEGNERIA INDUSTRIALE
CURRICOLO INGEGNERIA CHIMICA, DEI MATERIALI E MECCANICA
CICLO XXIX

Mass Transport Processes in vegetated wetlands-Optimal design of FWS wetlands

Coordinatore: Ch.mo Prof. Paolo Colombo

Supervisore: Ch.mo Prof. Andrea Marion

Co-Supervisore: Dr. Andrea Bottacin-Busolin

Dottorando : Nima Sabokrouhiyeh

January 2018

Abstract.

The hydraulic efficiency of wetlands for wastewater treatment was investigated as a function of wetland shape and vegetation density using a 2D depth-averaged numerical model. First, the numerical model was calibrated and validated against field data and then was applied to 8 hypothetical wetlands of rectangular and elliptical shape and different aspect ratio (i.e. 1/1 to 4/1). The vegetation density was varied from 0 to 1000 stems m^{-2} . The effect of inlet-outlet configuration was analyzed by simulating the hydraulic response of wetlands with different alignment of the flow inlet and outlet and wetlands with multiple inlets. The resulting Residence Time Distributions (RTDs) were derived from numerical simulations of the flow field and the temporal evolution of the outlet concentration of a passive tracer injected at the inlet. The simulated velocity field demonstrated that wetland shape can have significant impact on the size of dead zone areas, which is also reflected in the RTD. Efficiency metrics associated with detention time and degree of mixing improved for an elliptical shape compared to a rectangular shape. An ellipse shape improved the wetland performance by reducing the area of dead zones at the corners, and thereby increasing the effective wetland volume contributing to the treatment process. Configurations in which inlet and outlet were located at opposite corners of the wetland, and wetlands with multiple inlets produced smaller dead zones, which reduced the variance of the RTD. The simulation results also revealed an interesting threshold behavior with regard to stem density. For stem density above 300 stems m^{-2} , which is typical of treatment wetlands, the model predictions were not sensitive to the exact value of stem density selected, which simplifies the parameterization of models.

The presence of heterogeneous vegetation patterns in constructed wetlands was also analyzed by numerical model to simulate flow, mass transport and contaminant removal in a conceptual free water surface (FWS) wetland with heterogeneous vegetation patterns. The main objectives were (1) to quantify the effectiveness of FWS wetlands of different vegetation patterns in reducing water contamination and, if possible, give such patterns a physical interpretation to increase the insight into the governing processes, and (2) to evaluate if there exists an optimum pattern that would maximize contaminant removal. First, the model was calibrated and validated against survey data from a wide variety of vegetated types, sizes, and shapes of large, shallow wetlands, and subsequently, simulations were performed for different random vegetation fields characterized by imposed statistical properties, including mean, variance and correlation length of the stem density distribution. The patterns were designed to mimic vegetation patterns that occur in natural wetlands. Results show that the concentration reduction efficiency increased monotonically with average stem density, whereas mass removal had a peak for an intermediate value of average stem density. The ensemble average of the total mass removal decreased for increasing stem density variance and correlation length, because the presence of vegetation patches, localized regions of high or low stem density, promoted preferential flow paths. In particular, preferential flow paths parallel to the mean flow direction were found to reduce the hydraulic efficiency of wetlands by producing short-circuiting, whereas, for the same mean stem

density, alternating stripes of stem density perpendicular to the flow direction provide higher concentration and mass reduction efficiencies. The results provide guidance for designers of constructed wetlands by developing a quantitative understanding of the hydraulic impact of spatial heterogeneity in vegetation. This quantitative analysis of the effect of wetland shape, inlet-outlet configuration and vegetation distribution can help engineers to achieve more efficient and cost-effective design solutions for wastewater treatment wetlands.

Keywords: wetlands, FWS, Shallow water model, Detention time, Dispersion, Vegetation, short-circuiting, random fields, water quality, Design.

Processi di trasporto di massa in zone umide vegetate - Progettazione ottimale delle "FWS wetlands"

Sommario.

L'efficienza idraulica delle zone umide per il trattamento delle acque reflue è stata studiata in funzione della forma delle zone umide e della densità della vegetazione utilizzando un modello numerico bidimensionale mediato sulla verticale. In primo luogo, il modello numerico è stato calibrato e validato sulla base di dati sperimentali e quindi è stato applicato a 8 zone umide ipotetiche di forma rettangolare ed ellittica con differenti proporzioni (cioè da 1: 1 a 4: 1). La densità della vegetazione è stata variata da 0 a 1000 steli / m². Inoltre è stato analizzato l'effetto della configurazione dell'ingresso-uscita, simulando la risposta idraulica di zone umide con diversi allineamenti dell'ingresso e dell'uscita e di zone umide con più ingressi. Dalle simulazioni numeriche del campo di flusso e dall'evoluzione temporale della concentrazione di uscita di un tracciante passivo iniettato all'ingresso sono state ricavate le risultanti distribuzioni del tempo di residenza (RTD). Il campo di velocità simulato ha dimostrato che la forma delle zone umide può avere un impatto significativo sulle dimensioni delle zone morte, che si riflette anche nella RTD. Le metriche di efficienza associate al tempo di detenzione e al grado di miscelazione migliorano per una forma ellittica rispetto a una forma rettangolare. Una forma ad ellisse migliora le prestazioni delle zone umide riducendo l'area delle zone morte agli angoli, aumentando così il volume efficace che contribuisce al processo di trattamento. Le Configurazioni in cui l'ingresso e l'uscita erano situati agli angoli opposti della zona umida, e le zone umide con più ingressi producevano zone morte più piccole, che riducevano la varianza della RTD. I risultati delle simulazioni hanno anche rivelato un comportamento soglia interessante per quanto riguarda la densità dello stelo. Per densità di vegetazione oltre 300 steli / m², che è tipica delle zone umide deputate al trattamento di acque reflue, le previsioni del modello non erano sensibili al valore esatto della densità di vegetazione, il che semplifica la parametrizzazione dei modelli.

anche La presenza di distribuzioni eterogenee di vegetazione nelle zone umide artificiali è stata analizzata mediante un modello numerico in grado di simulare il flusso, il trasporto di massa e la rimozione dei contaminanti in una zona umida concettuale a superficie libera (FWS). Gli obiettivi principali erano (1) quantificare l'efficacia delle FWS wetlands con diverse distribuzioni di vegetazione nel ridurre la contaminazione dell'acqua e, se possibile, dare a tali schemi un'interpretazione fisica per aumentare la conoscenza dei processi che li governano e (2) valutare se esiste un modello ottimale che massimizza la rimozione dei contaminanti. Innanzitutto, il modello è stato calibrato e validato rispetto a dati di indagine provenienti da un'ampia varietà di tipi, dimensioni e forme vegetate di vaste zone umide superficiali e successivamente sono state eseguite simulazioni per diversi campi random di vegetazione caratterizzati da proprietà statistiche imposte, tra cui media, varianza e lunghezza di correlazione della distribuzione della densità dello stelo. le distribuzioni di vegetazione sono state generate in modo da imitare le distribuzioni che si verificano nelle zone umide naturali. I risultati hanno mostrato che l'efficienza di riduzione della concentrazione aumentava monotonicamente con la densità di vegetazione media, mentre la rimozione di massa aveva un picco per un valore intermedio della densità di vegetazione media. La media di insieme della rimozione totale della massa diminuiva

all'aumentare della varianza della densità di vegetazione e della lunghezza di correlazione, poiché la presenza di macchie di vegetazione, regioni localizzate con densità di steli alta o bassa, promuoveva percorsi di flusso preferenziali. In particolare, è stato rilevato come percorsi di flusso preferenziali paralleli alla direzione media del flusso riducano l'efficienza idraulica delle zone umide producendo cortocircuiti, mentre, per la stessa densità media staminale, strisce alternate di densità dello stelo perpendicolari alla direzione del flusso forniscono maggiore concentrazione e efficienze di riduzione di massa. I risultati forniscono una guida per i progettisti di zone umide artificiali grazie allo sviluppo di una comprensione quantitativa dell'impatto idraulico dell'eterogeneità spaziale nella vegetazione. Questa analisi quantitativa dell'effetto della forma delle zone umide, della configurazione dell'ingresso e della distribuzione della vegetazione può aiutare gli ingegneri a realizzare soluzioni di progettazione più efficienti ed economicamente vantaggiose per le zone umide di trattamento delle acque reflue.

Parole chiave: zone umide, FWS, modello di acque poco profonde, tempo di detenzione, dispersione, vegetazione, corto circuito, campi casuali, qualità dell'acqua, design.

Acknowledgments

Thanks to Andrea Marion for his creativity, scientific advice, and continuous support. I would not have come this far in this field without his support and encouragement.

I also express my gratitude to my other supervisor, Andrea Bottacin for providing constructive comments and encouragement. His guidance in numerical modeling have been essential during this work.

I would like to offer my special thanks to Heidi Nepf, who provided insightful comments and suggestions and perspective.

I will always be grateful to my parents for their unending support and enthusiasm; and the rest of my family for their continued love.

Finally, I am grateful to the the Initial Training Network (ITN) HYTECH 'Hydrodynamic Transport in Ecologically Critical Heterogeneous Interfaces', N. 316546, that provided funding for my PhD through the Seventh Framework Programme of the European Union, (Marie Curie-FP7-PEOPLE-2012-ITN).

Contents

| | |
|--|----|
| 1 Transport processes in aquatic systems | 12 |
| 1.1 Introduction..... | 12 |
| 1.2 Physical transport processes | 13 |
| 1.2.1 Advection and molecular diffusion..... | 13 |
| 1.2.2 Turbulent diffusion | 15 |
| 1.2.3 Dispersion | 16 |
| 1.2.3.1 Two dimensional depth-averaged model | 17 |
| 1.2.3.2 One dimensional cross-sectional averaged model | 18 |
| 1.2.3.3 Additional fluxes on the boundary..... | 19 |
| 1.3 The effect of physical features | 21 |
| 1.3.1 The role of bed topography..... | 21 |
| 1.3.2 The effect of vegetation | 22 |
| 1.3.3 Effect of evapotranspiration..... | 22 |
| 1.4 Tracer tests | 23 |
| 1.4.1 Tracers..... | 23 |
| 1.4.2 Designing stream tracer tests to quantify retention phenomena | 26 |
| 1.4.3 Limitations and challenges in inverse modeling of transport processes..... | 27 |
| 1.5 Work scope | 27 |
| 2 Effects of vegetation density and wetland aspect ratio variation on hydraulic efficiency of wetlands | 29 |
| 2.1 Contaminant removal in FWS wetlands | 29 |
| 2.2 Plug flow and nominal residence time..... | 32 |
| 2.3 Wetland aspect ratio..... | 32 |
| 2.4 Vegetated wetlands | 33 |
| 2.5 Importance of wetland aspect ratio in vegetated wetlands | 34 |
| 2.6 Depth-averaged two-dimensional numerical model | 34 |
| 2.6.1 Hydrodynamic model..... | 34 |
| 2.6.2 Solute transport model | 36 |
| 2.7 Residence time distribution..... | 38 |
| 2.8 Model application | 39 |
| 2.8.1 Model calibration and validation | 41 |

| | |
|--|----|
| 2.9 Numerical simulations of vegetation effects..... | 42 |
| 2.10 Numerical simulations of aspect ratio effects..... | 45 |
| 2.11 Wetland aspect ratio and vegetation effect on hydraulic efficiency..... | 46 |
| 3 Study of the effect of wetland shape and inlet-outlet configuration on wetland performance .. | 47 |
| 3.1 Wetland shape..... | 47 |
| 3.2 Inlet-outlet configuration..... | 48 |
| 3.3 Importance of wetland configuration..... | 48 |
| 3.4 Wetland characteristics and boundary condition..... | 49 |
| 3.5 Model application..... | 49 |
| 3.6 Results of numerical model..... | 50 |
| 3.6.1. Wetland Shape simulations..... | 52 |
| 3.6.2 Inlet-outlet configuration and size..... | 55 |
| 3.7 Shape and inlet-outlet effect on hydraulic efficiency..... | 58 |
| 4 Assessment of the nutrient removal effectiveness of free water surface wetlands with different configurations..... | 60 |
| 4.1 Nitrogen removal..... | 60 |
| 4.2 Contaminant removal efficiency in connection to design parameters..... | 63 |
| 4.3 Model application..... | 64 |
| 4.4 nitrogen removal model..... | 64 |
| 4.5 Nitrogen removal and hydraulic efficiency..... | 65 |
| 5 Contaminant removal efficiency as a function of vegetation distribution in free water surface wetlands..... | 68 |
| 5.1 Heterogeneity of vegetation patterns..... | 68 |
| 5.2 Vegetation distribution effect..... | 71 |
| 5.3 Spatial vegetation patterns..... | 71 |
| 5.4 Efficiency metrics..... | 73 |
| 5.5 Numerical simulations..... | 74 |
| 5.5.1 Model calibration..... | 75 |
| 5.6 Numerical model results..... | 77 |
| 5.6.1 Isotropic vegetation patterns..... | 77 |
| 5.6.2 Anisotropic vegetation patterns..... | 83 |
| 5.7 Effect of vegetation heterogeneity on wetland performance..... | 85 |
| Chapter 6..... | 87 |

| | |
|---|----|
| 6 Discussion and conclusions | 87 |
| 6.1. Design recommendations..... | 87 |
| 6.1.1 Wetland size..... | 88 |
| 6.1.2 Aspect ratio | 89 |
| 6.1.3 Wetland shape..... | 89 |
| 6.1.4 Inlet-outlet configuration | 89 |
| 6.1.5 Vegetation density and distribution | 90 |
| 6.1.6 Wind effect..... | 90 |
| Bibliography | 91 |

List of figures

| | |
|--|----|
| Figure 1.1 Reynolds time-averaging procedure: average of an erratic signal of velocity over two different time scales..... | 15 |
| Figure 1.2 Example of the three mixing zones in an aquatic system..... | 17 |
| Figure 1.3 Differences in longitudinal transport processes in relation to the value of transversal mixing..... | 19 |
| Figure 1.4 Illustration of the transport processes acting in an aquatic system..... | 21 |
| Figure 2.1 Basic elements of a FWS wetland..... | 31 |
| Figure 2.2 Simulations for a uniformly vegetated wetland (aspect ratio 4/1), tracer concentration distribution-After elapsed time=1.2 days..... | 40 |
| Figure 2.3 Volumetric efficiency derived from field data (black curve, Thackston et al. 1987) and from the numerical simulations..... | 42 |
| Figure 2.4 Normalized residence time distributions (RTDs) for six different vegetation densities..... | 43 |
| Figure 2.5 Rectangle-shape wetlands efficiency parameters variation for different aspect ratios (a) dimensionless retention time, (e_v), (b) Persson hydraulic index, (λ_h)..... | 45 |
| Figure 3.1 Illustration of a rectangular wetland with centrally aligned inlet and outlet and uniform vegetation coverage: (a) plan view, (b) side view..... | 49 |
| Figure 3.2 Simulated RTDs of wetlands with different aspect ratio and different shape..... | 50 |
| Figure 3.3 Simulated velocity fields for different wetland shapes of 1 ha area and a centrally aligned inlet-outlet..... | 53 |
| Figure 3.4 The effect of (a), (c) aspect ratio and (b), (d) wetland shape on volumetric and dispersion efficiency of wetlands with different vegetation density..... | 54 |
| Figure 3.5 The effect of (a) aspect ratio and (b) shape variation on hydraulic efficiency of wetlands with different vegetation density..... | 55 |
| Figure 3.6 Simulated velocity fields for different inlet and outlet configurations for a rectangular wetland with 100 stems m^{-2} vegetation density and an outlet of 10 m width: (a) Case R4-a, left inlet of 10 m width and central outlet ($b/W=0.1$); (b) Case R4-b, a left inlet of 10 m width and right outlet; (c) Case R4-2i, double inlet of 5 m width; (d) Case R4-3i, triple inlet of 3.33 m width. Black regions represent dead zones, i.e. regions of zero velocity..... | 56 |
| Figure 3.7 Effect of (a), (c) inlet-outlet position and (b), (d) number of inlets on volumetric and dispersion efficiency of rectangular wetlands of aspect ratio 4/1 with 100 stems m^{-2} vegetation coverage and different inlet width..... | 57 |

| | |
|--|----|
| Figure 3.8 Effect of wetland (a) inlet-outlet position and (b) number of inlets on hydraulic efficiency of rectangular wetlands of aspect ratio 4/1 with 100 stems m ⁻² vegetation density and different inlet width..... | 58 |
| Figure 4.1 Biological-chemical processes involved in nitrogen removal present in FWS wetlands..... | 61 |
| Figure 4.2.a Hydraulic efficiency and 4.2.b Nitrogen removal rate variation for wetland aspect ratios..... | 67 |
| Figure 5.1. Schematics of flow patterns in a free water surface wetland with non-uniform vegetation distribution. Such a system can create preferential flow paths and short-circuiting, which allow a significant fraction of solute to reach the outlet before adequate treatment has been achieved. Low velocity zones may also occur with minimal contribution to the treatment process..... | 70 |
| Figure 5.2 Examples of random vegetation fields with average stem density 2000 m ⁻² , standard deviation $\sigma/n = 0.50$, and relative correlation length (a), (b). $l_x/L = 0.30$, (c). $l_{cx}/L = 0.30$, $l_{cy}/L = 0.03$, (d) $l_{cx}/L = 0.03$, $l_{cy}/L = 0.30$ | 73 |
| Figure 5.3 Illustration of the a vegetated conceptual wetland: (a) plan view, (b) side view..... | 74 |
| Figure 5.4 Volumetric efficiency derived from field data is compared with the results of the numerical model..... | 77 |
| Figure 5.5 Behavior of (a) concentration reduction efficiency and (b) flow discharge as a function of average stem density. The points represent the ensemble mean of the simulation results, with corresponding standard deviation bars..... | 78 |
| Figure 5.6 Types of vegetation patterns from wetlands of the same mean steam density ($\bar{n} = 2000$ stems m ⁻²), the same relative correlation length ($\frac{L_{cx}}{L} = \frac{L_{cy}}{L} = 0.30$) and different variance..... | 80 |
| Figure 5.7 The concentration reduction efficiency, Ec , and mass removal rate, \dot{m} , as a function of mean stem density for and relative stem density variance..... | 81 |
| Figure 5.8 Types of vegetation patterns from wetlands of the same mean steam density ($\bar{n} = 2000$ stems m ⁻²), the same variance ($\sigma/n = 0.50$);, and relative correlation length | 82 |
| Figure 5.9 The concentration reduction efficiency, Ec , and mass removal rate, \dot{m} , as a function of mean stem density and relative correlation length, l_c | 83 |
| Figure 5.10 Types of vegetation patterns of the same mean stem density and the same variance considered in the simulations: (a) dotted pattern; (b) striped pattern aligned with the flow direction; (c) striped pattern perpendicular to the flow direction..... | 84 |
| Figure 5.11 Concentration removal efficiency as a function of mean stem density for the different vegetation patterns presented in Figure 5.10..... | 85 |

Figure 5.12 Mass removal rate versus vegetation density for the different vegetation patterns presented in Figure 5.10.....85

Chapter 1

1 Transport processes in aquatic systems

1.1 Introduction

The fate of pollutants in rivers is controlled by surface hydrodynamics and by exchange processes with the surrounding environment. A solute transported in a natural watercourse can be temporarily trapped in vegetated zones or in the sediment, follow deep flow paths in the porous medium and return to the surface water after some time. These solute trapping phenomena are generally referred to as “retention” processes or “transient storage”, and produce signatures on solute concentration patterns that can be observed by injecting a tracer in the surface water and by measuring the concentration at a distance downstream.

The hydrodynamic exchange with storage zones can be conceptually classified into short and long term retention. Short term retention is commonly due to surface dead zones, such as side pockets of recirculating water or vegetated zones, whereas long term retention is due to temporary storage of solutes in the upper part of the sediment bed. In addition to that, interactions between the stream water and the aquifer can occur over longer timescales. They are driven by gradients between the groundwater table and the river free surface, and depend on the

hydraulic conductivity of the aquifer and bed morphology. Solute losses from wetland systems also occur as a consequence of evapotranspiration, which accounts for evaporation and plant transpiration from the water body and the soil. The mass and momentum exchange between the water flowing in the wetland and the surrounding environment plays an important role in controlling the pollution of water bodies and connected ecological systems.

1.2 Physical transport processes

This chapter discusses an overview of the transport processes in aquatic systems. Main equations were derived, describing the main variables involved mixing processes over two dimensional domains. The conceptual description of transport processes depends on the scale of observation, which can range from the molecular scale to the watershed scale. Depending on the problem, it can be convenient to consider physical quantities averaged over certain spatial and temporal scales, or to operate a conceptual distinction between different parts of a continuum. This leads us to the identification of different physical process that are relevant to different spatial and temporal scales, or physical domains. The main processes governing the fate of solutes in fluvial systems are described in the following sections.

1.2.1 Advection and molecular diffusion

In transport processes, the quantity of interest is the mass of a dissolved substance subject to advection and diffusion. Advection is the process by which a conserved quantity is transported in a fluid in motion whereas diffusion is the process by which matter is transported from one part of the domain to another as a result of random molecular motions. Fluid motion is characterized by the velocity vector field $U = (u_x; u_y; u_z)$, in which u_x , u_y and u_z are the velocity components along the x , y and z directions and the mass of a dissolved substance per unit volume is described by a concentration C . Time averaging was assumed in calculation of velocity. The mass flux, that account for both diffusion and advection processes, can be written as:

$$\phi = Uc - D_m \nabla c \quad (1.1)$$

First term uc represents the convective component of the mass flux and the second term $D_m \nabla c$ represents the diffusive component written as proposed by Fick (1855). Fick's approach

describes the net mass flux of solute as the product of the concentration gradient and the molecular diffusion coefficient D_m . Negative sign accounts for the direction of the flux from higher concentrations to lower concentrations. To note that molecular diffusion does not exist as a physical phenomenon but represents only an ensemble behavior of solute particles. Indeed, each single particle does not feel the effect of the concentration gradient but moves following the Brownian motion: only at a larger scale small Brownian movements produce, under probabilistic point of view, a mass transport from zones characterized by high concentrations to zones characterized by low concentrations of solute.

The net flux ϕ can be coupled with the mass balance equation to model diffusion and transport processes of solutes in fluids. The mass balance equation can be written as:

$$\frac{\partial c}{\partial t} = -\nabla \cdot (cU - D_m \nabla c) \quad (1.2)$$

Molecular diffusion coefficient D_m can be regarded as a constant and depends on solute and solvent characteristics. If we develop the previous equation, for isotropic molecular diffusion and an incompressible fluid ($\nabla \cdot u=0$), equation (1.2) becomes:

$$\frac{\partial c}{\partial t} + U \cdot \nabla c = D_m \nabla^2 c \quad (1.3)$$

that is, in extended notation:

$$\frac{\partial c}{\partial t} + u_x \frac{\partial c}{\partial x} + u_y \frac{\partial c}{\partial y} + u_z \frac{\partial c}{\partial z} = D_m \left(\frac{\partial^2 c}{\partial x^2} + \frac{\partial^2 c}{\partial y^2} + \frac{\partial^2 c}{\partial z^2} \right) \quad (1.4)$$

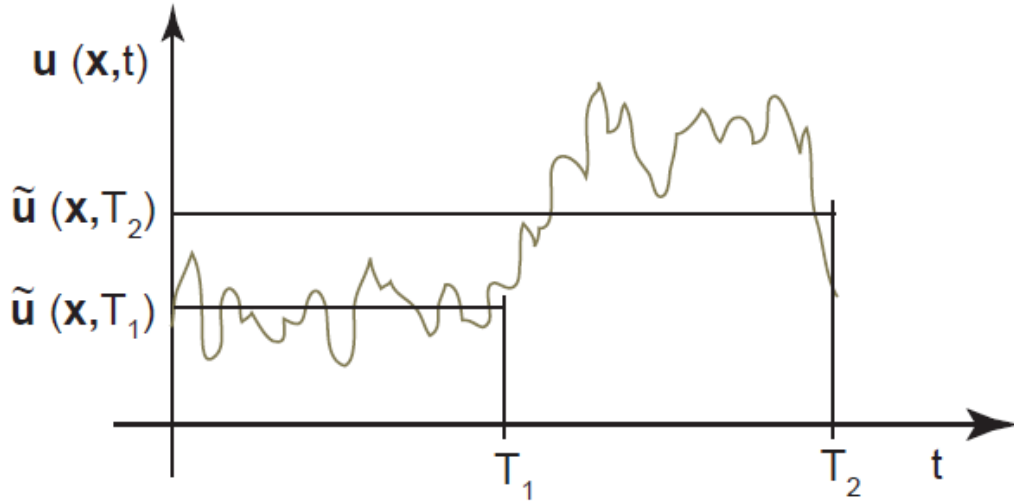


Figure 1.1 Reynolds time-averaging procedure: average of an erratic signal of velocity over two different time scales. The choice of the time step for the average can change averaging results.

Equation (1.4) is valid for conservative solutes (no mass consumption or production of solute) and neutral solutes (not affected by gravity forces). The structure of this latter equation is similar to the Navier-Stokes equations, for which the transported variable is the momentum and the kinematic viscosity ν (m^2/s) replaces the molecular diffusion coefficient. Kinematic viscosity has indeed the same role of molecular diffusion coefficient D_m in momentum diffusion process.

1.2.2 Turbulent diffusion

Molecular diffusion produced by Brownian motion is no longer the dominant diffusion mechanism when the flow velocity becomes fast enough to overcome viscous forces and the flow becomes turbulent. Under these conditions diffusion is controlled by continuous displacement of fluid elements in all directions induced by turbulence. While molecular diffusion is isotropic, turbulent diffusion is typically different in each direction, as eddies are continuously stretched and deformed by the flow. Turbulent flows are usually modeled splitting the physical quantities into time-averaged mean values and fluctuations around the mean. After manipulation of the advection-diffusion equation, the time-averaged mass transport equation becomes:

$$\frac{\partial \bar{c}}{\partial t} + \bar{u} \frac{\partial \bar{c}}{\partial x} + \bar{v} \frac{\partial \bar{c}}{\partial y} + \bar{w} \frac{\partial \bar{c}}{\partial z} = \frac{\partial}{\partial x} \left(D_{xx}^T \frac{\partial \bar{c}}{\partial x} \right) + \frac{\partial}{\partial y} \left(D_{yy}^T \frac{\partial \bar{c}}{\partial y} \right) + \frac{\partial}{\partial z} \left(D_{zz}^T \frac{\partial \bar{c}}{\partial z} \right) \quad (1.5)$$

where D_{xx}^T , D_{yy}^T , and D_{zz}^T are eddy diffusion coefficients in the three spatial directions x, y and z, respectively, and the bar notation denotes temporal average. The expression for the vertical dispersion coefficient $D_{zz}^T = 0.067u^*d$ in rivers can be derived from the logarithmic velocity profile where d is the water depth and u^* is the shear velocity. An approximate expression of the coefficient valid for uniform straight channels was empirically derived by Fischer et al. (1979) based on laboratory and field experiments: $D_{yy}^T = 0.15u^*d$, suggesting $D_{yy}^T = 0.6u^*d$ for irregular channels where geometrical variations enhance transverse mixing. For longitudinal mixing it can often be assumed that $D_{yy}^T = D_{xx}^T$. These relationships can be used to estimate the distance mix from an injection (for a lateral injection the distance is 4 times greater):

$$L_{mix} = 0.1 \frac{Ub^2}{D_{xx}^T} \quad (1.6)$$

where b is the channel width.

1.2.3 Dispersion

Dispersion is the mixing process that arises from advection and diffusion in presence of velocity gradients. Role of velocity gradients becomes clear if, after the time-averaging procedure, also a spatial-averaging procedure is performed. A spatial-averaging procedure is often convenient to simplify the description of mass transfer by averaging velocity and concentration over the vertical direction (shallow water approach), over a transverse direction or over a cross-section (unidirectional approach). Each mixing process is characterized by its typical spatial scale(s) of interest and therefore can be described only by a specific spatial-averaging procedure.

The example of an aquatic system (Figure 1.2) can be chosen to explain this concept: immediately around the injection point, the mass transfer is strongly three dimensional and is strongly dependent on the type of the injection and on the local flow regime. For this reason, to adequately model mass transfer near the injection point, is important to use a three dimensional model that takes into account the complete set of spatial and temporal variables. At some distance from the injection, when the complete mixing along the vertical direction is already happened, transversal and longitudinal concentration gradients control the process. In this case, a vertical (depth) averaging procedure can be performed reducing the complexity of the model to a two dimensional, depth-averaged model. Further downstream, when also transversal

concentration gradients have been modulated, only longitudinal concentration gradients control the mixing process. In this case a cross sectional-averaging procedure can simplify the model leading to a one-dimensional model.

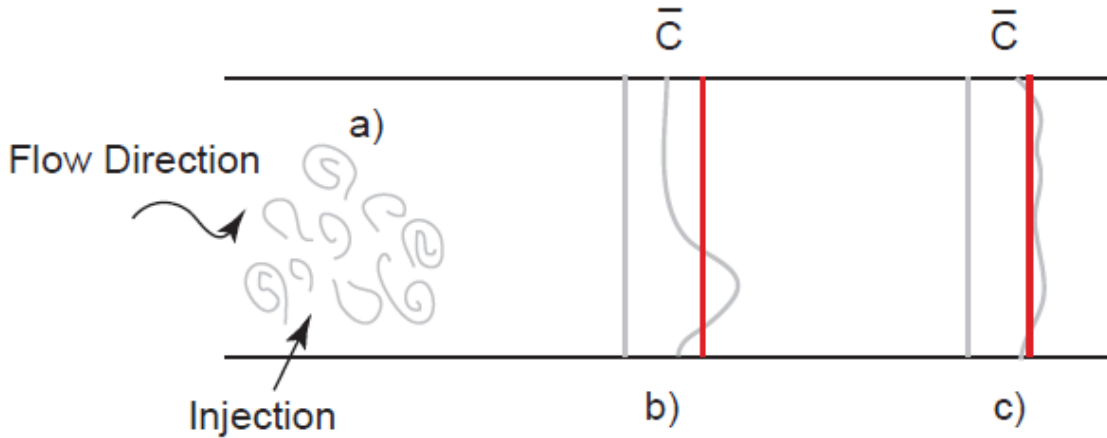


Figure 1.2 Example of the three mixing zones in an aquatic system. Near the injection (a) there is a strongly three dimensional process whereas further downstream the concentration has only an evident transversal gradient (b). When transversal concentration gradients are averaged by lateral mixing, only longitudinal gradients are relevant (c). The averaging process over the transversal area, typical of a one-dimensional models, can give good approximation of the real process only in (c) whereas other more complex models should be applied to model zones (a, b).

1.2.3.1 Two dimensional depth-averaged model

To model a natural system for which the depth is small compared to the other two horizontal dimensions, equation (1.7) is integrated over the depth obtaining:

$$\frac{\partial(hC)}{\partial t} + \frac{\partial(hu_x C)}{\partial x} + \frac{\partial(hu_y C)}{\partial y} = \frac{\partial}{\partial x} \left(hE_{xx} \frac{\partial C}{\partial x} \right) + \frac{\partial}{\partial y} \left(hE_{yy} \frac{\partial C}{\partial y} \right) \quad (1.7)$$

where U ; V ; C are depth averaged quantities and E_{ii} are horizontal dispersion coefficients. Values of these coefficients depend on the handled problem and specific formulations can be used. Some examples related to vegetation density have been introduced in the next chapters.

1.2.3.2 One dimensional cross-sectional averaged model

In the case of cross-sectional averaging of the physical quantities, and no additional exchange fluxes through the lateral boundary are considered, the mass balance equation is reduced to the one-dimensional form:

$$\frac{\partial C}{\partial t} + U \frac{\partial C}{\partial x} = \frac{1}{A} \frac{\partial}{\partial x} \left(AK \frac{\partial C}{\partial x} \right) \quad (1.8)$$

where C and U are the cross-sectional average concentration and flow velocity, respectively, A is the flow cross-sectional area, and K is the longitudinal dispersion coefficient. Under the assumption of constant A and K , the solution of equation (1.8) for an instantaneous injection of a mass of tracer M_0 in $x = 0$ at time $t = 0$ is given by:

$$C(x, t) = \frac{M_0/A}{\sqrt{4\pi Kt}} \exp\left(-\frac{(x-Ut)^2}{4Kt}\right) \quad (1.9)$$

The magnitude of the longitudinal dispersion coefficient K varies from case to case and is strongly related to the mixing velocity along the transversal direction. Usually, when transversal turbulent diffusivity D_{yy} is small, longitudinal dispersion is high and, in contrast, when transversal turbulent diffusivity D_{yy} is high the value of longitudinal dispersion is small. The competitive role of the transverse turbulent mixing process against the non-uniformity of the velocity distribution in determining the variance of the concentration distributions is due to the ability of the solute particle to sample the cross sectional area (Figure 1.3). If the transverse mixing process is fast, solute particles sample the entire cross sectional area experiencing the whole velocity profile. Particles move with the same average velocity U and the spreading of the solute along the longitudinal direction is therefore limited. On the contrary, if transverse mixing is slow, particles tend to maintain the same position in the flow domain experiencing only a limited velocity range. This characteristic produces a longitudinal spreading of the solute cloud that lead to an higher value of longitudinal dispersion coefficient. To note that vertical turbulent mixing act in the same manner as transverse turbulent mixing but has a limited role due to the fact that vertical mixing can be regarded, in natural rivers, as instantaneous. An approximated relationship for K valid for streams with large width-to-depth ratios was suggested by Fischer (1975):

$$K = 0.011 \frac{U^2 B_r^2}{h u_*} \quad (1.10)$$

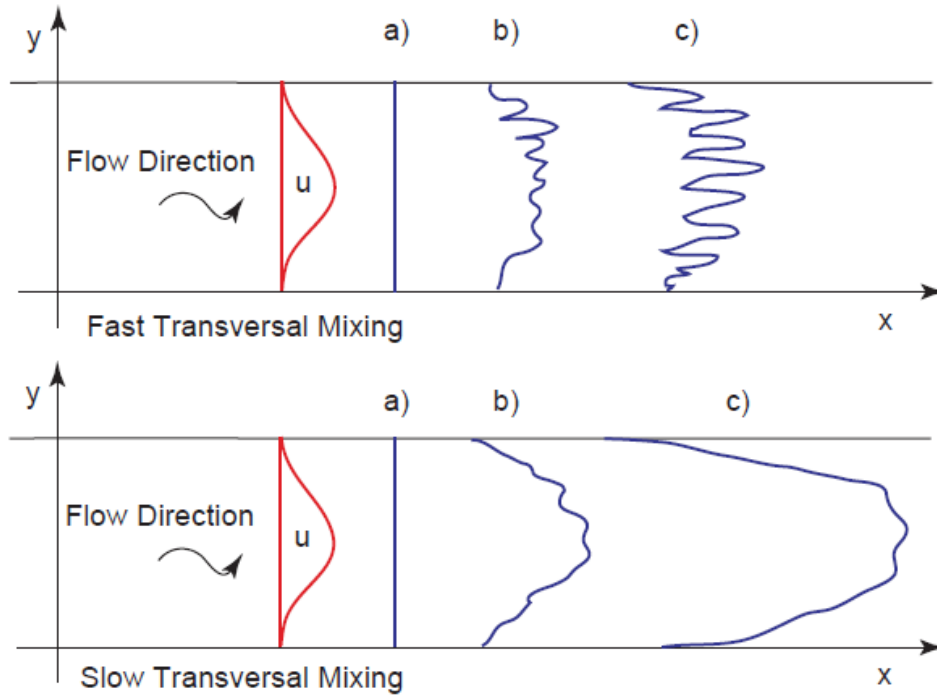


Figure 1.3 Differences in longitudinal transport processes in relation to the value of transversal mixing. In presence of fast transversal mixing, the solute particles move with the average flow velocity and thus longitudinal dispersion has a low value. In presence of slow transversal mixing, the solute moves with local velocity of flow leading to a relevant longitudinal dispersion.

1.2.3.3 Additional fluxes on the boundary

It was discussed how a formulation of one-dimensional mass transfer equation has been proposed assuming the absence of mass solute fluxes through the bed and through water surface. Although very useful, this simple model can describe only a small part of the real mixing processes in natural environments. Presence of retention in dead zones, advection and diffusion of decaying or volatile solutes, hyporheic contamination and solute consumption by biological components can clearly modify the mass transfer equation. For this reason, equation (1.8) can be extended in order to account for these different processes as follows:

$$\frac{\partial CA}{\partial t} + U \frac{\partial QC}{\partial x} = \frac{\partial}{\partial x} \left(AK \frac{\partial C}{\partial x} \right) \pm F_B P \pm F_A B_r \pm S - k_0 \quad (1.11)$$

where Q is the discharge rate, F_B is the mass flux of solute through the wetted perimeter P , F_A is the mass flux of solute through the surface B_r , k_0 is a decay rate and the term S ($\text{Kg m}^{-1} \text{s}^{-1}$) is a general production-consumption term. The decay of a solute represented by the term $-k_0CA$ is a spontaneous phenomenon independent of the presence of other substances and is almost ever associated with the radioactive decay of the substances. Radioactive decay is however a very rare mechanism that acts at very long time scales. For common engineering purposes, this mechanism is often discarded but its mathematical formulation is very helpful to treat other non-conservative processes in natural environments. Other phenomena, although not related with the natural radioactive decay, can be indeed rewritten with the same mathematical formulation. This is the case of a first order decay chemical breakdown in wetlands or the loss of a volatile solute through the water surface. Other mass exchanges with different types of storage zones as vegetated pockets, dead zones and permeable layers can happen in natural environments, as illustrated in Figure 1.4. Experimental observations of the presence of these additional boundary fluxes that cannot be represented with the classical advection-diffusion equations. These domains have fundamental role in determining the fate of transported substances for three reasons: first of all, they increase the dispersion of solute in the surface water; second, they control the exchange between the stream water and the surrounding aquifer; third, they govern the storage of contaminants into the bed sediments (A. Marion et al., 2008; Marion and Zaramella, 2005).

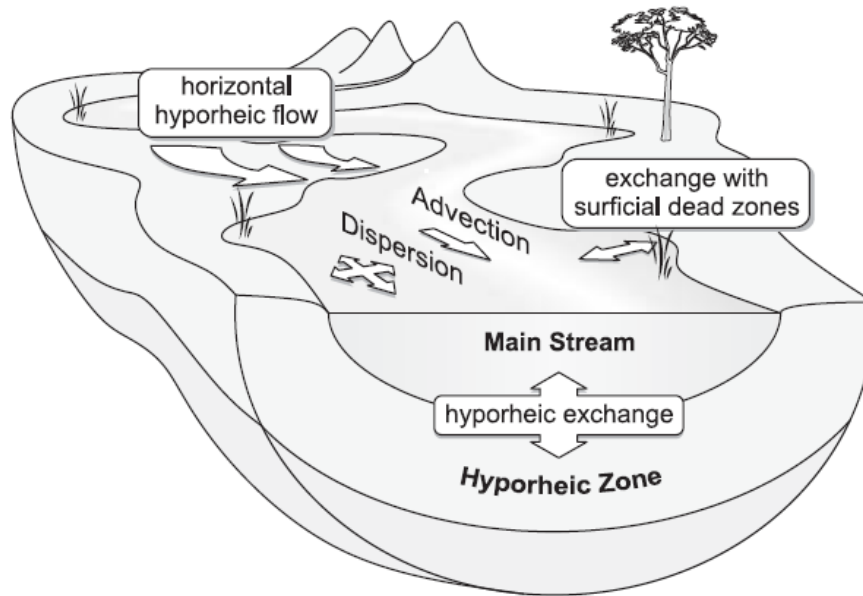


Figure 1.4 Illustration of the transport processes acting in an aquatic system. The downstream transport of solutes is governed by advection and hydrodynamic dispersion in the main stream, and by mass exchanges with different retention zones. These include vertical exchanges with the underlying sediments, where adsorption process may take place; lateral exchanges with surficial dead zones, typically vegetated pockets; and horizontal hyporheic flows induced by planimetric variation of the stream direction. (Figure from (A. Marion et al., 2008)).

1.3 The effect of physical features

1.3.1 The role of bed topography

Bed surface forms and obstructions (bedforms, berms, obstacles, etc.) play a direct role in driving flow hydrodynamics and mass transport processes: the water pressure variations induced by the interaction between flow and topography induce flows into and out the bed sediments (F. Arega and Sanders, 2004; Cardenas et al., 2004; Franken et al., 2001). Bedforms with small wavelengths and amplitude produce effects on relatively small spatial and temporal scales. However, the resulting subsurface flows play a significant role in determining larger hyporheic flow patterns (Harvey and Bencala, 1993).

The role of stream bedforms and roughness on hyporheic exchange processes has been studied in controlled laboratory studies (Marion et al., 2002; Packman et al., 2004; Salehin et al., 2003) and

models have been proposed for homogeneous (Elliott and Brooks, 1997; Bottacin-Busolin and Marion, 2010) and heterogeneous sediment beds (Andrea Marion et al., 2008).

Wörman et al. (2002) modeled the hyporheic exchange in the Säva Brook, Sweden, coupling a longitudinal in-stream solute transport with a physically based representation of storage in the hyporheic zone.

It should be also considered that, for densely vegetated aquatic systems the bed shear stress might be small compared to the vegetation drag, and can be dropped from the equations. A study on vegetative resistance by (Nepf, 1999) showed for vegetation densities as small as certain threshold, the bed drag and bed shear stress are negligible compared to their vegetation components. Such circumstances has been discussed in next chapters.

1.3.2 The effect of vegetation

It is well known that vegetation increases flow resistance and can have considerable impact on turbulence and flow patterns (Nepf, 1999). By decreasing the local flow velocity and producing complex wake structures, vegetation can generate trapping phenomena that significantly delay the downstream migration of a contaminant. Moreover, it is demonstrated that vegetation alters streambed permeability, with the introduction of organic matter to sediments and intrusion of plant roots having a pronounced effect on solute transfer to the dead zone (Packman and Salehin, 2003). The presence of in-stream vegetation thereby reduces the exchange rates, increasing the release timescale of solute retention (Cardenas et al., 2004; Dierberg et al., 2005; Lynn et al., 2002). A number of studies have attempted to quantify the effect of submerged and emergent vegetation on the dispersion of solutes (Nepf et al., 2007; Shucksmith et al., 2011; Nepf, 1999) and the storage effects associated with microbial biofilms (Battin et al., 2003; Bottacin-Busolin et al., 2009).

1.3.3 Effect of evapotranspiration

Evapotranspiration (ET) is a process through which plants roots “pump” water from the riparian sediments exploiting capillarity forces. This water is then lost as vapor through stomata in leaves

during diurnal hours. The “pumping” effect of ET drives fluxes of stream water to the sediments, enhancing the solute exchange processes from surface water to the surrounding hyporheic areas.

ET had a pronounced effect on solute residence times in the dead zones (Kadlec and Wallace, 2009; Larsen et al., 2014), diminishing them as a result of enhanced bidirectional flux across the interface between the hyporheic zone and surface water. This flux prevent hyporheic interstitial water from being caught by deep groundwaters, limiting the extent of the exchange layer and recalling upward water fluxes from the aquifer.

1.4 Tracer tests

Wetlands are complex environmental systems characterized by irregular geometry and heterogeneous properties. Field tracer tests provide a way to quantify reach-averaged transport quantities by measuring the solute concentrations at a section in response to a tracer injection upstream.

1.4.1 Tracers

A tracer is usually a soluble substance that follows the movement of water. Some of these substances are conservative, as they do not decay or react with any other compounds, and are not subject to sorption and deposition processes. Sometimes, non-conservative tracers can be used to study the physical or chemical properties of the surface water, the sediment bed or the storage zones. These tracers allow to investigate the behavior of solid particles in the water (i.e. heavy suspended sediments, colloids, spores, etc.) or to understand the retardation or degradation potential of a substrate containing surface or sub-surface water. Tracers that are purposely introduced in the environment are called “artificial”

Ward et al. (1998) in opposition to environmental tracers, which are those substances or water properties that naturally exist in the environment. Environmental tracers can be particular chemical compounds or water properties like conductivity or temperature, but also microbes or algae. The analysis of these tracers can be particularly useful when groundwater and surface water, with different tracer content, mix at the sediment-water interface. An example of environmental tracer is the use of radon-222 (Ellins et al., 1990). Radon (^{222}Rn) is an environmental tracer released from radon-bearing rock. Radon concentrations are higher in

groundwater than in surface water and can be used to identify groundwater inputs to a stream (Yoneda et al., 1991).

Anthropogenic environmental tracers result from their accidental release into the environment due to human activities. Frequently such tracers are widely distributed, have weak signals and result from prolonged accidental release. An example of anthropogenic environmental tracer is CFCs, which were released between the 1950s and 1980s and can be used to trace 50 year old water at a low detection limit (Busenberg and Plummer, 1992).

Tracers must be chosen in order to obtain the best experimental control during an investigation. The addition of an artificial tracer to stream water may be used to provide improved understanding of hyporheic retention and natural attenuation processes. Radioisotopes like tritium (conservative, ^3H as tritiated water) and chromium (reactive, ^{51}Cr as Cr(III)), were used in field studies in the Säva Brook, Sweden (Johansson et al., 2001; Jonsson and Worman, 2001). By using different tracers at the same time, the investigators were able to detect the retardation of the non-conservative (reactive) tracer relative to the conservative (inert) tracer.

The sorption of strontium (Sr) and potassium (K) tracers in bed sediments was investigated by (Bencala and Walters, 1983). Other researchers used caesium (Cs) to investigate the sorption processes in aquatic sediments (Comans and Hockley, 1992; N.J. Comans et al., 1991; Nyffeler et al., 1984; Smith and Comans, 1996). In these studies Caesium (Cs) was an environmental tracer originated from the 1986 Chernobyl accident in the Ukraine.

(Fuller and Harvey, 2000) used the reactive environmental tracer bromide (Br^-) to track the fate of metals in the hyporheic zone of a stream contaminated by mining in Arizona, pointing out an active uptake and retardation of these metals by hyporheic flow-paths along the study reach.

Particular attention was devoted to the analysis of transport and retention of nitrate in the hyporheic zone (Duff and Triska, 1990; Triska et al., 1993, 1990, 1989). Chloride and bromide (inert tracers) were injected in the study reach and recovered from the hyporheic zone by wells positioned at the side of the stream. The use of an inert solute provides information on the retardation and biological properties of the hyporheic zone. By injecting nitrate (NaNO_3) into the stream water and directly in the hyporheic sediments, it was demonstrated that biotic uptake within the hyporheic zone sediments acted as the major retention and storage mechanism.

Groundwater and surface water mixing in the hyporheic zone was found to govern the denitrifying capacity of sediments, due to the different dissolved oxygen concentration (DOC) provided by the two sources of water.

(Storey et al., 2003) used the ^{15}N isotope to describe denitrification processes in laboratory column experiments with sediments cores.

Temperature is another environmental tracer largely used in groundwater studies. Groundwater has a relatively constant temperature compared to surface or stream waters (Constantz, 1998). Conant (2004) investigated stream-groundwater exchange profiling water temperature through a depth profile of hyporheic sediments. Confirmation of the delineation of zones of groundwater discharge or recharge within the hyporheic zone derived from temperature measurements can be provided by the simultaneous injection of conservative solute tracers in the study reach. Becker (2004) used heat as a tracer and measured the longitudinal variation of the stream discharge to quantify the stream-groundwater fluxes. The work of (Anderson, 2005) offers a comprehensive background review of existing literature on the use of temperature as a tracer.

Fluorescent dyes are an important group of tracer for hydrologic field studies in rivers and wetlands. Among a variety of commercial dyes available in a variety of colors, uranine, lissamine FF and rhodamine WT are the most used fluorescent water tracers (Wilson et al., 1986). Since fluorescent dyes are cost effective, highly soluble, low-toxic and easily detectable with specific fluorometers, they have been widely used for stream tracing applications, especially rhodamine WT (Atkinson and Davis, 2000; Bencala, 1984; Bottacin-Busolin et al., 2011; Fernald et al., 2001).

Among the fluorescent dyes, particular attention should be given to “smart” tracers, like resazurin. Resazurin is a type of fluorescent, non-toxic, redox-sensitive phenoxazine dye. An important property of resazurin is the reduction to the strongly fluorescent resorufin under mildly reducing conditions, most commonly in the presence of aerobic respiration (Karakashev et al., 2003). These tracers have been recently used to analyze microbial activity in the hyporheic zones (Haggerty et al., 2009).

1.4.2 Designing stream tracer tests to quantify retention phenomena

Tracer tests are conducted by injecting a tracer in a study reach. Injection is usually performed with a constant (plateau) concentration of fixed duration to ensure proper dilution along the reach. The concentration distributions generated by the injection, known as breakthrough curves (BTCs), are measured over time at one or more sections downstream from the injection point, at a distance greater than the length scale of transverse mixing. BTCs contain information relevant to surface processes, namely advection and longitudinal dispersion, but also signatures of retention phenomena that produce deviations from the asymptotic dispersion regimes described by Taylor dispersion theory. Tracer BTCs carry signatures of complex stream-storage zone mixing and exchange dynamics, and the challenge of modeling and designing field tracer tests lies in the identification and the parameterization of these signatures. It is known that the tails of surface concentration distributions are affected by transient storage processes, but the major issue with their characterization is given by the detection limit of solute concentrations. Only the use of highly detectable tracers allows the analysis of long-term retention phenomena.

Davis and Atkinson (2000) observed that longitudinal dispersion leaves clear signatures only within a short distance from the upstream boundary section and that the fast exchange with the dead zones overwhelm the effect of surface mixing at longer distances. In other words, longitudinal dispersion and fast exchange processes act as a bulk process over longer distances from the injection point. The geometry of the study reaches and the choice of the tracer are thereby important factors for the success of an experimental campaign aiming to determine surface dispersion, fast exchange and the deeper transfer of solutes into the hyporheic zones. It must be stressed that the use of tracer tests to quantify long-term retention phenomena is limited by a number of factors, including the experimental timescale, the concentration detection limit, and the presence of background noise in the measurements. The surface water point of view is thereby blind to those processes characterized by small exchange fluxes and by temporal scales that are much longer than the duration of the experiment.

A work on how signatures of different mechanisms can be observed on BTC was presented by Bottacin-Busolin et al. (2011). BTCs were obtained with a controlled plateau injection of rhodamine WT in two different small Italian rivers, the Desturo and the Brenton channels. The

two study reaches were divided in 4 sub-reaches, hence 4 BTCs for each reach were produced. BTCs were analyzed using a numerical model. Two components of the residence time distribution were considered. A multiple domain solute transport model properly characterize river transient storage processes in terms of average retention times, and show that retention patterns at different timescales can be detected. The information contained in the tail comprehend the sum of different exchange processes that only a model implementing multiple compartments of storage can properly describe.

1.4.3 Limitations and challenges in inverse modeling of transport processes

Tracer tests in surface water provide a picture of stream transport and exchange processes through BTCs of designed solute injections. Modern technologies and new generation tracers improved the quality of information collected with field tests. Transient storage and exchange models offer an important tool to interpret BTCs and to extrapolate the different mechanisms of interaction between the surface water and the surrounding environment. The future of tracers tests and models is to push further the detection of long timescales exchange mechanisms and to link hydrodynamics to these processes.

A proper survey of the study reach including bed elevations, planimetric variations (bends, stream width), obstacles, vegetation status combined with surface and groundwater sampling (temperature profiling in the hyporheic zones, use of wells) can lead to a comprehensive understanding of solute transfer processes between the surface water and the surrounding environment.

1.5 Work scope

In this study, the performance of FWS wetlands for wastewater treatment was studied as a function of wetland configuration (i.e. wetland aspect ratio, shape and inlet-outlet position) and vegetation density and distribution. Previous work has suggested that high aspect ratio ($L:W$) may be an important factor in the ability of FWS wetlands to improve performance. However, it is still not known how much performance improvement can be achieved under varying vegetation coverage. In addition, the effect of wetland shape and vegetation distribution on mass transport mechanisms through the entire wetland system is not well understood. In this study,

these two important questions were explored to help creating design guidelines for more efficient constructed wetlands.

First, a hydrodynamic model to solve the shallow-water equations and a solute transport model to solve the depth-averaged advection-diffusion equations was used to create a conceptual mathematical model that examined the effect of wetland properties on treatment performance. Numerical simulations of a set of hypothetical wetlands were performed to obtain detailed velocity field of the distribution, and flow through wetland area. The Residence Time Distributions (RTDs) were derived from numerical simulations of the flow field and the temporal evolution of the outlet concentration of a tracer injected at the inlet. It has been proposed that application of an ellipse shape improves the wetland performance by reducing the area of dead zones at the corners, and thereby increasing the effective wetland volume contributing to the treatment process. Moreover, it was suggested the application of wetlands with different alignment of the flow inlet and outlet and wetlands with multiple inlets effect the wetland treatment performance.

Next, the depth-averaged two-dimensional numerical model was coupled with a random field generator, which allowed the study of the effect of the Heterogeneity of vegetation patterns and the presence of fast flowpaths on jet-induced spreading within the wetland area. Note that here both vegetation bands oriented parallel and perpendicular to the flow direction were considered. It was shown bands that run parallel to the flow direction will create short-circuiting by conveying flow directly to the outlet, whereas, perpendicular bands will improve the treatment performance through aligning potential fast flowpaths.

The numerical model was used to show that perpendicular vegetation bands can improve wetland performance through two separate mechanisms. When lateral mixing is present within the vegetation band, it dilutes passed water through the fast flowpath and reduces the fraction of water that short-circuits the entire wetland length. In addition, by dissipating the high velocity associated with the fast flowpaths, there is a high possibility that vegetation bands reduce the probability that fast flowpaths will align throughout the entire wetland. Therefore, in the absence of lateral mixing is within the vegetation band, it is likely that all water will receive more treatment, causing a higher performance.

Chapter 2

2 Effects of vegetation density and wetland aspect ratio variation on hydraulic efficiency of wetlands

2.1 Contaminant removal in FWS wetlands

Treatment wetlands are man-made systems that designed according to specific characteristics of wetland ecosystems and to provide wastewater treatment capacity. Treatment wetlands can be constructed based on a variety of hydrologic and hydraulic criteria. At the current stage of technology development, different types of wetlands can be categorized in three main groups: (1). Free water surface (FWS) which are mainly vegetated aquatic systems similar in appearance to natural marshes, (2). Horizontal subsurface flow (HSSF) wetlands consist of a gravel bed planted with wetland vegetation. The wetland system works based on horizontal water flow below the surface of the bed from the inlet to the outlet, and (3). Vertical flow (VF) wetlands employ surface flooding of a sand or gravel bed in a single-pass configuration to treat the water when percolate it through the plant root zone.

In this study, FWS wetlands and their design configuration was discussed comprehensively. Constructed FWS wetlands contain areas of open water and floating or emergent vegetation, and their water treatment performance is a function of the design configuration. As the wastewater passes through the wetland, it is exposed to a variety of physical, biological and chemical processes (i.e. sedimentation, filtration, oxidation, nitrification and reduction). Figure 2.1 illustrates the components of a typical FWS wetland. FWS constructed wetlands mimic natural wetlands, and similarly they are inhabited by a wide variety of wildlife, namely insects, mollusks, fish, amphibians, reptiles, birds, and mammals (Kadlec and Wallace, 2009; Thullen et al., 2005). Free Water Surface (FWS) wetlands are an efficient ecological system for treating different forms of wastewater through biochemical processes (Arheimer and Wittgren, 2002; Meng et al., 2014) that are linked to hydrodynamic processes (Bodin et al., 2012; Savickis et al., 2016). The effectiveness of constructed wetlands in reducing different contaminants is well documented (Vymazal, 2014; Vymazal and Březinová, 2015), with several studies demonstrating the efficiency of wetlands in removing BOD (80.8%) (Katsenovich et al., 2009), COD (61.0%) (Chen et al., 2006), total suspended solids TSS (75.0%) (Martín et al., 2013), total nitrogen (TN) (62.3%), and NO₃-N (75.3%) (Zhang et al., 2015), ortho-phosphate (PO₄-P) and total phosphorus (TP), (53.9%), (56.0%) respectively. (Kotti et al., 2010), FCs (52%) and E.coli (58%) (Cameron et al., 2003).

FWS wetlands can be used for advanced treatment of effluent from secondary or tertiary treatment processes (Vymazal, 2013). However, due to the potential for human exposure to pathogens, the application of FWS wetlands for secondary treatment is not common (Meng et al., 2014). Although the treatment performance of FWS wetlands may decrease for temperature-dependent reactions (e.g. nitrogen removal), they still remain suitable. Moreover, the transfer of oxygen from the atmosphere may be disturbed, when ice covers the wetland surface, leading to decreasing oxygen-dependent treatment processes (Kotti et al., 2010). Other processes, such as TSS removal, are more effective under the ice than in summer conditions. It is generally more efficient to store water during winter and treat it during the warm part of the year (Kadlec and Wallace, 2009).

There are also extra benefits for FWS wetlands, including human uses and wildlife habitat. Treatment marshes are not inexpensive, but are usually capital cost-competitive with alternative

technologies. Operating costs are typically quite low compared to alternatives (Kadlec and Wallace, 2009; Yang and Tsai, 2011).

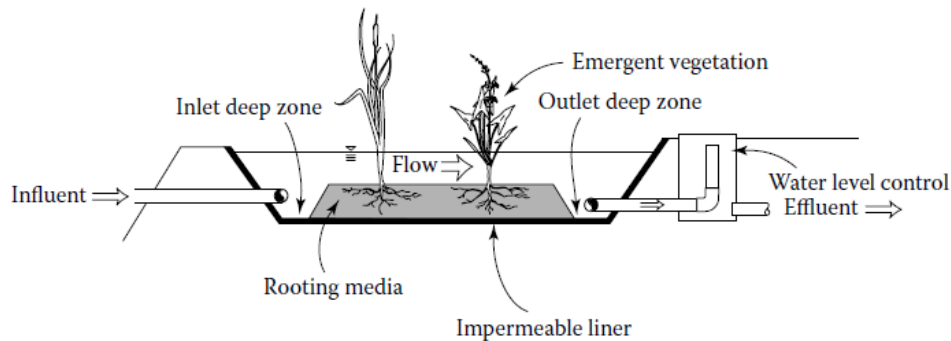


Figure 2.1 Basic elements of a FWS wetland.

Free water surface constructed wetlands (FWS CWs) can remove a variety of contaminants from municipal wastewater (Cameron et al., 2003; Kipasika et al., 2014), storm water (Carleton et al., 2001; Mangangka et al., 2015), industrial wastewater (Vymazal, 2014; Wu et al., 2015), agricultural wastewater (Maucieri et al., 2014; Vymazal and Březinová, 2015), road runoff (Gill et al., 2014), woodwaste leachate (Tao et al., 2006), and landfill leachate (Yang and Tsai, 2011). The effectiveness of constructed wetlands in removing different forms of contaminants is well documented (Vymazal, 2013). For example, phosphorus removal has been documented in over 250 FWS wetlands, for a wide range of inflow concentrations, from below 20 $\mu\text{g/L}$ to over 100 mg/L (Kadlec and Wallace, 2009). Hsueh et al. (2014) reported 85% removal of TN (total nitrogen) in a subtropical free water surface CW in Taiwan with retention time of 3.7 days. Batty and Younger (2002) found that where dissolved iron concentrations in wetland waters were at or below 1 mg/L , direct uptake of iron by plants could account for 100% of iron removal. Kotti et al. (2010) investigated the performance of five FWS CWs and observed average removal values of 77.5%, 67.9%, 60.4%, 53.9%, 56.0% and 51.7% for BOD, COD, TKN, ammonia ($\text{NH}_4\text{-N}$), ortho-phosphate ($\text{PO}_4\text{-P}$) and total phosphorus (TP), respectively. Although CWs have the potential to improve water quality significantly, there is a large variability in their hydraulic efficiency and removal rates (Persson et al., 1999). Wetland characteristics including wetland shape, inlet-outlet configuration, vegetation coverage and water depths affect the hydraulics of CWs, which directly influences removal rates. Designing a constructed wetland to achieve a certain performance level requires optimization of these wetland properties (Marion et al., 2014).

2.2 Plug flow and nominal residence time

The hydraulic design of a wetland has two main requirements: (1) the resulting hydraulic residence time (HRT) must be sufficiently long to allow for the natural treatment processes to remove the contaminants (Thackston et al., 1987); (2) the wetland must provide a condition close to plug flow, for which dispersion is minimum, so that all water parcels experience a residence time close to the HRT (Holland et al., 2004; Persson et al., 1999). Hydraulic retention time (HRT) is the average amount of time a passive solute spends in a wetland system. A longer retention time provides more time for biochemical reactions to occur in the wetland, and thus increases pollutant removal (Kadlec and Wallace, 2009). Toet et al. (2005) evaluated the pollutant removal in a FWS under four hydraulic retention times from 0.3 to 9.3 days and found that increasing HRT led to considerable increase in the removal of total nitrogen, ammonium, and nitrates. A minimum HRT of 4 days was found to be necessary for a nitrogen removal efficiency of approximately 45%, corresponding to an annual mass loading rate of $150 \text{ gr m}^{-2} \text{ yr}^{-1}$. The hydraulic efficiency of a wetland is characterized in terms of two non-dimensional parameters. The first is the dimensionless retention time, defined as $e_v = t_m/t_n$, in which t_m is the observed mean residence time, and $t_n = V/Q$ is the nominal residence time, in which V is the volume of the wetland and Q is the input discharge rate (Thackston et al., 1987). The optimum residence time would be achieved when the ratio approaches unity ($t_m = t_n$), which implies that there are no dead zones in the wetland, and the whole wetland volume actively contributes to the treatment processes. The second design criterion describes the departure from plug flow due to dispersion processes. Dispersion arises from inlet and outlet effects, vegetation distribution patterns, bottom topography, wind effects and shear stresses from sides. Dispersion makes some parcels of water exit before and after the nominal residence time (t_n). Because the biochemical reactions impacting pollutant removal are mostly first-order reactions, there is a greater disbenefit to pollutant removal for parcels of water leaving before t_n compared to the benefit for parcels leaving after t_n , so that any dispersion, which creates a greater variance in individual residence times, will diminish the overall pollutant removal.

2.3 Wetland aspect ratio

Most constructed treatment wetlands are rectangular, to maximize the wetland treatment area (on a rectangular land parcel) and minimize the construction costs (Kadlec and Wallace, 2009; Su et

al., 2009). Therefore, wetland aspect ratio, (length/width ratio, L/W), is an important design feature, determining wetland footprint and number of berms. In addition, a long and narrow shape with high aspect ratio reduces short-circuiting in wetlands that vegetation is not distributed uniformly. For example, Jenkins and Greenway (2005) developed a numerical model and studied hypothetical wetlands of aspect ratios in range of 1 to 18 and concluded that higher aspect ratio improves treatment capability of wetlands through increasing residence time.

Abbas et al. (2006) simulated waste stabilization ponds with multiple berms and found that BOD5 removal rate increased about 10% for a pond with a L/W ratio of 1/1, compared to a pond with a L/W ratio of 4/1. Persson et al. (1999) developed a two-dimensional numerical model and simulated the tracer release in wetlands of different aspect ratio. A rectangle wetland of 10/1 aspect ratio was found to have the highest retention time. However, A high aspect ratio (L/W) is not always useful, for example, Reed et al. (1995) noted that there is a higher possibility of short-circuiting for FWS wetlands of very high aspect ratios (above 10/1) due to the increased level of head drop within the system. In addition, a high aspect ratio increases the required berm length per wetland area, and berm construction costs increase wetland costs (Hammer and Knight, 1994).

2.4 Vegetated wetlands

Vegetation is an essential component of wetland systems and its properties influence wetland efficiency (Jenkins and Greenway, 2005). The most important effects of vegetation on CWs are (1) the uptake of nutrient pollution and oxygen release from roots, (2) the contribution of additional hydrodynamic drag that impacts the wetland hydraulics. Several studies have investigated the effects of vegetation type and density on CWs hydraulics. Jenkins & Greenway (2005) applied a numerical model to study the effects of emergent fringing and banded vegetation on the hydraulic characteristics of constructed wetlands. The results proved that inappropriate layout of wetland vegetation results in poor performance of a wetland system. Musner et al. (2014) used a two-dimensional depth-averaged model to study the residence time distribution of a tracer under different vegetation patterns in a channelized wetland and reported that increasing vegetation densities produce an increasingly pronounced bimodality of the RTDs reflecting a separation between flow traversing the channels and flow traversing the vegetated regions.

2.5 Importance of wetland aspect ratio in vegetated wetlands

Considering the importance of wetland aspect ratio and vegetation coverage in wetland design, there is a need to further investigate the significance of these parameters on wetland hydraulics. This chapter introduces a two-dimensional numerical model to study the wetland hydrodynamics and mass transport patterns. The model is used to study the interaction between the vegetation density, wetland aspect ratio and the hydraulic efficiency of a constructed surface water wetland system. The aim of chapter is to investigate design parameters in wetlands to provide a quantitative understanding of hydraulic efficiency in connection with wetland vegetation and wetland shape. Such an understanding might help engineers to design more efficient and cost-effective water systems.

2.6 Depth-averaged two-dimensional numerical model

A depth-averaged 2-dimensional numerical model of a wetland was developed to simulate the velocity field and the transport of a dissolved tracer under steady flow conditions. The hydrodynamic model solved the shallow-water equations and a solute transport model solved the depth-averaged advection-diffusion equations.

2.6.1 Hydrodynamic model

Under the assumption of hydrostatic pressure, stationary flow, and negligible wind and Coriolis forces, the depth-integrated velocity field and water depth can be described by the following equations (Wu, 2007):

$$\frac{\partial(hU_x)}{\partial x} + \frac{\partial(hU_y)}{\partial y} = 0 \quad (2.1)$$

$$\frac{\partial(hU_x^2)}{\partial x} + \frac{\partial(hU_xU_y)}{\partial y} = -gh \frac{\partial(z_s)}{\partial x} - \frac{\tau_{bx}}{\rho} - \frac{\tau_{vx}}{\rho} \quad (2.2)$$

$$\frac{\partial(hU_xU_y)}{\partial x} + \frac{\partial(hU_y^2)}{\partial y} = -gh \frac{\partial(z_s)}{\partial y} - \frac{\tau_{by}}{\rho} - \frac{\tau_{vy}}{\rho} \quad (2.3)$$

in which u_x and u_y are the velocity components along the x and y directions; h is the mean water depth; z_s is the water surface elevation; ρ is water density; τ_{bx} and τ_{by} are the bed shear stresses in

the x and y directions; and τ_{vx} and τ_{vy} are the shear stresses due to vegetation in the x and y directions. The bed shear stresses can be determined as (Kadlec and Wallace, 2009).

$$\tau_{bi} = \rho C_{bD} U_i \sqrt{u_x^2 + u_y^2}, \quad (2.4)$$

with bed-drag coefficient,

$$C_{bD} = \frac{3\mu}{h\rho\sqrt{u_x^2 + u_y^2}} + \frac{M^2 g}{h^3} = \frac{3}{Re} + \frac{M^2 g}{h^3} \quad (2.5)$$

in which μ is the water dynamic viscosity and M is the Manning friction coefficient. The bed drag coefficient consists of two terms. Under laminar and transitional flow ($Re = Uh/\nu \leq 500$, with Re the Reynolds number, U the cross-sectionally averaged velocity and ν kinematic viscosity), the first term dominates, whereas the second turbulent term becomes important for larger Reynolds numbers ($Re \geq 1250$) (Musner et al., 2014). Following (Werner and Kadlec, 1996), vegetation drag is modeled using the following expressions for the drag exerted by the stems,

$$\tau_{vi} = \rho C_{vD} a l \frac{U_i}{2} \sqrt{u_x^2 + u_y^2} \quad (2.6)$$

in which C_{vD} is the vegetation-drag coefficient (dimensionless) and l is the submerged stem height, equal to the water depth in the case of emergent vegetation. C_{vD} is a function of the stem Reynolds number $Re_d = Ud/\nu$. The drag coefficient for a circular cylindrical stem within a canopy may be represented as $C_{vD} = 1 + 10Re_d^{-2/3}$, $1 < Re_d < 10^5$, for an isolated circular cylinder (White, 1991), when the canopy density $ad < 0.1$ (Nepf, 1999; Stone and Shen, 2002). Therefore, under the laminar flow in the simulated wetlands (velocity in the range between 0.05, 0.22 cm s⁻¹), C_{vD} was set ranging between 3 and 9. If the plants are modeled as cylinders, the average vegetation density parameter, \bar{n} , can be defined as $\bar{n} = n_s D$, in which n_s is the number of stems per unit area (m⁻²), and d is the stem diameter (m) (Nepf, 1999; Stoesser et al., 2010). The stem diameter can be assumed to be in the range $d = 3$ mm-15 mm, which is a reasonable assumption for the type of vegetation found in FWS wetlands (Serra et al., 2004; Tanino and Nepf, 2008).

2.6.2 Solute transport model

The depth-integrated concentration, C , of a reactive tracer passing through the wetland was simulated using the 2D, depth-integrated, advection-diffusion equation with a first-order reaction,

$$\frac{\partial(hC)}{\partial t} + \frac{\partial(hu_x C)}{\partial x} + \frac{\partial(hu_y C)}{\partial y} = \frac{\partial}{\partial x} \left(hE_{xx} \frac{\partial C}{\partial x} + hE_{xy} \frac{\partial C}{\partial y} \right) + \frac{\partial}{\partial y} \left(hE_{yx} \frac{\partial C}{\partial x} + hE_{yy} \frac{\partial C}{\partial y} \right) - hkC \quad (2.7)$$

The coefficients E_{ij} account for both turbulent diffusion and shear dispersion due to vertical velocity gradients. Since we cannot assume that the x-axis is everywhere parallel to the local flow vector, the mixed dispersion coefficients, E_{ij} , must be retained. They can be written in terms of their longitudinal (E_L) and transverse (E_T) components (Feleke Arega and Sanders, 2004),:

$$E_{xx} = E_L + (E_L - E_T) \frac{u_x^2}{u_x^2 + u_y^2} \quad (2.8)$$

$$E_{xy} = E_{yx} = E_L + (E_L - E_T) \frac{u_x u_y}{u_x^2 + u_y^2} \quad (2.9)$$

$$E_{yy} = E_L + (E_L - E_T) \frac{u_y^2}{u_x^2 + u_y^2} \quad (2.10)$$

In this study k (s^{-1}), the solute volumetric removal rate, is assumed to be proportional to the vegetation density (s^{-1}).

$$k = k_0 \frac{\bar{n}}{\bar{n}_0} \quad (2.11)$$

Where k_0 is the decay rate for the reference vegetation density, \bar{n}_0 . The non-reactive tracer was used in this chapter, so with assumption of $k_0 = 0$ the term related to equation (2.11) drops from the equation (2.7). An equation to determine transverse diffusion for flow through emergent vegetation was proposed by Nepf (1999). The total transverse diffusion is expressed as the combination of both mechanical and turbulent diffusion Eq. (2.12):

$$\frac{E_T}{U_x d} = \alpha_h (C_{vD} ad)^{\frac{1}{3}} + \frac{\beta^2}{2} ad \quad (2.12)$$

The first term, associated with turbulent diffusion, is based on the assumption that all the energy extracted from the mean flow through stem drag appears as turbulent kinetic energy. The second term accounts for the mechanical diffusion and arises from the dispersal of fluid particles due to obstruction of flow by vegetation stems. Nepf (1999) compared the predictions of Eq. (2.12) with experimental data from laboratory experiments in the range of stem Reynolds number $Re_d = \frac{Ud}{\nu} = 400$ to 2000 and field experiments in the range $Re_d = 300$ to 600 and found a good agreement for scale factors of $\alpha_h = 0.81$, $\beta = 1$. Turbulent diffusion is not present ($\alpha_h=0$) for conditions with $Re_d < 200$, for which the viscous drag, which dissipates mean flow energy without generating turbulence, is a key factor.

Longitudinal dispersion (E_L) reflects the effects of stem-scale longitudinal dispersion processes and the dispersion induced by vertical velocity gradients. Lightbody and Nepf (2006) used field velocity measurements in the range between 0.1 and 0.24 cm s⁻¹ ($Re_d = Ud/\nu = 2-360$, with d the stem diameter) to determine longitudinal dispersion coefficient E_L . The non-dimensional form of the longitudinal dispersion coefficient is written as a combination of the stem-scale and the depth-scale dispersion process as:

$$\frac{E_L}{u_x d} = \frac{1}{2} (C_{vD})^{\frac{3}{2}} + \frac{u_x h}{D_z} \Gamma \quad (2.13)$$

in which $D_z = \alpha_z (C_{vD} a d)^{\frac{1}{3}} U d$ is the vertical turbulent diffusion coefficient, $\alpha_z = 0.81$ (Lightbody and Nepf, 2006), and Γ is the non-dimensional velocity shape factor. The shape factor is a function solely of canopy morphology and can be determined from the normalized vertical diffusion $\frac{Ud}{D_z}$ and the normalized depth-shear dispersion coefficient, $\frac{K_h}{Uh} \left(\frac{Ud}{D_z} \Gamma = \frac{K_h}{Uh} \right)$. In this study, here $ad = 0.009$ to 0.04, Γ was set to the range 0.02 to 0.08, which is comparable to the range observed by Nepf et al. (1997) in a laboratory flume study of an emergent dowel array ($\frac{D_z}{ud} = 0.04 \pm 0.01$ for $ad = 0.014$ and $\frac{D_z}{ud} = 0.09 \pm 0.01$ for $ad = 0.053$), and the assumption of fairly uniform frontal area over depth (i.e. *Atriplex portuloides*), $\frac{K_h}{Uh} = 0.8$ (Leonard and Reed, 2002). As noted by Lightbody and Nepf (2006), over length-scales greater than the flow depth the first term of equation (2.13) is typically smaller than the second term, and can be neglected. For the

range of stem Reynolds numbers investigated in this study it is reasonable to consider only the first term of equation (2.12) and only the second term of equation (2.13).

2.7 Residence time distribution

Tracer tests are used to evaluate the hydraulic efficiency of a wetland (Bodin et al., 2012; Holland et al., 2004; Koskiaho, 2003). A non-reactive tracer is introduced at the wetland inlet, and the outlet concentration is measured as a function of time, $C_{out}(t)$, from which the residence time distribution, $r(t)$, can be found.

$$r(t) = \frac{Q_{out}(t)C_{out}(t)}{\int_0^{\infty} Q_{out}(t)C_{out}(t)dt} \quad (2.14)$$

with volumetric outflow $Q_{out}(t)$. The first moment of the RTD is the mean residence time, t_m , which is the average time that tracer particles remain in the wetland (Bodin et al., 2012),

$$t_m = \int_0^{\infty} t r(t)dt \quad (2.15)$$

If the flow passes through the entire volume (i.e. there are no dead-zones), the measured mean residence time equals the nominal residence time, i.e. $t_m = t_n = V/Q$. The second moment of $r(t)$, i.e. the variance (σ^2), is:

$$\sigma^2 = \int_0^{\infty} (t - t_m)^2 r(t)dt \quad (2.16)$$

which describes the range of possible residence times for different individual fluid parcels. A large variance indicates that there is a large variation in the times spent by individual parcels of water within the wetland. This variation can be caused by the presence of different flow paths, e.g. short-circuiting flow paths and recirculation zones, or by a high level of turbulent mixing. For plug flow, for which there is no mixing and a perfectly uniform flow field, the variance is equal to zero.

A wetland can be modeled as a number (N) of continuous stirred tank reactors (CSTRs) in series (Kadlec and Wallace, 2009). In the case of a single tank ($N = 1$), water is uniformly and instantly mixed over the entire wetland, and the wetland behaves as a well-mixed reactor, resulting in an exponential RTD with $\sigma = t_n$. In contrast, a model with a large number of tanks (large N) produces a system approaching plug flow, with a low degree of overall mixing and

small variance (σ^2). According to Fogler (1992), the number of tanks in series, N , can be determined from the inverse of the dimensionless variance ($\sigma_\theta = \sigma/t_n$):

$$N = (\sigma_\theta)^{-2} = \left(\frac{\sigma}{t_n}\right)^{-2} \quad (2.17)$$

The dimensionless variance or the number of CSTRs can be used to compute the dispersion efficiency of the wetland (Persson et al., 1999):

$$e_d = 1 - (\sigma_\theta)^2 = 1 - \left(\frac{1}{N}\right) \quad (2.18)$$

In the ideal limit of plug flow, $\sigma^2 = 0$, resulting in $e_d = 1$. This represents the best treatment conditions with the lowest exit concentration.

Another metric of wetland efficiency is the volumetric efficiency, e_v , (Persson et al., 1999), representing the effective volume of a wetland system. It is determined as the ratio of the mean residence time (t_m) and the nominal residence time (t_n).

$$e_v = \left(\frac{t_m}{t_n}\right) = \left(\frac{A_{\text{effective}}}{A_{\text{total}}}\right) \quad (2.19)$$

Assuming a uniform depth, this also indicates the ratio of effective flow area ($A_{\text{effective}}$) to total pond surface area (A_{total}). Low values of e_v (<1) indicate the presence of dead zones ($A_{\text{effective}} < A_{\text{total}}$). Persson et al. (1999) also defined a hydraulic efficiency index, λ_h , incorporating both the effects of retention time and dispersion.

$$\lambda_h = e_v \left(1 - \frac{1}{N}\right) \quad (2.20)$$

A high value of this index indicates that few dead zones are present ($e_v \approx 1$) and low levels of dispersion are present, both of which lead to better wetland performance.

2.8 Model application

The numerical model study was undertaken to simulate velocity fields and tracer transport patterns for a free water surface (FWS) wetland system (Fig. 2.2). In this study, four different wetland configurations (aspect ratios 1/1, 2/1, 3/1, 4/1) each with the area of 1 hectare and 0.5 m

depth and variable vegetation densities were simulated. The boundary conditions were defined for the equations (2.1) and (2.3), by the inflow at the inlet, 0.83 L/s, and the water depth at the outlet, 0.5 m , producing a nominal hydraulic retention time of $t_n = 7$ days. In all the studied cases, the flow was modeled for a constant discharge rate through an inlet of 10 m width and an outlet with 10 m width and 0.5 m height, under atmospheric pressure. Both the inflow and outflow were centrally located. These design values were chosen according to the values described by (Persson et al., 1999; Thackston et al., 1987).

For the solute transport equation, the boundary conditions were given by an instantaneous tracer injection at the inlet, $C = 1 \text{ kg/m}^3$, an open boundary condition at the outlet, and the no-flux condition on the remaining part of the flow boundary. The equations were solved via a finite element method using COMSOL Multiphysics® with quadratic shape functions. The computational grid was made of approximately 150000 triangular elements, with higher spatial resolution near the inlet and the outlet, and a maximum element size of 2m. C_{out} was calculated from the averaging over the outlet element.

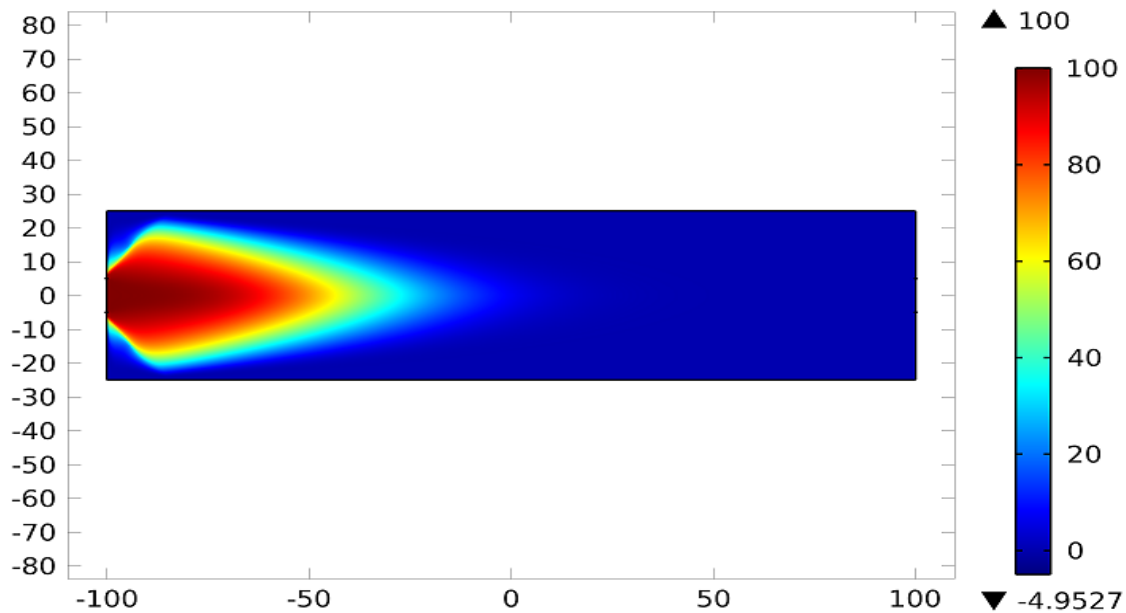


Figure 2.2 Simulations for a uniformly vegetated wetland (aspect ratio 4/1), tracer concentration distribution- After elapsed time=1.2 days.

A numerical tracer study was performed to generate RTDs for all configurations. Response to the tracer injection was simulated for rectangular wetlands of vegetation densities 20 to 1500 stems m^{-2} . The vegetation shear stresses were determined by the Eq. (2.6) by assuming that all of the vegetation had a diameter of $d= 10$ mm, which is reasonable for a constructed FWS wetland. Marsh grasses are relatively sparse; the vegetation volume fraction is in the range of $VF=0.001-0.15$ associated with the stem diameter of $d=1-12$ mm (Jadhav and Buchberger, 1995; Lightbody and Nepf, 2006). In contrast, in constructed wetlands aquatic vegetation conditions may be designed quite dense with diameters up to 15 mm (Serra et al., 2004). The wetland Manning coefficient for bottom friction was $0.035 \text{ s/m}^{1/3}$.

2.8.1 Model calibration and validation

Four parameters; vegetation density, transverse diffusivity, E_T , longitudinal dispersion coefficient, E_L , and Manning coefficient (M); were used for model calibration. A sensitivity analysis was carried out by initially considering parameters that represented average values of E_T and E_L determined from Eq. (2.13) using the scale factors $\alpha_h = 0.1$, $\beta = 1$, as derived from the experimental studies (Nepf, 1999) and $\alpha_v = 0.1$ (Eq. 2.12) (Lightbody and Nepf, 2006; Tanino and Nepf, 2008). The model output was used to calculate the volumetric efficiency, e_v , which was compared to the following empirical relation derived by Thackston et al. (1987), based on survey data from a wide variety of vegetated types, sizes, and shapes of large, shallow wetlands (Fig. 2.3).

$$e_v = 0.85 \left(1 - \exp \left(-0.59 \left(\frac{L}{W} \right) \right) \right) \quad (2.21)$$

Applying a best-fit calibration for a vegetation density of 50 stems m^{-2} , the Manning coefficient that produced the best match between the model and the design curve was found to be $M = 0.02 \text{ m}^{-1/3} \text{ s}$. The vegetation density of 50 stems m^{-2} was chosen because the contribution of bed friction is higher at low density. In the calibration, 60% of the simulations were used (with L/W aspect ratios of 1/1, 2/1, 5/1, 6/1, 8/1, 10/1) whereas the remaining 40% was applied for model validation. As shown in Figure 2.3, the numerical model results fit well with the field data presented by Thackston et al. (1987). The relative errors of rectangular and ellipse wetlands to the field data were 8% and 11%, respectively (Fig. 2.3). The numerical modeling studies by

Jenkins and Greenway (2005) and Minsu et al. (2009) have also calibrated sets of hypothetical wetlands according to the design curve proposed by Thackston et al. (1987), and both found a good fit between L/W and the simulated detention time.

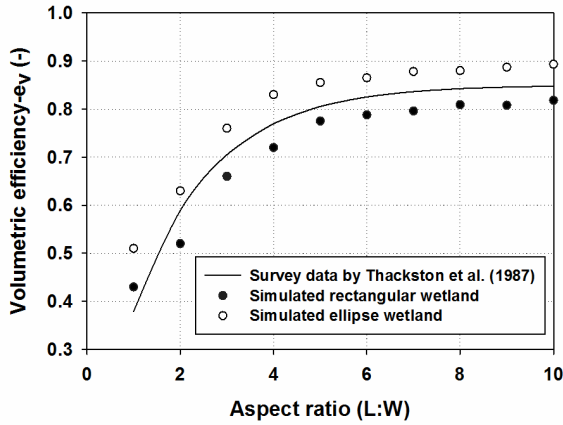


Figure 2.3 Volumetric efficiency derived from field data (black curve, Thackston et al. 1987) and from the numerical simulations.

2.9 Numerical simulations of vegetation effects

The outlet tracer concentration variation and corresponding RTDs simulated by the numerical model grouped for different vegetation densities are illustrated in Fig. 2.4. The summary of wetland hydraulic efficiency indexes is given in Table 2.1. Similar positively skewed RTDs with elongated tails to the right were observed for different vegetation densities. However, the data points showed a tendency to be closer to the centroid, as the vegetation density increased. Moreover, there was also an increase in the mean retention time with increasing stem density.

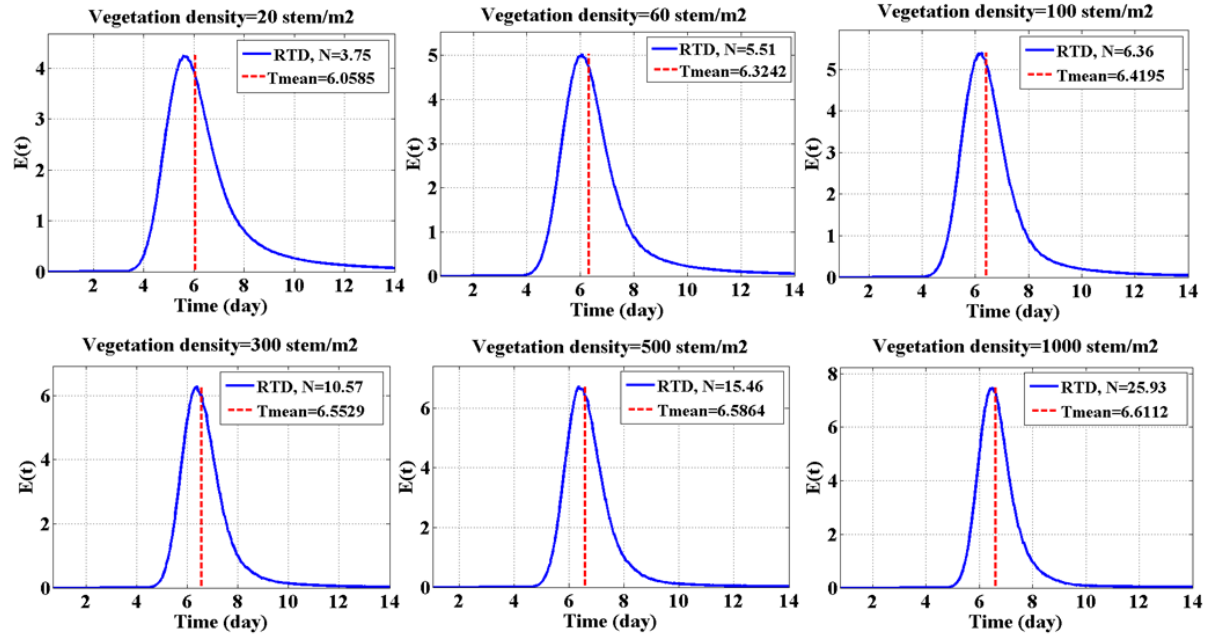


Figure 2.4 Normalized residence time distributions (RTDs) for six different vegetation densities.

The numerical simulations returned different values of the variance of the RTDs (Fig. 2.4), which revealed that wetlands of dissimilar vegetation density experience different hydraulic performances. Generally, an increase in vegetation density produced an increase of mean retention time and variance before reaching an approximately constant value of efficiency (Table. 2.1).

In response to a vegetation density boost from 20 stems m⁻² to 260 stems m⁻², the efficiency measure related to retention time, e_v , and measure of mixing, λ_h , improved by respectively 7% and 20%, whereas each of the hydraulic efficiency parameters exhibited smaller changes due to vegetation density increase for densities higher than 260 stems m⁻² (i.e. $e_v \approx 1\%$ and $\lambda_h \approx 8\%$). Above the threshold vegetation density, in this case 260 stems m⁻², changes in wetland performance were not significant and suggested negligible improvement in efficiency factors. As already mentioned, the number of CSTRs in series, N , can be used as a measure of mixing, and to quantify the heterogeneity of mixed tracers. In this manner, the sparse vegetation density of 20 stems m⁻² can be compared to a series of $N=3.75$ and the more dense vegetation pattern of 260 stems m⁻² compares to a series of $N=9.86$. The higher numbers of CSTRs were achievable by increasing the vegetation density (i.e. $N=25.93$ for $\bar{n}=1000$ stems m⁻²); however, such a change

for very dense vegetation covers did not necessarily improved the mixing efficiency factor (Table. 2.1).

Table 2.1. Estimated statistic-hydraulic parameters of a wetland (aspect ratio 4/1). Mean residence time (t_m), the variance of RTD (σ), number of continuously stirred tank reactors, CSTRs, (N), dimensionless retention time (e_v), Persson hydraulic index (λ_h).

| Vegetation density (stems m ⁻²) | t_m -day | σ -day | N | e_v | λ_h |
|--|------------|---------------|-------|-------|-------------|
| 20 | 6.06 | 3.13 | 3.75 | 0.86 | 0.63 |
| 60 | 6.32 | 2.69 | 5.52 | 0.90 | 0.74 |
| 100 | 6.42 | 2.55 | 6.36 | 0.92 | 0.77 |
| 180 | 6.50 | 2.31 | 7.91 | 0.93 | 0.81 |
| 260 | 6.54 | 2.10 | 9.68 | 0.93 | 0.84 |
| 340 | 6.56 | 1.92 | 11.68 | 0.94 | 0.86 |
| 420 | 6.58 | 1.79 | 13.46 | 0.94 | 0.87 |
| 500 | 6.59 | 1.68 | 15.46 | 0.94 | 0.88 |
| 700 | 6.60 | 1.48 | 19.77 | 0.94 | 0.89 |
| 800 | 6.60 | 1.40 | 22.20 | 0.94 | 0.90 |
| 1000 | 6.61 | 1.30 | 25.93 | 0.94 | 0.91 |
| 1500 | 6.62 | 1.41 | 33.67 | 0.95 | 0.92 |

More dense vegetation coverage is associated with higher variances of RTDs and larger number of continuously stirred tank reactors (N) (Table 2.1). This indicates better efficiencies are most likely related to the high coverage of emergent vegetation in wetlands. However, it was observed that the factors λ_h and e_v remained almost constant and increasing vegetation density did not significantly improve the efficiencies above a certain value of density. From a design and management point of view, determining this vegetation density threshold is necessary for a cost effective wetland design.

2.10 Numerical simulations of aspect ratio effects

The impact of aspect ratio on wetland efficiencies was investigated by analyzing four different wetland configurations of 1-hectare area with aspect ratios of 1/1, 1/2, 1/3 and 1/4. It was observed that an evolving wetland shape from a square to a narrow rectangle (i.e. $L/W \geq 1$) led to a better hydraulic performance. As it can be seen from Fig. 2.5.b, Persson hydraulic index (λ_h) for a rectangular-shaped wetland with aspect ratio of 1/4 was approximately 25% larger than a square wetland of same area and same vegetation density. The dimensionless retention time, e_v , experienced a moderate increase of approximately 5% for the same cases.

According to Persson et al (Persson et al., 1999), wetlands with $\lambda_h \leq 0.50$ are wetlands with ineffective hydraulic conditions. Thackston et al. (Thackston et al., 1987) has also categorized wetlands as those with a moderate amount of dead zones ($0.5 \leq e_v \leq 0.75$), and others with large dead areas values below ($e_v \leq 0.5$). Considering the above mentioned evaluation criteria, it can be seen from Fig. 2.5 that low hydraulic performance can result from a poor geometric design and/or sparse vegetation coverage. However, the better efficiencies are achievable by considering proper geometric design criteria and sufficient vegetation densities.

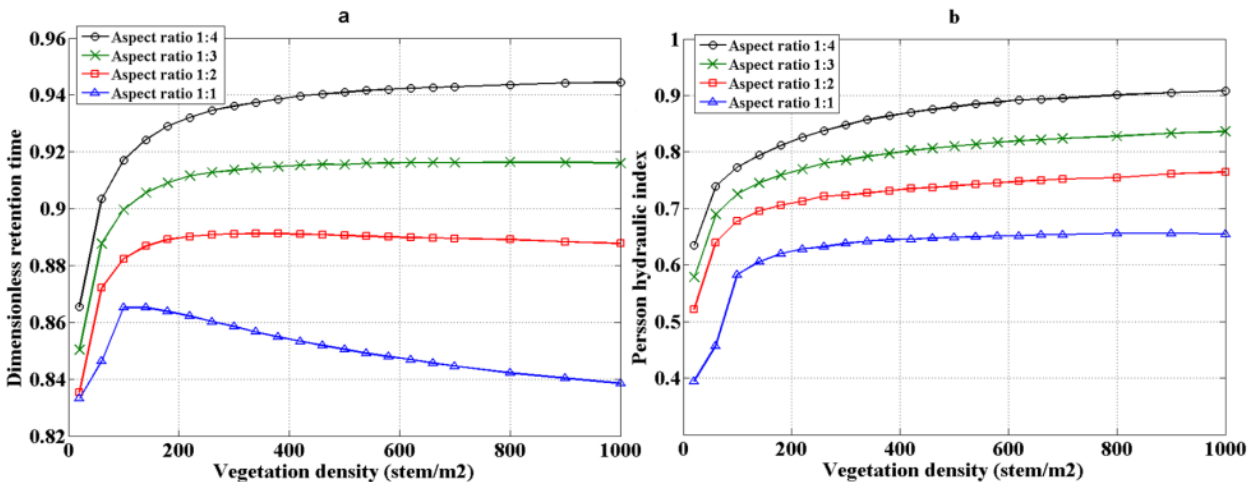


Figure 2.5 Rectangle-shape wetlands efficiency parameters variation for different aspect ratios (a) dimensionless retention time, (e_v), (b) Persson hydraulic index, (λ_h).

These results confirmed the observations by Jadhav & Buchberger (1995) who found that a wetland might exhibit static or dynamic behavior. Under static conditions, the wetland behaves like a pond in which displacement effects caused by submerged plant mass invariably decrease detention times. Under dynamic conditions, stem drag induced by aquatic plants predominates

and wetland detention times increase with vegetation density. It can be seen from Fig. 2.5.a, a square-shaped wetland (i.e. aspect ratio 1/1) behaved statically where the detention time fell after reaching a maximum for vegetation density of 200 stems m^{-2} . Unlike the square-shape wetland, rectangle wetlands showed a proper dynamic behavior. In summary, it can be concluded narrow rectangle-shape wetlands (i.e. $L/W \geq 1$) are more likely to show a dynamic behavior than a square wetland (1/1).

2.11 Wetland aspect ratio and vegetation effect on hydraulic efficiency

Vegetation density variation and aspect ratio changes affect the hydraulic residence time distribution. This means that these factors should be carefully taken into account for wetland design and management. It was observed that the efficiency measure related to retention time, ev , and the measure of mixing, λ_h , improved before reaching a maximum in response to vegetation density increase. The wetland exhibited negligible hydraulic efficiency improvement due to vegetation growth after reaching the threshold value. It can be concluded that vegetation density higher than a certain level might not be necessarily useful. More dense vegetation density gives rise to a slightly elevated retention times in wetlands, whereas it considerably improves mixing efficiency of a wetland. Results showed that as the vegetation density increases, square wetlands experience a decrease of retention time after an initial increase for sparse vegetation covers. The study confirmed some of the results obtained by Persson et al (1999) who observed narrow rectangular wetlands (i.e. $L/W \geq 1$) have a better hydraulic performance than square wetlands. In this paper, the analysis was extended by considering variable vegetation density. Results showed that low coverage of emergent vegetation in combination with aspect ratio causes more dispersion and larger dead zones and consequently lead to poor hydraulic efficiency. The resulting performance was quantified in this study. The analysis of the hydraulic efficiency presented in this chapter was complemented by the analysis of the concentration reduction efficiency, by inclusion of an appropriate uptake function in the solute transport model in Chapter 4. This is left for future work. More complex geometric wetland shapes and heterogeneous vegetation patterns on wetland performance were investigated in Chapters 3 and 5.

Chapter 3

3 Study of the effect of wetland shape and inlet-outlet configuration on wetland performance

3.1 Wetland shape

Wetland shape can significantly affect both dead zones (Kotti et al., 2010) and dispersion (Holland et al., 2004) in wetlands. Thackston (1987) found that distinct dead zones and mixed zones are present in every wetland, and their size and location varies as a function of wetland shape and inlet-outlet positions. Persson (1999) studied 13 rectangular ponds of different aspect ratio (i.e. L/W , length-to-width ratio) and concluded that higher aspect ratios decrease the dead-zone area by as much as 20 %. Sabokrouhiyeh et al. (2016) showed that a low aspect ratio in combination with sparse vegetation coverage causes more dispersion and larger dead zones in rectangular wetlands. Despite the importance of the subject, only a few studies have investigated the effects of wetland shape on the behavior of inert tracers and on the performance of ponds and wetlands for pollutant reduction (Kadlec and Wallace, 2009). Instead, the focus of most published studies has been on the effects on wetlands hydraulics as a function of aspect ratio

(Jenkins and Greenway, 2005; Persson et al., 1999; Su et al., 2009; Thackston et al., 1987). It has been shown that long, narrow wetlands (high aspect ratios) give rise to plug-flow conditions and consequently provide higher hydraulic efficiencies than wider (low aspect ratio) wetlands. However, narrow, long wetlands can produce operational problems associated with high surface water slopes at high hydraulic loading rates (Koskiaho, 2003). For example, Reed et al. (1995) reported that a FWS wetland constructed with aspect ratio of 20/1 experienced overflow due to a dramatic head drop. In addition, construction costs are higher for a narrow wetland, because such a design requires a larger berm length per wetland area (Kadlec and Wallace, 2009). Therefore, there is a need to further investigate other wetland geometries, and other factors, such as inlet-outlet geometry, that may positively impact wetland performance.

3.2 Inlet-outlet configuration

The flow pattern generated by the inlet impacts the distribution of flow within the wetland (Somes et al., 1999). An appropriate design of inlet-outlet configuration increases HRT and enhances the flow uniformity (Persson et al., 1999; Su et al., 2009; Suliman et al., 2006). Su et al. (2009) showed the highest wetland hydraulic performance (greatest pollutant removal) was obtained with a uniform inlet and an outlet located at mid-width. They also found that the use of subsurface berms could be an efficient way to improve the wetland performance. Numerical simulation of a pond with low aspect ratio ($L/W = 2/1$) indicated that changing a single inlet to multiple inlets increased wetland effective volume ratio from 60 to 75 % (Su et al., 2009). For a higher aspect ratio ($L/W = 5/1$), having the outlet placed close to the inlet produced an effective volume ratio of just 40 %, compared to nearly 80 % if the outlet was placed at the opposite end of the pond (Persson et al., 1999). Numerical simulations by Koskiaho (2003) showed that the number of inlets and their position do not significantly affect flow patterns in wetlands of high aspect ratio, but did have an impact for aspect ratios less than 4/1.

3.3 Importance of wetland configuration

The present chapter analyzed the impact of wetland design parameters on wetland efficiency (degree of pollutant removal), considering different wetland shapes, vegetation densities and inlet-outlet configurations. The 2-D depth-averaged model which was already introduced in chapter 2 (section 2.6) was applied to simulate flow hydrodynamics and mass transport. The

objective of the study was to provide quantitative understanding of how different performance metrics are affected by wetland geometry and vegetation density.

3.4 Wetland characteristics and boundary condition

This numerical model study investigated the effects of wetland shape, inlet-outlet configuration, and vegetation density on the hydrodynamics and mass removal capabilities of FWS wetlands. The size of all basins (Fig. 3.1) was set at 1 hectare, and a range of vegetation density was assumed, from non-vegetated to 1000 stems m^{-2} (Kadlec and Wallace, 2009; Serra et al., 2004). Applying the numerical model introduced in chapter 2 (section 2.6), the boundary conditions were defined for Eqs. (2.1)– (2.3), by the inflow at the inlet, 7.7 L/s, and the water depth at the outlet, 0.5 m, producing a nominal hydraulic retention time of $t_n = 7.5$ days. The vegetation drag was described by Eq. (2.6) by assuming that the stem diameter was uniform and equal to $d = 5$ mm, which is a typical assumption for vegetation found in a FWS constructed wetland (Serra et al., 2004).

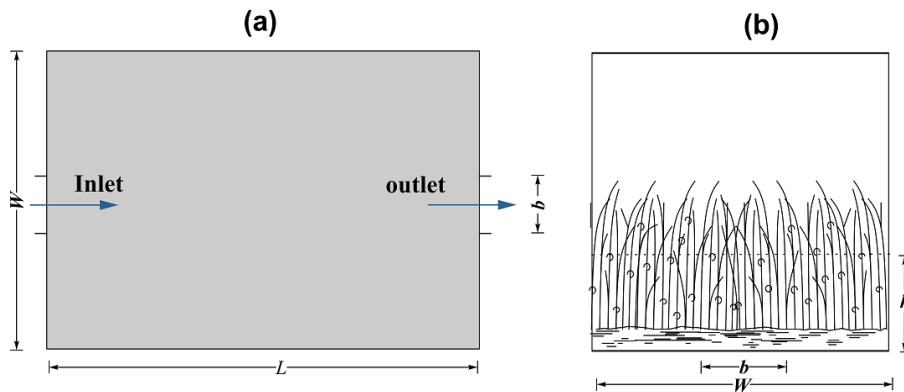


Figure 3.1 Illustration of a rectangular wetland with centrally aligned inlet and outlet and uniform vegetation coverage: (a) plan view, (b) side view.

3.5 Model application

Eight hypothetical wetlands, including four rectangular (R) and four elliptical wetlands (E) of aspect ratios (1/1, 2/1, 3/1, 4/1), were modeled (Table. 3.1). Elliptical wetlands were considered because this geometry is likely to increase the detention time by reducing the area of dead zones at the corners of the wetland, which should reduce the variance and increase the volumetric efficiency (e_v) of the RTD. The flow was modeled for a constant discharge rate through an inlet

of 10 m width and an outlet with 10 m width. Both the inlet and the outlet were centrally located (Fig. 3.1). The effect of inlet-outlet configuration was also examined. In these cases the shape, area and discharge rate were kept constant, and four different inlet-outlet configurations for a rectangular wetland of aspect ratio 4/1, R4, were considered, including a single inlet in the right corner and single central outlet (i.e. case R4-a); a single right corner inlet and the outlet located in left corner (i.e. Case R4-b); a double-inlet wetland (i.e. R4-i2) and a triple-inlet (i.e. R4-i3). The inlet width of 10 m was used for all the cases. The aspect ratio 4/1 complies with common design guidelines which recommend aspect ratios higher than 3/1 (EPA, 2000; Kadlec and Wallace, 2009).

The boundary conditions were defined according to the assumption of an open boundary condition at the inlet-outlet, and a no-flux condition on the remaining part of the flow boundary. Then, the solute transport equations were solved to simulate the varying outlet concentration as a function of time and in response to an instantaneous tracer injection at the inlet, $C = 1 \text{ kg/m}^3$. A finite element method (FEM) using COMSOL Multiphysics® with quadratic shape functions were applied to solve the equations. The computational grid was made of approximately 200,000 triangular elements with a higher spatial resolution around inlet and outlet, with maximum element size of 1 m.

3.6 Results of numerical model

The RTDs (Fig. 3.2) and velocity fields (Fig. 3.3 and 3.5) were generated for all configurations.

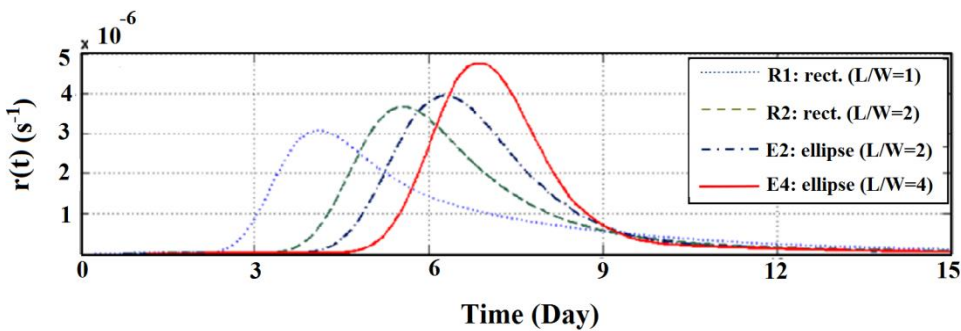
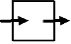
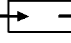
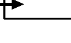



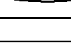
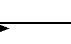
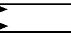
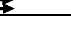




Figure 3.2 Simulated RTDs of wetlands with different aspect ratio and different shape.

Table. 3.1 shows the several parameters derived from the RTDs for each of the simulated wetlands for vegetation coverage 100 stems m^{-2} and inlet width to wetland width ratio of 0.1

($b/W=0.1$). The mean residence time was in the range $t_m = 1.6$ to 6.9 days, which was less than the nominal residence time of 7.5 days. The number of tanks in series, N , for FWS wetlands are generally in the range $0.3 < N < 10.7$ with a mean of $N = 4.1 \pm 0.4$ (Holland et al., 2004; Kadlec and Wallace, 2009). Therefore, the range of $NTIS$ values obtained in this study, $1.2 < N < 11.1$, was representative of FWS wetlands and not unusual for free water surface wetlands.

Table 3.1 Summary of configurations and simulated results for a wetland with nominal residence time $t_n = 7.5$ days and a vegetation coverage of 100 stems m^{-2} .

| Case | Dimension (m × m) | L/W | t_m (day) | σ^2 | e_v | e_d | λ_h | Config. |
|-------|----------------------|-------|-------------|------------|-------|-------|-------------|---|
| R1 | (100 × 100) | 1 | 5.3 | 0.50 | 0.71 | 0.50 | 0.36 |  |
| R2 | (141 × 71) | 2 | 6.1 | 0.24 | 0.82 | 0.76 | 0.62 |  |
| R3 | (173 × 58) | 3 | 6.3 | 0.18 | 0.84 | 0.82 | 0.69 |  |
| R4 | (200 × 50) | 4 | 6.8 | 0.16 | 0.91 | 0.84 | 0.77 |  |
| E1 | (113 × 113) | 1 | 6.1 | 0.34 | 0.81 | 0.66 | 0.53 |  |
| E2 | (160 × 80) | 2 | 6.5 | 0.25 | 0.86 | 0.75 | 0.65 |  |
| E3 | (195 × 65) | 3 | 6.6 | 0.16 | 0.88 | 0.84 | 0.74 |  |
| E4 | (224 × 56) | 4 | 7.1 | 0.09 | 0.95 | 0.91 | 0.86 |  |
| R4-a | | | 5.3 | 0.29 | 0.82 | 0.71 | 0.58 |  |
| R4-b | | | 6.6 | 0.12 | 0.94 | 0.88 | 0.83 |  |
| R4-2i | (200 × 50) | 4 | 6.9 | 0.08 | 0.93 | 0.92 | 0.85 |  |
| R4-3i | | | 7.1 | 0.06 | 0.94 | 0.94 | 0.88 |  |

3.6.1. Wetland Shape simulations

Persson (1999) categorized wetlands into three categories. A wetland with good performance must have hydraulic efficiency $\lambda_h \geq 0.75$, whereas hydraulic efficiencies of $0.50 \leq \lambda_h \leq 0.75$ correspond to satisfactory performance, and $\lambda_h \leq 0.5$ correspond to low performance. First, for both elliptical and rectangular wetland shapes, increasing the aspect ratio (L/W) increased both the volumetric efficiency, e_v , and dispersion index, e_d , indicating improved treatment performance (Table 3.1). This was consistent with previous studies for rectangular wetlands (Jenkins and Greenway, 2005; Persson et al., 1999). For example, for rectangular wetlands with 100 stems m^{-2} e_v and e_d increase by 28% and 68%, respectively, with an increase in aspect ratio from $L/W = 1/1$ to $L/W = 4/1$ (Table 3.1). Likewise, for elliptical wetlands with 100 stems m^{-2} e_v and e_d increased by 17% and 38%, respectively, between $L/W = 1/1$ to $4/1$ (Table 3.1).

Second, for the same area, depth, discharge rate, and aspect ratio elliptical wetlands consistently had better performance than rectangular ones, i.e. produced higher values of e_v , e_d , and λ_h , (Table 3.1). The better performance arose from the difference in flow pattern, as shown in Figure 3.3 Larger dead zones (denoted by black color in Figure 3.3) occurred in the corners of rectangular wetlands than in elliptical ones. The presence of dead zones (regions of zero velocity) meant that some fraction of the wetland was excluded from the main flow path, and consequently the effective wetland area ($A_{effective}$) was reduced, reducing e_v from 1. Shifting from a rectangular to an elliptical shape, the dead zones were replaced by regions of moving fluid, increasing the effective wetland area, which then increased e_v . The difference was largest for the wetlands with the smallest aspect ratio ($L/W = 1/1$), for which e_v increased from 0.71 to 0.81 between a rectangular and elliptical shape. Further, at the inlet the elliptical shape provided a gradual expansion in width, which produced a more uniform cross-sectional velocity profile. This can be seen in the more uniform color of the velocity maps in Figure 3.3. The range of color (black to red) also provided a general picture of the degree of spatial variation in the velocity field. A smaller spatial variation in the velocity field is associated with smaller wetland scale dispersion. Consistent with this, the elliptical wetlands produce higher values of e_d (Table 3.1). Recall from chapter 2 and Eq. (2.18) that $e_d = 1$ for plug-flow, for which there is no dispersion.

The trends were consistent across all stem densities. Specifically, for the same aspect ratio, elliptical wetlands consistently produced higher values of both e_v and e_d (Figure 3.4).

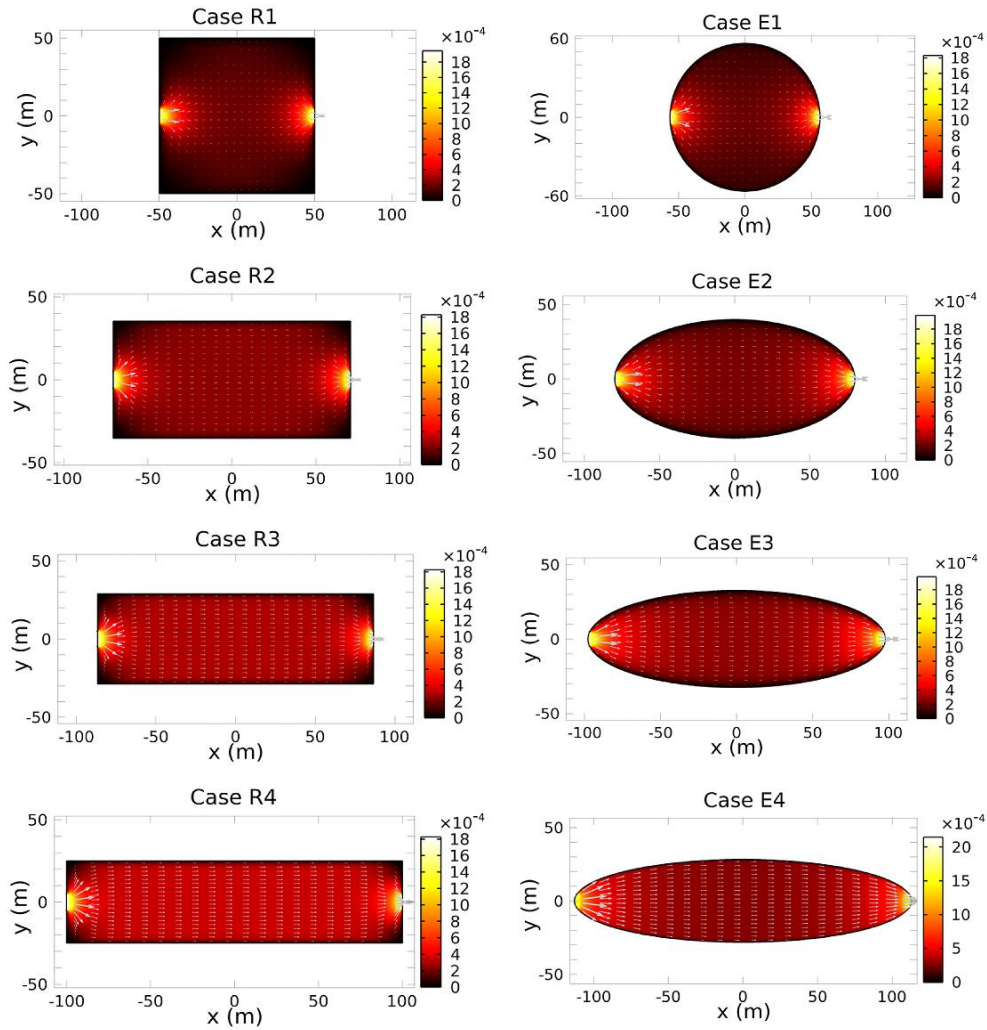


Figure 3.3 Simulated velocity fields for different wetland shapes of 1 ha area and a centrally aligned inlet-outlet of 10 m width and 100 stems m^{-2} vegetation density.

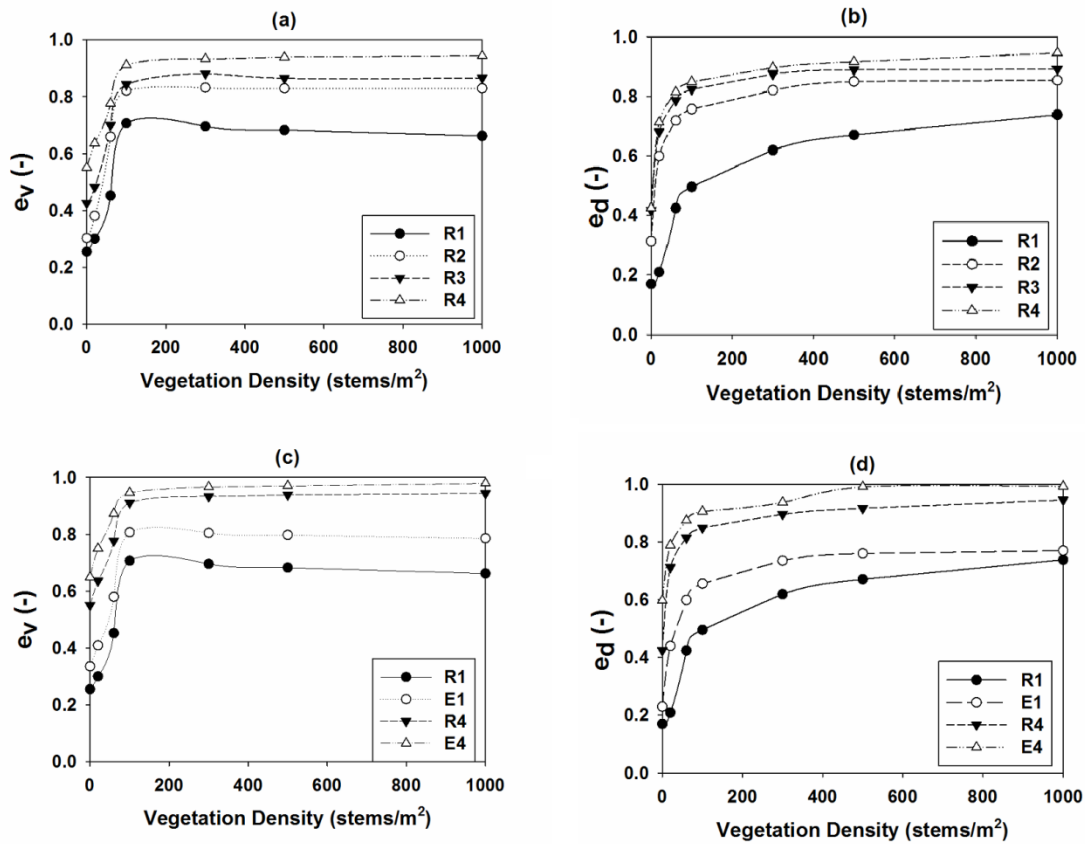


Figure 3.4 The effect of (a), (c) aspect ratio and (b), (d) wetland shape on volumetric and dispersion efficiency of wetlands with different vegetation density.

The simulation results revealed an interesting threshold behavior with regard to stem density (Figure 3.4). A change in wetland vegetation density between zero and 150 stems m^{-2} was associated with a significant increase in volumetric efficiency, e_v (Figure 3.4a and 3.4c), but further increasing stem density provided little additional improvement. A similar threshold was observed for dispersion efficiency, e_d , but occurred at a slightly higher stem density, 300 stems m^{-2} (Figure 3.4b and 3.4d). The same threshold (300 stems m^{-2}) was also observed in the overall hydraulic efficiency parameter, λ_h (Figure 3.5). The presence of this threshold has important implications for predictive modeling, because it suggests that knowledge of the exact stem density may not be necessary. As long as the stem density is above 300 stems m^{-2} , which is typical of treatment wetlands (Serra et al., 2004), predictions will not be sensitive to the exact value of stem density selected, which simplifies the parameterization of models.

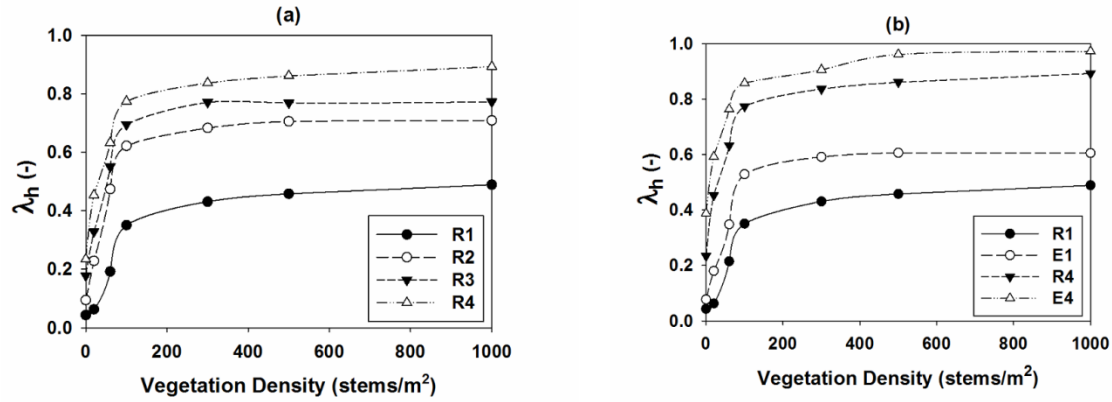


Figure 3.5 The effect of (a) aspect ratio and (b) shape variation on hydraulic efficiency of wetlands with different vegetation density.

3.6.2 Inlet-outlet configuration and size

Modification of the inlet-outlet position and size affected the flow distribution within the wetland systems (Figure 3.6). First, consider the cases for which the inlet width (b) to wetland width (W) ratio was $b/W = 0.1$. An asymmetric alignment of inlet and outlet, case R4-a (Fig. 3.6a), produced a larger dead-zone away from the inlet-outlet couple (lower left corner in Figure 3.6a), compared to a symmetric inlet-outlet, R4 (Fig. 3.3). The larger dead-zone reduced the effective volume of wetland, which resulted in a lower value of volumetric efficiency, e_v . Specifically, e_v dropped from 0.91 for the symmetric case R4 to 0.82 for the asymmetric case R4-a (Fig. 3.7.a, 3.7.b). On the other hand, moving the inlet and outlet to opposite corners, case R4-b, improved the volumetric efficiency, relative to the symmetric base case R4. In fact, the opposite corner configuration produced the highest volumetric efficiency of $e_v = 0.94$ (Fig 3.6.b, Fig. 3.7.a). Similarly, the opposite corner configuration (R4-b) also produced the highest value of $e_d = 0.88$, compared to 0.84 for the symmetric base case R4 and $e_d = 0.71$ for the asymmetric case R4-a, indicating that the opposite corner inlet-outlet configuration produced the least dispersion (Fig. 3.7.a, 3.7.b). Consistent with this, the opposite corner configuration also produced the highest hydraulic efficiency, with $\lambda_h = 0.83$, compared to 0.77 for the symmetric base case (R4) and just 0.58 for the asymmetric case R4-a. Finally, for each inlet-outlet configuration the ratio between the inlet width (b) and the wetland width (W) was varied between 0.1 to 1 (Fig. 3.7). As b/W increased, cases R4 and R4-a experienced a consistent increase in e_v and e_d from 0.82 and 0.98

and 0.71 and 0.97, respectively (Fig. 3.7). However, for the opposite corner case R4-b the variation of the inlet width had little impact on the efficiency parameters (Fig. 3.7).

The use of multiple inlets improved all of the efficiency metrics (e_v , e_d , λ_h). The velocity field showed that the area of dead zone (black areas) was diminished in the both the double-inlet (case R4-2i, Fig 3.6.c) and the triple inlet (case R4-3i, Fig. 3.6.d) systems, compared to the symmetric, single-inlet reference wetland (case R4, Fig. 3.3). In addition, multiple inlets (Figure 3.6c, 3.6d) produced a more uniform velocity field (more uniform color in Figure 3.6), compared to the single inlet case R4 (Fig. 3.3).

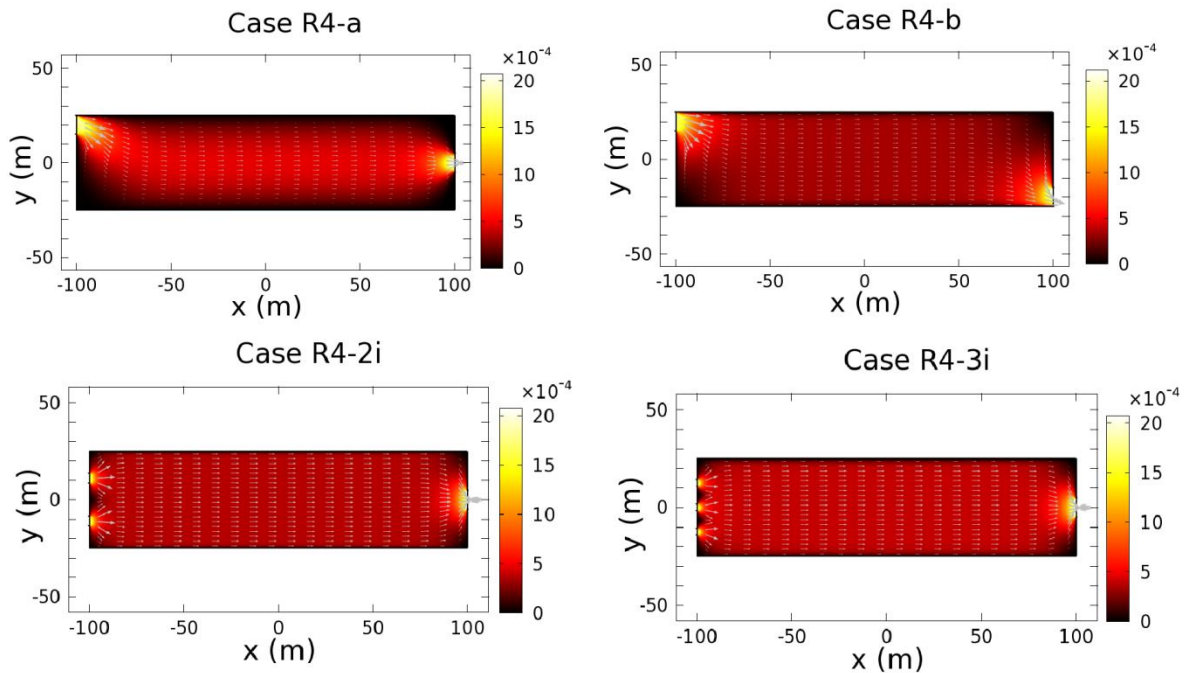


Figure 3.6 Simulated velocity fields for different inlet and outlet configurations for a rectangular wetland with 100 stems m^{-2} vegetation density and an outlet of 10 m width: (a) Case R4-a, left inlet of 10 m width and central outlet ($b/W=0.1$); (b) Case R4-b, a left inlet of 10 m width and right outlet ; (c) Case R4-2i, double inlet of 5 m width; (d) Case R4-3i, triple inlet of 3.33 m width. Black regions represent dead zones, i.e. regions of zero velocity.

The presence of multiple inlets significantly changed the values of retention time and RTD variance (Table 3.1). For $b/W = 0.1$, the velocity field became more uniform as the number of inlets increased (see Figure 3.6), which resulted in lower RTD variance (smaller σ_θ), and thus high values of the dispersion parameter e_d . Specifically, e_d , was 0.84 for a single-inlet (Case R4),

0.92 for a double-inlet (Case R4-2i) and 0.94 for a triple-inlet (Case R4-3i) (Fig. 3.7d). The use of multiple inlets also decreased dead-zone area, which increased the values of volumetric efficiency, e_v , from 0.91 for R4 to 0.93 for R4-2i and changed to 0.94 for R4-3i (Fig. 3.7c).

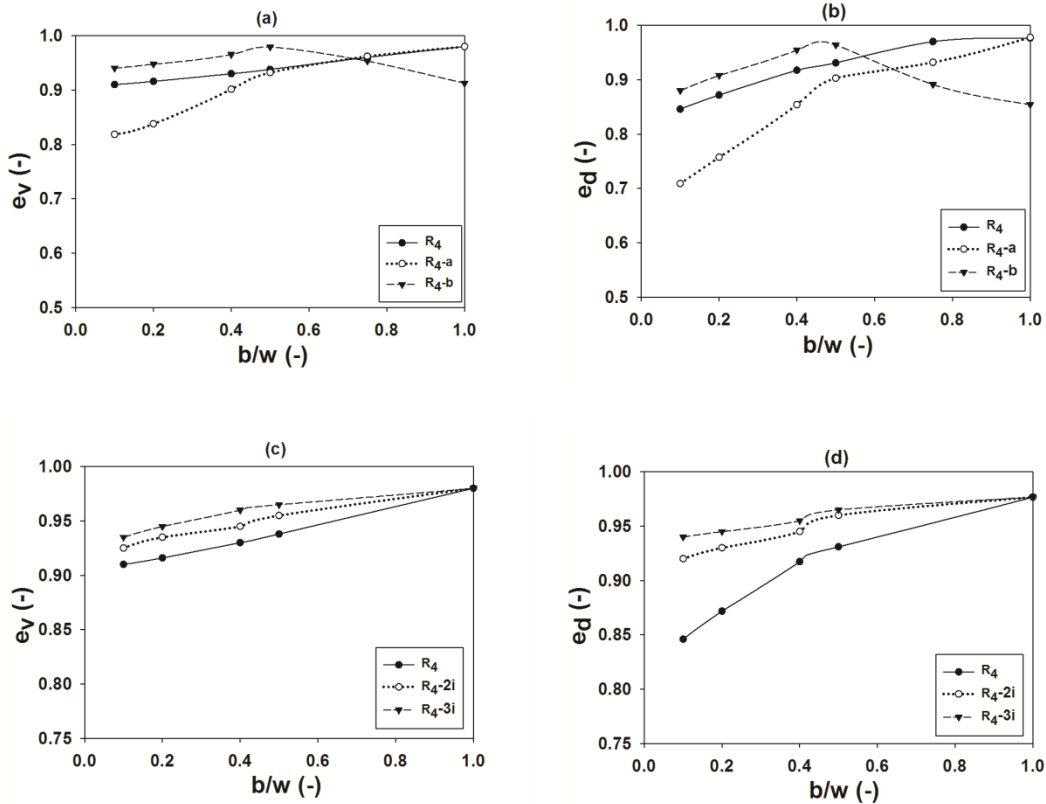


Figure 3.7 Effect of (a), (c) inlet-outlet position and (b), (d) number of inlets on volumetric and dispersion efficiency of rectangular wetlands of aspect ratio 4/1 with 100 stems m^{-2} vegetation coverage and different inlet width.

The use of a double inlet (R4-2i) also improved the hydraulic efficiency (λ_h) by 8%, relative to the base case with a single inlet R4 (Figure 3.8). However, increasing to a third inlet (case R4-3i), did not produce further improvement (Figure 3.8). The primary advantage of widening the inlet or using multiple inlets was to create a more uniform velocity field with smaller dead-zone area. Therefore, as the inlet width increased (increasing b/W), the added benefit of multiple inlets diminished, and the efficiency parameters converge to a single value for $b/W = 1$ (Figure 3.8).

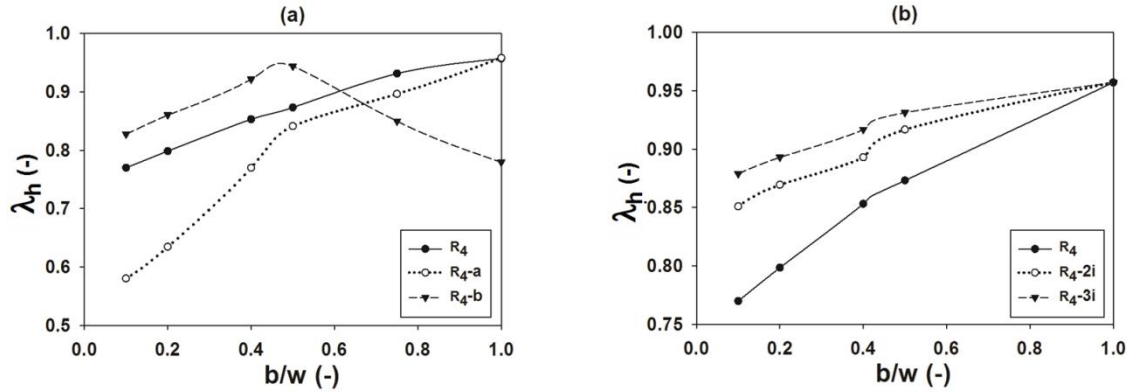


Figure 3.8 Effect of wetland (a) inlet-outlet position and (b) number of inlets on hydraulic efficiency of rectangular wetlands of aspect ratio 4/1 with 100 stems m^{-2} vegetation density and different inlet width.

3.7 Shape and inlet-outlet effect on hydraulic efficiency

This study showed that performance of a wetland can be improved by appropriately designing wetland shape, aspect ratio and inlet-outlet configuration. Ellipse-shaped wetlands yielded higher detention time (higher e_v) and less dispersion (higher e_d) compared to rectangular wetlands with similar characteristics. Unlike a rectangular wetland, in which prominent dead-zones formed in each corner of the wetland, an elliptical wetland produced a more uniform velocity distribution with fewer (or no) dead zones, increasing e_v , reducing RTD variance and thus increase the dispersion efficiency e_d . The reduction in dead-zone size and the more uniform velocity field of the elliptical wetland implies performance greater potential for pollutant removal.

Higher vegetation density was associated with lower variances in the RTD and larger NTIS. However, above a threshold stem density of about 300 stems m^{-2} , the dispersion efficiency (e_d), and volumetric efficiency (e_v) remained almost constant, i.e. increasing vegetation density further did not significantly improve these efficiency metrics. From a design and management point of view, determining this threshold vegetation density can be useful for a cost-effective wetland design and operation.

Both parameters related to volumetric retention time and dispersion rate, e_v and e_d , can also be improved by adjusting the inlet-outlet configuration. The minimum dead zone area (greatest effective area) and the lowest dispersion were achieved with the opposite corner-to-corner inlet-outlet configuration, which produced the maximum values of e_v and e_d , respectively (Figure 3.7).

On the other hand, an asymmetric inlet-outlet layout with the inlet at a corner and a centrally aligned outlet produced the lowest hydraulic efficiency. This is due to the fact that the flow can pass from the inlet to the outlet without entering the opposite side of the wetland volume, such that a large fraction of the wetland volume is excluded from the circulation. Finally, using multiple inlets and increasing the inlet to wetland width ratio (b/W) both improved the hydraulic efficiency by reducing dead zone area and producing a more uniform velocity field within the wetland.

Chapter 4

4 Assessment of the nutrient removal effectiveness of free water surface wetlands with different configurations

4.1 Nitrogen removal

The nitrogen removal processes in FWS wetlands, which represent the purification capacity, are well known from a chemical point of view; however, there is a further need to study their nature and their close interconnection with flow hydrodynamics (Marion et al., 2014; Somes et al., 1999). The two main mechanisms which can be attributed to the self-purification capacity of a wet area are the separation of the solid phase from the liquid and the transformation of the substances present in the water. Here the important processes that determine the removal of the nitrogen is explained.

The most common forms of nitrogen compounds present in FWS wetlands are nitrate, nitrite, ammonia and organic nitrogen. All mentioned forms, including gas nitrogen, are biochemically interconnected and they circulate within the nitrogen cycle. The nitrogen as nitrate and also as

ammonia is a common form of pollutant produced in the form of industrial, agricultural and domestic wastewater (Hsueh et al., 2014; Kotti et al., 2010). Nitrogen presence in the waters, mostly due to the use of fertilizers and the oxidation of organic forms and ammonia contained in wastewaters, is one of the main causes of eutrophication (Martín et al., 2013). Nitrogen can be removed both through chemical and biochemical reactions, forming together the nitrogen cycle, and also through physical separation (Arheimer and Wittgren, 1994; Yang and Tsai, 2011). Physical separation requires the same considerations made for suspended solids including flocculation, sedimentation and filtration. Providing a set of effective biological-chemical processes, FWS wetlands has shown a good capacity in treating nitrogen compounds (Fig. 4.1).

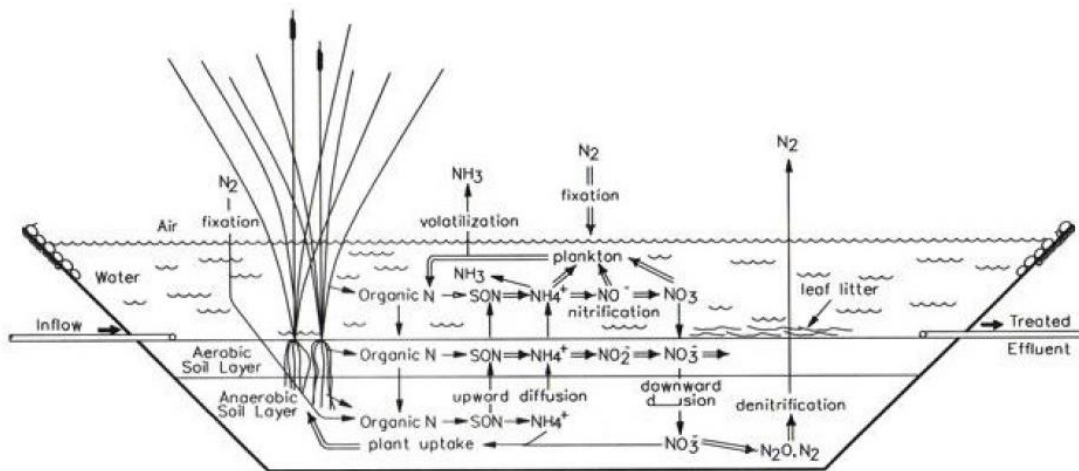


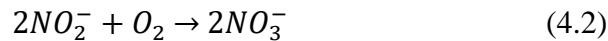
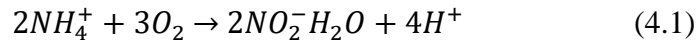
Figure 4.1 Biological-chemical processes involved in nitrogen removal present in FWS wetlands

The vegetation acts as a temporary storage zone, where nitrogen compounds are exposed to the treatment reactions. Such reactions occur by the process of assimilation which allows the use of inorganic nitrogen compounds for the synthesis of organic macromolecules that involves the plant biomass.

The emerging macrophytes and, in less amount the submerged vegetation assimilate the mineral nutrients in dissolved form through the roots located in the sediment, whereas, phytoplankton and floating macrophytes assimilate the nutrients dissolved in the water column.

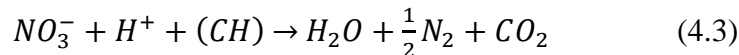
The organic matter resulting from the death of the organisms and from the settlement of suspended solids, is decomposed with the release of organic nitrogen, usually in a dissolved form

(urea, amino acids, proteins). The mineralization is the process, in which an organic form of nitrogen compound transforms to an inorganic ammonium ion (NH_4^+). This process is mainly dependent on the temperature variation, and can take place under both anaerobic and aerobic conditions. The mineralized nitrogen in the soil can be taken up by plant roots, circulating into the aqueous phase, or it can be directly the subject of other biochemical transformations. It is likely that the ammonium ion may participate in the ion exchange in the presence of clay, combined to sedimentation processes (by diffusion or decomposition of organic matter). It should be noted that, this exchange capacity is a short-term potential, because it is subjected to saturation. The nitrification of (NH_4^+) occurs in an aerobic environment. The process involves the transformation of ammonium ion (NH_4^+) into nitrate (NO_3^-), which is likely to take place in presence of microbial species (i.e. Nitrosomonas and Nitrobacter). The mentioned process can be represented by the following two chemical reactions:



Speed of redox reaction (4.1), (4.2) depends mainly on temperature and also on redox potential and pH of environment. In addition, the presence of oxygen is necessary for the reaction, and therefore, they are more likely to take place in the aqueous phase by the microbial film attached on the vegetation. The other suitable environments for reactions are in the oxidized layer of the sediment in contact with water, and oxidizing environment created by plants marsh around their roots and aerobic micro-climates created by bioturbation.

An intermediate product of nitrification is nitrite (NO_2^-), which is generally found in very low concentrations, because its oxidation is much faster than production rate. The produced nitrate may have different fates. In the soil profiles, it may be absorbed by plants through their roots, or it may be reduced under anaerobic conditions, it may also be denitrified by facultative anaerobic bacteria, which use the nitrate instead of oxygen as electron acceptor in the respiration process. The stoichiometry of denitrification process can be represented as:



The denitrification returns molecular nitrogen in gas form which return to the atmosphere, passing through the sediment and plant tissues. A beneficial aspect of this process is the transfer of nitrogen from the aqueous interface to the atmosphere, which represents an environment-friendly type of removal in water treatment processes (Kadlec and Wallace, 2009).

Denitrification becomes a significant process, due to the presence of aerobic micro-zones, which are necessary for the synthesis of nitrate, surrounded by anaerobic environments. It should be noted that, denitrification requires an oxidized form of nitrogen and an anaerobic environment; which are two conflicting conditions. Area surrounding the roots (rhizosphere) of typical wetland plants represents a suitable environment for denitrification, where aerobic and anaerobic conditions are found simultaneously. Such an area is characterized with anaerobic sediment system and transferred oxygen from the air to the sediment through the root systems. Similar conditions are also present in the sediment-water or more generally in biofilm-water surface. Many processes of assimilation and denitrification can occur in the water column by phytoplankton communities and bacteria in the biofilm (Duff and Triska, 1990; Thullen et al., 2005).

The denitrification reaction requires a source of organic carbon, which in some cases can be a limiting factor. While the limitation by nitrate almost never occurs, due to the type of water which has to be treated, that is generally rich in this compound, the limitation of carbon in a wetland can be a limiting factor, impeding the process.

Other processes involving nitrogen within FWS wetlands are the volatilization of ammonia and the nitrogen fixation. Volatilization of ammonia is the process, in which (NH_3) goes into the gas phase and it is released in the atmosphere. The process is more likely to occur in high pH environment and high temperature. Moreover, the occurrence of Volatilization of ammonia might be more likely in warm seasons, when the photosynthetic production can induce high pH (Hammer and Knight, 1994). Whereas, fixation of atmospheric nitrogen is a process allows chemical-biological organisms to use it as a nutrient for their growth.

4.2 Contaminant removal efficiency in connection to design parameters

In this chapter, the performance of FWS wetlands in contaminant removal was quantified as a link to hydraulic efficiency index representing the combined effect of detention time and degree

of mixing. The two-dimensional numerical model (introduced in Chapter 2) was used to simulate the velocity field and the mass transport processes in hypothetical rectangular wetlands with different aspect ratio and variable vegetation density. The results were coupled with a calibrated concentration removal model to obtain the removal efficiency of nitrogen (N). The aim of this chapter is to study the contaminate removal efficiency of FWS wetlands in connection with wetland vegetation and wetland shape.

4.3 Model application

The numerical model introduced in chapter 2 (section 2.6) was applied to study the effects of wetland aspect ratio on the nitrogen removal rates in FWS wetlands. Therefore, Four rectangular wetlands (Cases, R1, R2, R3, R4) of the same properties, but different aspect ratios were selected. The properties of the mentioned wetlands are mentioned in Table 3.1. The boundary condition for the wetlands were set the same as values in section 3.4. In addition, the values of transverse diffusivity, E_T , and longitudinal dispersion coefficient, E_L , and Manning coefficient (M), were chosen according to the validated model (section 3.4). The size of all basins (i.e. R1, R2, R3, R4) (Fig. 3.3) was set at 1 hectare, and a range of vegetation density was assumed, from non-vegetated to 1000 stems m^{-2} . The boundary conditions were defined for equations. (2.1)–(2.3), by the inflow at the inlet, approximately 7.7 L/s, and the water depth at the outlet, 0.5 m, producing a nominal hydraulic retention time of $t_n = 7.5$ days. The vegetation shear stresses were determined by equation (2.6) by assuming that the stem diameter was uniform and equal to $d = 5$ mm. The results obtained from the 2-dimensional depth averaged model were combined with a nitrogen removal model (section 4.5)

4.4 nitrogen removal model

Applying tanks-in-series (TIS) model and assuming a series of continuously stirred tank reactors (CSTRs) in a wetland system can be used to describe removal of soluble pollutants, e.g., Nitrogen. Under such an assumption a substance is removed in each tank according to first-order kinetics. Arheimer & Wittgren (2002) described Nitrogen removal as an area-based and temperature-dependent process. Eq. (4.4) derived from a simple and robust first-order model, which was modified and evaluated against data from eight monitored surface-flow wetlands.

Such a model yields a solute pollutant removal model which is dependent on both degree of mixing, N , and volumetric efficiency of the wetlands, e_V (Persson, 2003).

$$\frac{C_e}{C_i} = \left(\frac{1}{1 + \left(\frac{A_{\text{effective}} K_{aT}}{QN} \right)} \right)^N = \left(\frac{1}{1 + \left(\frac{e_V A_{\text{total}} K_{aT}}{QN} \right)} \right)^N \quad (4.4)$$

Where C_e is the effluent Nitrogen concentration (mg/L), C_i the influent Nitrogen concentration (mg/L), $A_{\text{effective}}$ the active area of wetland (m^2), Q discharge rate (m^3/s), and K_{aT} is the area-based temperature-dependent removal rate constant. The temperature dependence of removal constant is described by Eq. 4.5.

$$K_{aT} = K_a T \quad (4.5)$$

Where K_a is defined as area-based removal rate constant ($\text{m s}^{-1} \text{ } ^\circ\text{C}^{-1}$); and T is average water temperature ($^\circ\text{C}$). The Nitrogen removal model has previously been calibrated for the four wetlands and was applied to study four wetlands situated in south of Sweden and was used to estimate potential catchment-scale wetland removal of a River. The wetlands were then calibrated simultaneously to yield the removal rate coefficient of $ka=0.0023$ ($\text{m s}^{-1} \text{ } ^\circ\text{C}^{-1}$) (Arheimer and Wittgren, 1994). In addition, the validity of ka -values has been shown by individual calibration against data from eight surface-flow wetlands (Arheimer and Wittgren, 2002).

4.5 Nitrogen removal and hydraulic efficiency

The simulated modeled velocity field (Fig. 3.3) and transport of a continuously injected tracer, were used to generate hydraulic efficiency indexes. Applying tanks-in-series (TIS) model and assuming a series of continuously stirred tank reactors (CSTRs) in a wetland system was used to describe removal of a soluble pollutants (i.e. Nitrogen) by applying Eq. 4.5 in $T=20$ ($^\circ\text{C}^{-1}$). Under such an assumption a substance is removed in each tank according to first-order kinetics. Hydraulic efficiency indexes were derived by analysis of RTDs. The summary of wetland configurations and hydraulic efficiency indexes of vegetation coverage 100 stems m^{-2} is given in Table 4.1.

Table 4.1. Summary of configurations and simulated results for vegetation coverage 100 stems m⁻²

| Case | L/W | Dimensions | e_v | e_d | λ_h | C_{out}/C_{in} |
|------|-------|------------|-------|-------|-------------|------------------|
| R1 | 1 | (100×100) | 0.71 | 0.50 | 0.36 | 0.32 |
| R2 | 2 | (141 × 71) | 0.82 | 0.76 | 0.62 | 0.35 |
| R3 | 3 | (173 × 58) | 0.84 | 0.82 | 0.69 | 0.38 |
| R4 | 4 | (200 × 50) | 0.91 | 0.84 | 0.77 | 0.47 |

The numerical experiments demonstrated that increasing the aspect ratio of the wetland leads to an increase in both volumetric efficiency, e_v , and dispersion index, e_d , indicating improved treatment performance. For example, e_v and e_d increase by approximately 20% and 35%, respectively, with an increase in aspect ratio from $L/W = 1/1$ to $L/W = 4/1$ for vegetation density of 100 stems m⁻² (Table 4.1, Fig. 3.4.a, b).

It can be seen from velocity field simulations (Fig. 3.3) and the derived efficiency results (Fig. 3.4.a, b) that a narrow wetland with a higher aspect ratio had better performance than a wide wetland. The results also showed a threshold behavior with regard to stem density (Fig. 3.4). Volumetric efficiency, e_v , increased significantly when wetland vegetation density changed between zero and 150 stems m⁻² (Fig. 3.4.a), but further increasing stem density caused a negligible additional improvement. The threshold was also observed in the dispersion efficiency, e_d , but occurred at a slightly higher stem density, 300 stems m⁻² (Fig. 3.4.b). Hydraulic efficiency index, combination of retention time measure and dispersion index, (Fig. 4.2.a) and the results of Nitrogen removal model (Fig. 4.2.b) approve the better performance of wetlands with higher aspect ratio. Hydraulic efficiency, λ_h , increased approximately 35%, for a high aspect ratio rectangular wetland (i.e. $L/W=4/1$) compared to a square shape (i.e. $L/W=1/1$). This increase was associated to an approximately 20% improvement in Nitrogen removal. Above the threshold vegetation density, in this case 300 stems m⁻², changes in nutrient removal were not significant and suggested negligible improvement in efficiency factors.

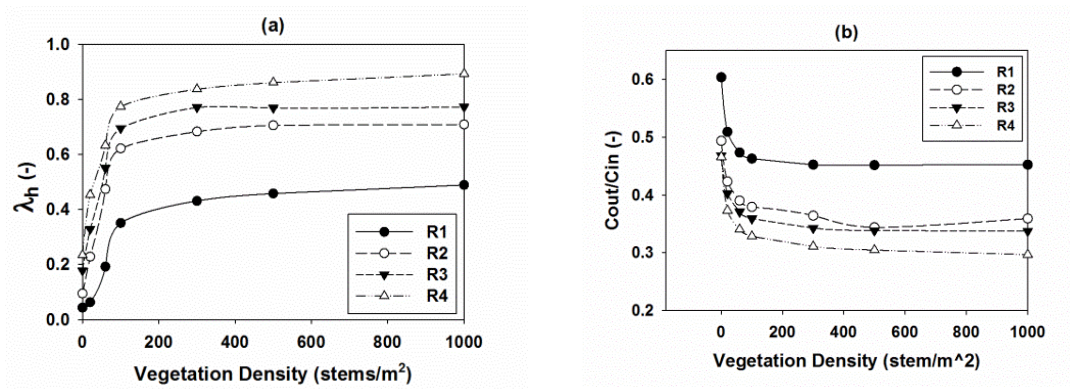


Figure 4.2.a Hydraulic efficiency and 4.2.b Nitrogen removal rate variation for wetland aspect ratios.

The results also showed nitrogen removal rate can be increased approximately 15 percent for a very dense vegetation density, whereas approximately 30 percent improvement in Nitrogen removal is achieved as a result of applying a high aspect ratio wetland compared to a lower aspect ratio case with the same characteristics. This means that these factors should be carefully taken into account for wetland design and management.

Chapter 5

5 Contaminant removal efficiency as a function of vegetation distribution in free water surface wetlands

5.1 Heterogeneity of vegetation patterns

Pollutant reduction in a treatment wetland is significantly influenced by vegetation density (Sabokrouhiyeh et al., 2017; Vymazal, 2013) and the spatial layout of vegetation (Jenkins and Greenway, 2005; Musner et al., 2014), because these parameters control (1) the residence time (Carleton et al., 2001; Jadhav and Buchberger, 1995) and (2) the level of mixing and recirculation in a wetland (Holland et al., 2004; Persson et al., 1999). The residence time and level of mixing control the contact time between contaminants and aquatic vegetation (Harvey et al., 2005), and thereby determine the treatment efficiency of a wetland. Generally, increased flow resistance results in a decrease in mean velocity and longer retention times, which are necessary for biological chemical reactions (Kadlec and Wallace, 2009; Sabokrouhiyeh et al., 2016). In addition, spatial heterogeneity in stem density can alter the flow distribution. Ideally, for optimum performance the flow distribution approach plug flow. In a plug flow, the flow is uniformly distributed and there is no dispersion, so that all the water parcels entering the wetland remain a time equal to the nominal residence time (t_n). (Lightbody et al., 2009; Thackston et al., 1987). However, perfect plug flow is never achieved in a wetland, and the spatial variations in the velocity produce a distribution of residence time that degrades the wetland performance

relative to plug flow. Heterogeneous velocity fields can result from the variation of vegetation density over the water depth, patches of dense and sparse vegetation, and non-vegetated channels (Lightbody and Nepf, 2006). For example, Nungesser and Chimney (2006) noted that large interspersed patches of submerged aquatic vegetation and emergent cattail stands altered the flow paths through a wetland in the Everglades Nutrient Removal Project.

Many natural wetlands are characterized by patches of different vegetation type and density (Cheng et al., 2011; Marani et al., 2006). The heterogeneity of vegetation patterns can create preferential paths of low resistance (Fig. 5.1), allowing a significant portion of flow to reach the outlet much faster than the nominal hydraulic residence time. This phenomenon is known as short-circuiting (Thackston et al., 1987) and is known to significantly reduce the treatment performance of a wetland (Kadlec and Wallace, 2009; Lightbody et al., 2007; Zheng et al., 2015). For example, aerial photographs and internal concentration measurements of the Everglades system (Dierberg et al., 2005) revealed 1.2-m-deep ditches oriented parallel to the main flow direction constituted only 8% of the surface area of the wetland but allowed 44% of the volumetric discharge to flow out of the wetland with only partial removal of total phosphorus (TP).

Jenkins and Greenways (2005) developed a numerical model to study the effect of fringing and banded vegetation patterns on the residence time and degree of mixing in a wetland, and found that the layout of wetland vegetation had a significant impact on the hydraulic efficiency of the wetland system. Musner et al. (2014) studied a conceptual wetland characterized by a main flow channel and adjacent vegetated zones. They reported that increasing vegetation density produced an increasingly pronounced bimodality of the RTD, reflecting the partition of the flow between the main channel and the lateral vegetated zones. Savickis et al. (2016) analyzed the effect of a meandering channel in a vegetated wetland with flat topography, and found that the hydraulic efficiency increased with the sinuosity of the channel. Sabokrouhiyeh et al (2017) studied uniformly vegetated wetlands of different shapes and vegetation density and observed a threshold behavior with regard to stem density, where further increasing stem density provided little additional improvement in pollutant removal efficiency indexes related to volumetric retention time and dispersion rate.

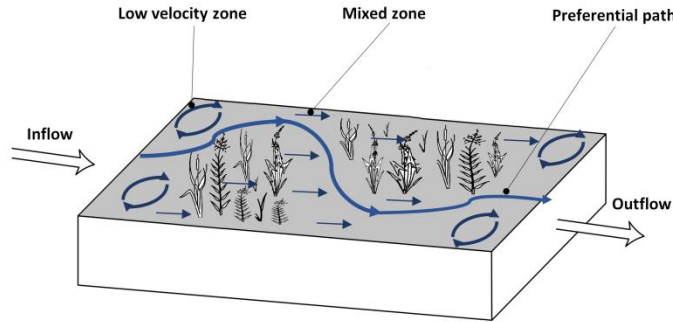


Figure 5.1. Schematics of flow patterns in a free water surface wetland with non-uniform vegetation distribution. Such a system can create preferential flow paths and short-circuiting, which allow a significant fraction of solute to reach the outlet before adequate treatment has been achieved. Low velocity zones may also occur with minimal contribution to the treatment process.

Several wetland studies have also reported the presence of vegetation bands perpendicular to the prevailing flow direction (Jenkins and Greenway, 2005; Rietkerk et al., 2004; Swanson and Grigal, 1988). The formation of these bands is explained by three different mechanisms, including peat accumulation (Hilbert et al., 2000), water ponding (Couwenberg and Joosten, 2005) and nutrient accumulation (Rietkerk et al., 2004). Cheng et al. (2011) developed an advection-reaction-diffusion model to investigate the effect of topography and vegetation self-organization on vegetation patterns and concluded, when the advection of water and nutrients along the longitudinal axis (i.e. flow direction) is much higher than the advection of water and nutrients induced by topography or transpiring vegetation in the lateral direction, biomass then grows laterally toward zones of relatively higher nutrients, and therefore, perpendicular vegetation bands form. Thullen et al. (2005) suggested that an effective tool to manage and sustain healthy vegetation is the use of hummocks, i.e. shallow planting beds perpendicular to flow. Using tracer studies, Keefe et al. (2010) showed that the incorporation of hummocks enhanced the hydraulic performance of the Tres Rios Wastewater Treatment Constructed Wetlands near Phoenix, AZ; however, the results were limited to the seasonal variation of stem density in a single wetland case study, and it did not investigate a wide parameter space. Jenkins and Greenways (2005) applied a numerical model to study the effect of hypothetical oriented vegetation patterns on retention time and mixing levels of wetlands. However, the prediction of wetland processes remains a significant challenge, in part because the link between wetland hydrodynamics and biochemical processes is poorly understood (Marion et al., 2014). Simplified modeling approaches such as the tanks-in-series (TIS) model have been widely used in the predictive evaluation of wetland performance. However, in most cases their applicability is

limited by the simplifying assumption of complete mixing within each tank (Kadlec and Wallace, 2009) or negligible transverse diffusion (Carleton and Montas, 2010). Therefore, there is a need for more sophisticated numerical wetland models (e.g. models with spatially distributed parameterization) that can produce more realistic circulation patterns that account for vegetation density and spatial heterogeneity.

5.2 Vegetation distribution effect

In this chapter, the two-dimensional depth-averaged hydrodynamic and solute transport model, introduced in Chapter 2 (section 2.6), was validated against survey data, and used to investigate the effect of heterogeneous vegetation patterns on the treatment performance of a wetland. The model applied recently developed parameterizations for mixing within emergent vegetation (Lightbody and Nepf, 2006; Nepf, 1999). In the simulations, the spatial vegetation distribution was represented as a 2-D random field of vegetation stem density characterized by the statistical properties of mean, variance and correlation length in the two spatial directions. The resulting concentration reduction and mass removal efficiencies were analyzed as a function of the statistical parameters of the random vegetation fields. We attempted to explain how velocity heterogeneity, and short circuiting in particular reduce treatment capabilities of wetlands. The research was also used to identify an efficient vegetation pattern by investigating pollutant removal capabilities of main vegetation patterns that occur in natural wetlands. Such a pattern, mimicking natural wetlands, can be utilized in constructed wetlands. The goal of this work was to provide insight into how spatial heterogeneity in the vegetation impacts wetland performance. Such an understanding can help wetland designers to achieve solutions that are more efficient and cost-effective.

5.3 Spatial vegetation patterns

A number of conceptual models have been proposed to simulate vegetation distribution patterns in wetland ecosystems (Cheng et al., 2011; Larsen and Harvey, 2011; Swanson and Grigal, 1988). It is well-recognized that wetland vegetation is often characterized by three main patterns (Cheng et al., 2011; Jenkins and Greenway, 2005; Musner et al., 2014); (1) dotted patterns consisting of emergent vegetation patches on flat ground, (2) vegetation bands parallel to the prevailing flow direction, and (3) vegetation bands perpendicular to the prevailing flow direction.

In the absence of anisotropy, e.g. on relatively flat ground, when the advection of water and dissolved nutrients towards the vegetation (local advection) is greater than regional advection in the direction of the gradient, the nutrients released from the turnover of vegetation is retained locally for growth, allowing producing a dotted pattern. On the other hand, when there is a large regional hydraulic gradient, vegetation patches aggregate and elongate in the direction of the downhill flow, promoting the formation of vegetated bands oriented parallel to the flow direction (Cheng et al., 2011; Ellery et al., 2003). Under moderate hydraulic gradients, and when the effect of lateral diffusion becomes important, fluxes of water and dissolved nutrients flow in the direction perpendicular of the flow, leading to the formation of vegetation bands perpendicular to the flow (Eppinga et al., 2009).

A pseudo-random correlated field generator based on a Gaussian Markov random field approach (Bellin and Rubin, 1996; Elliott and Aggoun, 1996; Mardia, 1988) was used to mimic spatial vegetation patterns. This generator uses an approximation of a field with an exponential covariance. For a two-dimensional domain $D \subset \mathbb{R}^2$, a random field, $\{Z(x): x \in D\}$, was defined with mean \bar{x} and an exponential covariance $Cov(x, y)$ associated with probability space $(\Omega, \mathcal{F}, \mathcal{P})$, in which Ω is a sample space with a set of possible outcomes, \mathcal{F} set of events, and \mathcal{P} a function from events to probabilities. The covariance is expressed as:

$$Cov(x, y) = \sigma^2 \exp\left(-\frac{\|x-y\|_2}{l_c}\right) \quad l_c > 0 \quad (5.1)$$

Where, σ^2 is the constant variance of the random field and $L_c, c = 1, \dots, N$ is correlation length. The spatial mean stem density, random variable, (\bar{n}) , standard deviation and correlation length-scale (for all the stochastic distributions) were assumed to be respectively equal to $1000 < \bar{n}, < 4000 \text{ stems m}^{-2}$, $0.01 < \sigma/\bar{n} < 0.75$, and $l_c = 30\text{m}$. Relative correlation length to the wetland domain scale was also defined as l_c/L , in which L is wetland length. Isotropic mappings (Fig. 5.2.a, b) was created, where the properties of vegetation distribution do not depend on the direction. Alternately, anisotropic patterns (Fig. 5.2.c, d) were generated, where vegetation distribution properties vary with different orientations. The generator also was used to create the banded vegetation patterns assuming different horizontal (l_{cx}) and vertical correlation lengths (l_{cy}). In order to randomize the realistic correlation length in a range to be close to nature the values was set between 1 and 30 m, $0.01 < \frac{l_c}{L} < 0.30 \text{ m}$. The same range values of mean stem

density and standard deviation used for homogenous patterns were applied to heterogeneous distribution too. The chosen values are reasonable for vegetation pattern of FWS wetland (Citations) (Kadlec and Wallace, 2009). As an example, relative vertical and horizontal correlation lengths of $\frac{l_{cx}}{L} = 0.30$ and $\frac{l_{cy}}{L} = 0.03$ were used to generate Fig. 5.2.c and Fig. 5.2.d was generated with the assumption of $\frac{l_{cx}}{L} = 0.03$ m and $\frac{l_{cy}}{L} = 0.30$ m.

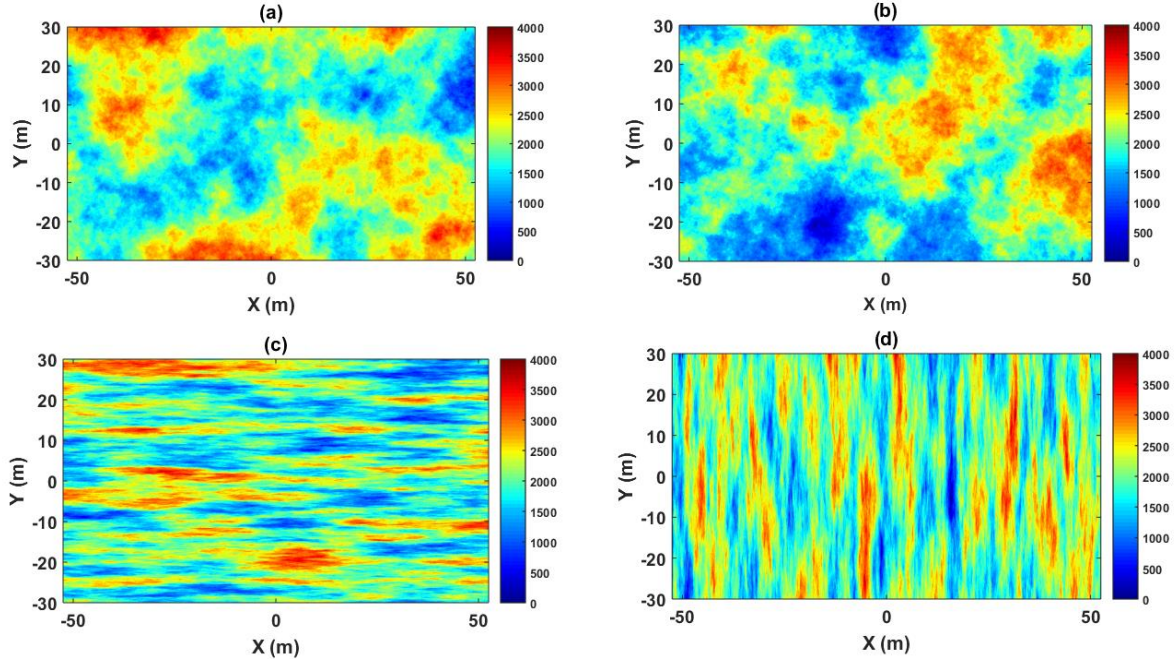


Figure 5.2 Examples of random vegetation fields with average stem density 2000 m^{-2} , standard deviation $\sigma/n = 0.50$, and relative correlation length (a), (b), $l_c/L = 0.30$, (c), $l_{cx}/L = 0.30$, $l_{cy}/L = 0.03$, (d) $l_{cx}/L = 0.03$, $l_{cy}/L = 0.30$.

5.4 Efficiency metrics

The removal efficiency of a wetland is controlled by the contact time between the contaminant and aquatic vegetation, which is responsible for natural treatment processes. The treatment performance of a wetland can be characterized in terms of either concentration reduction or total mass removal (Kadlec and Wallace, 2009). The concentration reduction efficiency is defined as

$$E_c = \frac{C_i - C_o}{C_i} = 1 - \frac{C_o}{C_i} \quad (5.2)$$

in which C_i and C_o are the concentration at the inlet (C_i) and outlet (C_o) of the treatment wetland..

The mass removal rate is defined as

$$\dot{m} = QC_i - QC_o \quad (5.3)$$

in which Q is the wetland discharge. Under steady-state flow conditions, Q is both the inflow and outflow discharge.

5.5 Numerical simulations

Simulations were performed for a 100 m long and 60 m wide rectangular wetland, with a centrally aligned inlet-outlet configuration and inlet-outlet widths of 5 m (Figure 5.3). It has been assumed (EPA, 2000) that Manning's equation, which defines flow in open channels, can be adapted to FWS wetlands $S^{\frac{1}{2}} = \frac{U}{\frac{1}{n}(h^{\frac{2}{3}})}$, in which M is the Manning's resistance coefficient ($s/m^{\frac{1}{3}}$), and S is hydraulic gradient or slope of water surface (m/m). By assuming that M is a function of the water depth as well as the resistance of submerged vegetation, hydraulic gradient of a wetland can be determined (Kadlec and Wallace, 2009). Belyea (2007) studied open water pools with different discharge rates and observed hydraulic gradients in the range from 0 to 0.015 $m\ m^{-1}$. (Reed et al.) (1995) use an equation for vegetated wetlands and estimate M values to vary from up to 1 to 14 $s/m^{1/3}$ corresponding to maximum required hydraulic gradients of 0.007 $m\ m^{-1}$. (Crites and Tchobanoglous) (1998) offer a series of values for slope of surface in wetlands from 1 in 1,000, or 1cm in 100 meters. In this chapter, a hydraulic gradient of 0.005 m was imposed between the inlet and the outlet, and the water depth at the outlet was set equal to 0.5 m. The condition on the hydraulic gradient and the range of vegetation densities were assumed to produce a nominal residence time $5 \leq t_n \leq 7.5$ days, which is reasonable for a FWS wetland (Kadlec and Wallace, 2009; Serra et al., 2004).

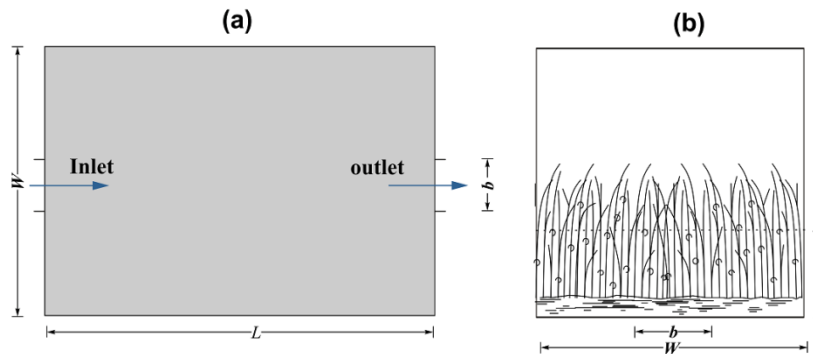


Figure 5.3 Illustration of the conceptual vegetated wetland: (a) plan view, (b) side view.

The solute transport equations were solved by applying a finite element method (FEM) using COMSOL Multiphysics®, assuming a no-flux condition on the remaining boundaries of the flow domain and an open boundary condition at the outlet. Similar to the modeling in chapters 2 and 3, a grid of 250,000 triangular elements of a maximum element size of 1.5 m was used. The mentioned mesh had a higher spatial resolution near the inlet and the outlet. The solute transport equations were solved for the outlet concentration as a function of time, responding to the instantaneous tracer injection of $C = 1 \text{ kg/m}^3$ at the inlet. In this study $k \text{ (s}^{-1}\text{)}$, the solute volumetric removal rate, is assumed to be proportional to the vegetation density (s^{-1}).

$$k = k_0 \frac{n_s}{n_{s0}} \quad (5.4)$$

Where k_0 is the decay rate for the reference vegetation density, n_{s0} . The reference vegetation was assumed to be 1000 stems m^{-2} and the volumetric removal rate, k_0 , was set equal to 23 yr^{-1} , corresponding to the wetland depth of 0.5 m and the mean value of the areal removal rate of ammonia, 11.5 m yr^{-1} , reported by (Kadlec and Wallace, 2009) for a set of 131 FWS wetlands.

5.5.1 Model calibration

The main model parameters include transverse diffusivity, E_T , longitudinal dispersion coefficient, E_L , and Manning coefficient, M . The parameters E_T and E_L were determined from Eq. (2.13) using the scale factors $\alpha_h = 0.1$, $\beta = 1$, as derived from the experimental studies (Nepf, 1999) and $\alpha_v = 0.1$ Eq. (2.12) (Lightbody and Nepf, 2006; Tanino and Nepf, 2008). The manning coefficient, M , was chosen so that the output volumetric efficiency (Eq. 2.19), e_v , best matched the value predicted by the empirical relationship derived by Thackston et al. (1987),

$$e_v = 0.85 \left[1 - \exp \left(-0.59 \frac{L}{W} \right) \right] \quad (5.5)$$

This equation is based on field data from a variety of large shallow wetlands of diverse size, shape and vegetation type.

To calibrate the model, a conceptual wetland of rectangular geometry was considered (Figure 5.3), with an area of $6,000 \text{ m}^2$, length-to-width ratios, L/W , spanning from 1/1 to 10/1, and same inlet and outlet width $b = 5 \text{ m}$ located in the middle of the shorter sides. Managing the water depth is necessary for the health and vigor of the plant community, which is typically sensitive to

it (Kadlec and Wallace, 2009). The water depth h at the outlet was set to be 0.5 m, and a head loss of 0.005 m between the inlet and the outlet sections was imposed in all the simulations. Inflow can be distributed by gravity flow or by pressurized flow. Considering that the gravity flow conserves energy and reduces operation and maintenance costs, and causes less erosion and sedimentation makes it a desirable solution in some cases (Kadlec and Wallace, 2009). Application of set up with constant head is a technique used for some lagoon-wetlands (Bragato et al., 2006) and stormwater ponds (Kadlec and Wallace, 2009). The value of hydraulic gradient was constrained below 0.005 m m^{-1} to maintain consistency with previous studies field observations (Crites and Tchobanoglous, 1998; Kadlec and Wallace, 2009; S. Reed et al., 1995). Random fields of vegetation patterns with prescribed statistical properties (Eq. 5.1) were generated as described in Section 5.4. The simulations assume a stem diameter of 5 mm and a range of average stem density from 1000 to 4000 stems m^{-2} , which is representative of the vegetation density found in a variety of wetlands (Kadlec and Wallace, 2009; Serra et al., 2004). Four sample fields generated for the same combination of parameters are shown in Figure 5.2.

The calibration of the two-dimensional hydrodynamic model calibration was performed by minimizing, for each aspect ratio, the relative error, $RE = \left| \frac{\sum_{i=1}^n (E-S)}{\sum_{i=1}^n (S)} \right|$, where E is the value from equation (5.5) and S is the mean model output for a set of 10,000 random field vegetation distributions. A study on vegetative resistance by (Nepf, 1999) showed for vegetation densities as small as 0.01 ($ad=0.01$), the bed drag and bed shear stress are negligible compared to their vegetation components. Based on this assumption and comparing the magnitude of the bed drag and the vegetation drag equations (2.6), it can be seen that the bed stress will always be small compare to the vegetation drag, and can be dropped from the equations. Then, applying a best-fit calibration (Fig. 5.4) was used as a verification of the random arrangement of vegetation, where a vegetation density of 2000 stems m^{-2} , stem diameter of 5 mm, $l_c = 30$ and standard deviation $\sigma = 1000$ produced realistic ranges of the e_v . Each point in Fig. 5.4 represents the ensemble average volumetric efficiency, e_v , of 10,000 wetlands of randomly distributed vegetation patterns (Eq.5.1).

Ensemble For the abovementioned vegetation density and distribution, the shear stresses are the result of the contribution of only vegetation. In the calibration, 60% of the simulations were used (i.e. the retention time of wetlands with aspect ratios $L/W = 1/1, 2/1, 5/1, 6/1, 8/1, 10/1$) whereas

the remaining 40% was applied for validation. As shown in Fig. 5.4, the numerical model results fit well within the field data presented by Thackston et al. (1987). The relative error (RE), of simulated wetlands to the field data was 0.08 (Figure 5.3). The numerical studies by Jenkins and Greenway (2005), Minsu et al. (2009) and (Sabokrouhiyeh et al., 2017) have also calibrated sets of hypothetical wetlands according to the design curve proposed by Thackston et al. (1987) and both found a good fit between L/W and the simulated detention time.

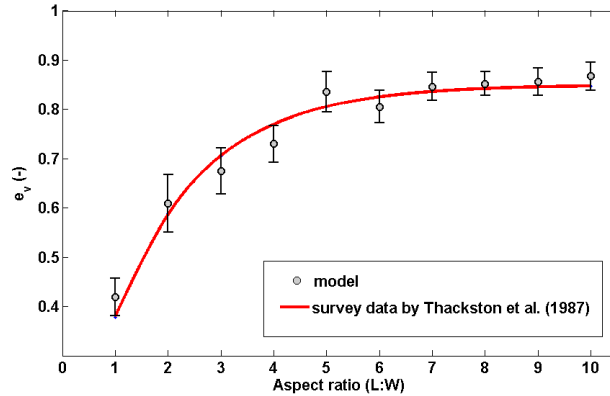


Figure 5.4 Volumetric efficiency derived from field data (Thackston et al. 1987) is compared with the results of the numerical model.

5.6 Numerical model results

5.6.1 Isotropic vegetation patterns

Figure 5.5a and 5.5b show the concentration efficiency, E_c , and discharge rate, Q , respectively, as a function of the mean stem density, \bar{n} . For each set of model simulations, based on 10,000 random vegetation fields with the same statistical parameters of , Figure 5.5 shows mean (circles) and standard deviation (bars) of the model results. Results show that the concentration reduction efficiency increases monotonically with the average stem density, and the flow discharge decreases consistently as a function of the average stem density. Theoretically, if Q approached zero, such that the residence time approached infinity, E_c would approach 1, which indicates that the best performance with regard to this metric occurs at the highest stem density.

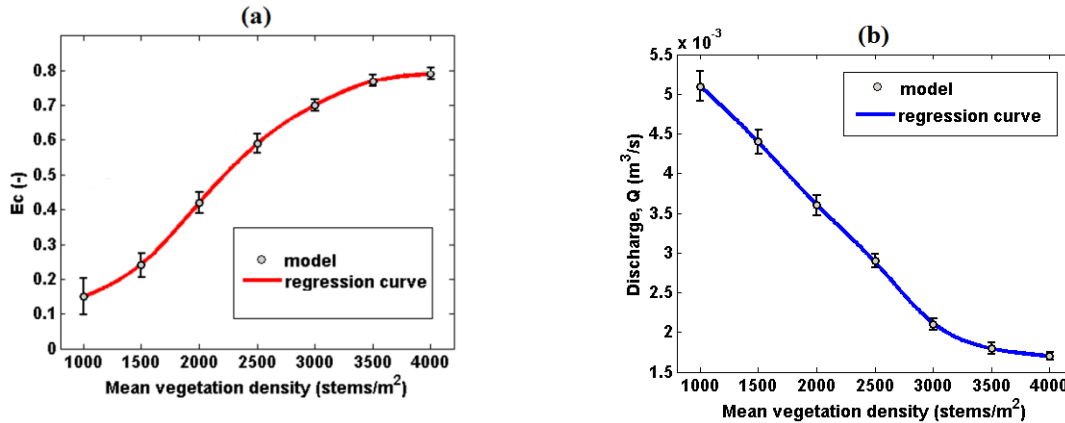


Figure 5.5 Behavior of (a) concentration reduction efficiency and (b) flow discharge as a function of average stem density. The points represent the ensemble mean of the simulation results, with corresponding standard deviation bars.

As seen in Fig. 5.5.b, the discharge decreases linearly with increasing stem density, but then appears to approach a constant value at 4000 stems m⁻². The progress from an initial sparse vegetation to a more densely vegetated coverage was associated by increases in the friction coefficient. Consequently the raised friction forces produced considerable increase in retention time and a decreased discharge rate through the wetland before converging to a maximum constant value. It can be seen from (Fig. 5.5.a) there is an increase in Ec (Eq. 5.2) from a sparse vegetation to a more densely vegetated condition (Fig. 5.5.a). Water moved more slowly because of the increased drag of the dense vegetation coverage. The reduced flow velocity created longer retention time, and thus lead to a longer exposure time to biological-chemical reactions and an enhanced Ec . There is also an additional influence from the higher volumetric removal rate, k (s⁻¹), associated with higher stem density (Eq. 5.4), where removal rate is assumed to be proportional to the vegetation density. These two effects combine to form an overall increasing pattern of contaminant removal. The result of such mixing is evidenced in the behavior of concentration reduction efficiency and as a function of average stem density (Figure 5.5.a).

The behavior of the total mass removal rate, \dot{m} , as a function of the average stem density for a prescribed head drop between the inlet and the outlet is shown in Figure 5.6. The graph shows that the total mass removal is not a monotonic function of the mean stem density, \bar{n} , but has a peak for a certain value of \bar{n} . For low vegetation density, $\bar{n} < 2500$ stems m⁻², mass removal

increases with increasing vegetation density, since the increasing vegetation density induces a higher removal of the solute that overcomes the reduced mass inflow from the inlet. Conversely, if the vegetation stem density is higher than approximately 2500 stems m^{-2} , mass removal decreased as the decrease in wetland discharge no longer compensated for the increase in concentration reduction efficiency. It can therefore be concluded that, for the same hydraulic gradient, vegetation density higher than a certain threshold will lead to a decreased mass removal rate.

To quantify the stochastic nature of short-circuiting, a field generator (Eq. 5.1) was used to generate the vegetation distribution from wetlands of the same mean stem density ($\bar{n} = 2000 \text{ stems } m^{-2}$), the same relative correlation length ($\frac{L_{cx}}{L} = \frac{L_{cy}}{L} = 0.30$), and different variance interval of $0.01 < \sigma/n < 0.75$. Figure 5.6 shows the resulting vegetation states from the sensitivity analysis of vegetation distribution variance ($\sigma/n = 0$). The range was chosen to be consistent to vegetation patterns occurring in FWS wetlands (Cheng et al., 2011; Kadlec and Wallace, 2009). Studying a wide range of variance was necessary, since spatial vegetation distributions is likely to change under seasonal variation of stem density (Keefe et al., 2010), destruction of the wetland vegetative infrastructure (Kadlec, 2007) and varying hydraulic gradients (Cheng et al., 2011).

For a data set stems densities with low variance ($\sigma/n = 0.01$), wetland vegetation appeared almost uniform, and the wetland had a fairly uniform flow characteristics (Fig. 5.6.a). However, the other vegetation patterns of higher variances ($\frac{\sigma}{n} = 0.25, 0.5, 0.75$) were more likely to exhibit heterogeneous patches of vegetation and channelized flowpaths (Fig. 5.6.b,c,d). These results suggest that short-circuiting may be more likely to be present in wetlands with high level of variance in stem distribution. It can also be seen from Fig. 5.6, more dense, intercepted patches and canals can be a result of high level of variance. Such a pattern can result in discernible flow paths and higher likelihood of short-circuiting. These flowpaths can be narrow or wide, to have different slow-flow or fast-flow zones, and to carry different fractions of the flow. The assumption that heterogeneity of vegetation patterns was made in analogy to field observations (D'Alpaos et al., 2006; Lightbody et al., 2008), where the vegetation distribution develops randomly and spontaneously, so it is impossible to predict the locations of the flowpaths in advance.

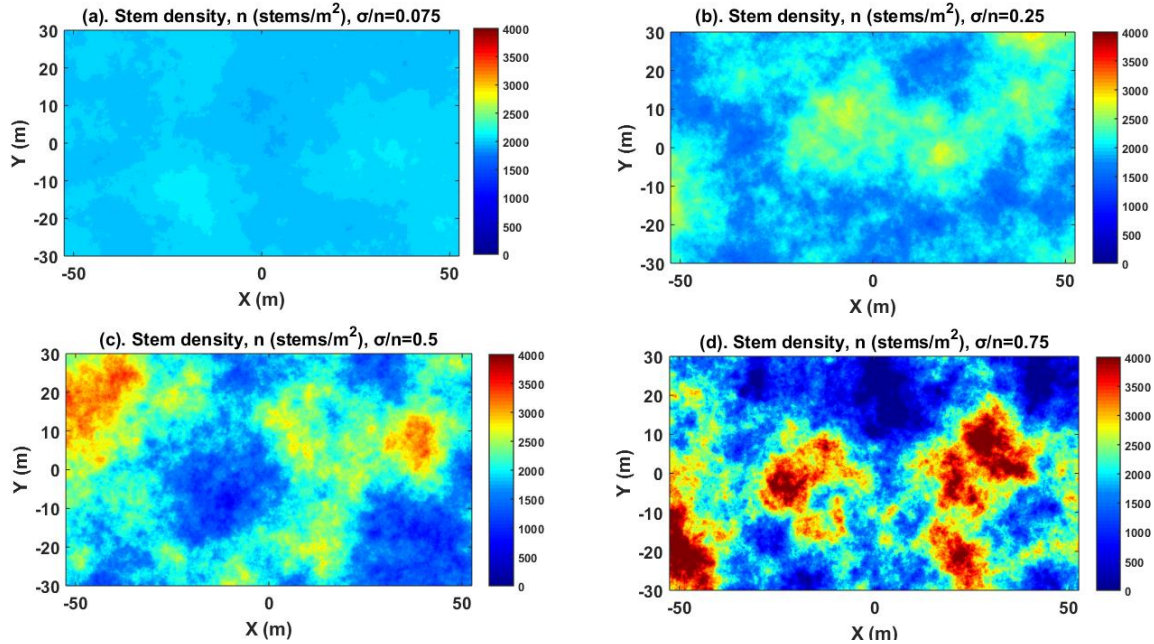


Figure 5.6 Types of vegetation patterns from wetlands of the same mean stem density ($\bar{n} = 2000 \text{ stems m}^{-2}$), the same relative correlation length ($\frac{L_{cx}}{L} = \frac{L_{cy}}{L} = 0.30$) and different variance of (a) $\sigma/n = 0.075$, (b) $\sigma/n = 0.25$, (c) $\sigma/n = 0.5$, (d) $\sigma/n = 0.75$.

The concentration reduction efficiency, E_c , and mass removal rate, \dot{m} , decreased with increasing stem density variance (Fig. 7). Each point and bar within Fig.7 represents the ensemble average from random field simulations of flow through 10,000 wetlands of the same properties of Fig 5.6.

The reason for this behavior was that the presence of fairly uniform vegetation patterns with low variance ($\sigma/n = 0.01$, Fig. 5.6.a) reduced the formation of preferential flowpaths, thereby reducing short-circuiting. Conversely, higher stem density variance was associated with more patchy vegetation patterns that were more likely to produce higher dispersion and preferential flowpaths. This results in a deviation from the plug flow behavior, and lower mass exchange with slow flowing regions of dense vegetation where treatment processes occur. For example, Low removal rates in a portion of a constructed wetland in Fig. 5.6.c.d was attributed to sparsely vegetated areas, which allowed water to flow directly through the wetland. The results is supported by previous field studies (Dierberg et al., 2005), where for example, internal phosphorus concentrations measurements showed higher phosphorus removal rates in shallow vegetated regions than within the deeper canals that created short-circuiting within the

Everglades Nutrient Removal Project, and numerical simulations in which, (Kadlec and Wallace, 2009) presented a numerical model to simulate short-circuiting in wetlands and concluded that the existence of different flow velocities and significant preferential flow paths decreased performance 30% below the plug-flow expectation.

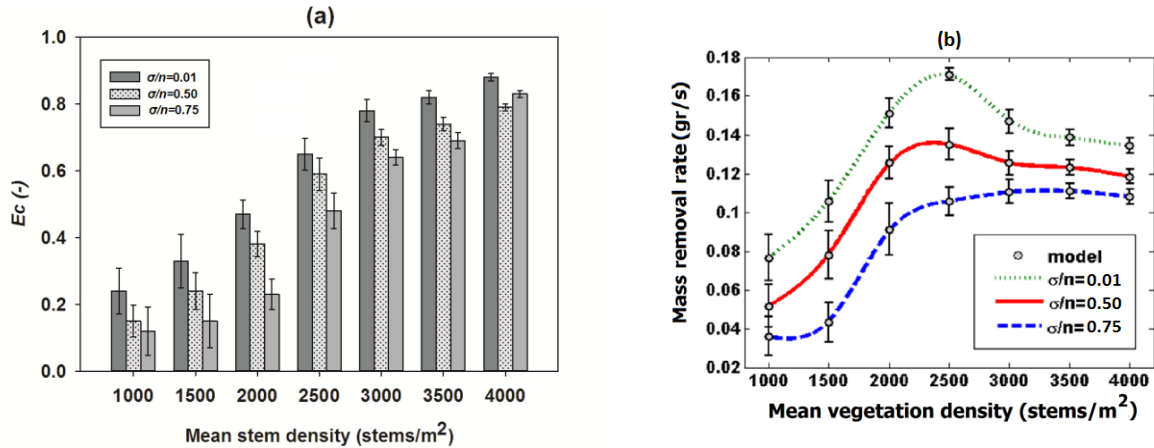


Figure 5.7 The concentration reduction efficiency, E_c , and mass removal rate, m , as a function of mean stem density for and relative stem density variance.

The random field generator (Eq. 5.1) was used to simulate spatial vegetation distribution for vegetation patterns from wetlands of the same mean steam density ($\bar{n} = 2000$ stems m⁻²), the same variance of ($\sigma/n = 0.25$), and different relative correlation length ($\frac{L_{cx}}{L} = \frac{L_{cy}}{L} = 0.01, 0.10, 0.30, 0.50$). As can be seen from Fig. 5.8, low relative correlation length (Fig. 5.8.a) lead to emergence of small patches, whereas, larger amounts of correlation lengths (Fig. 5.8.c, d) exhibited large-scale vegetation patchiness. More dense, larger interspersed patches of vegetation stands likely contributed more to the velocity heterogeneity, and emergence of short-circuiting throughout the wetland. The presence of patches of different scales in all patterns suggested that some amount of short-circuiting is always present in vegetated systems.

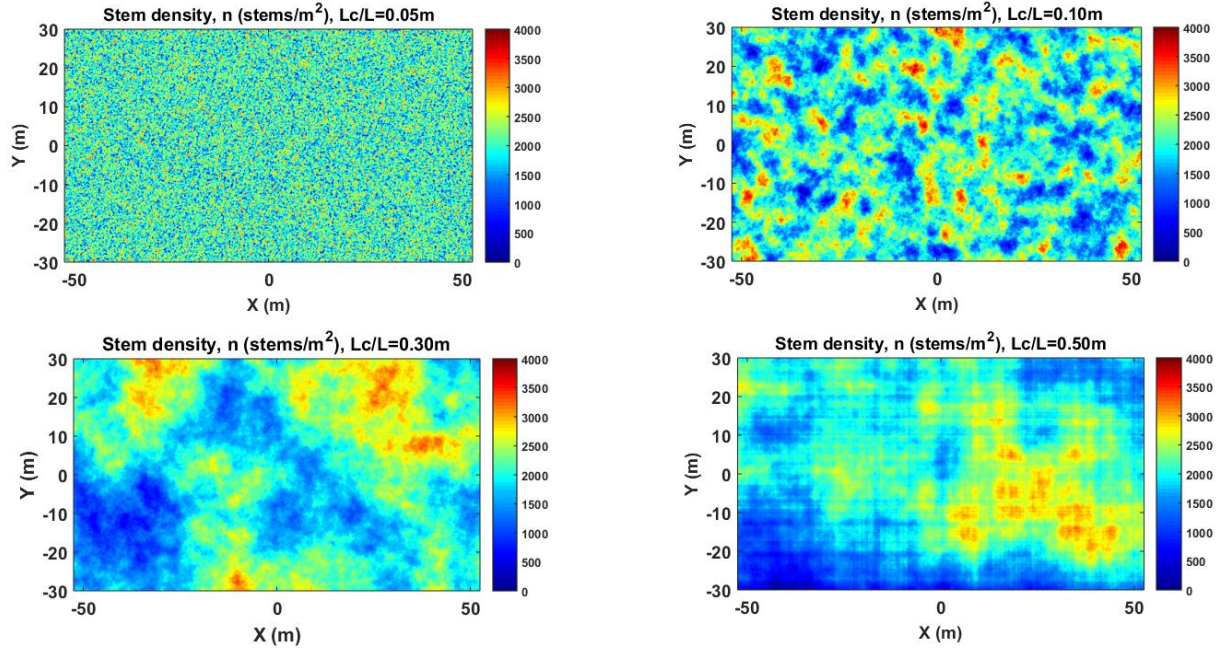


Figure 5.8 Types of vegetation patterns from wetlands of the same mean stem density ($\bar{n} = 2000 \text{ stems m}^{-2}$), the same variance ($\sigma/n = 0.50$), and relative correlation length of (a) ($\frac{L_{cx}}{L} = \frac{L_{cy}}{L} = 0.01$); (b) ($\frac{L_{cx}}{L} = \frac{L_{cy}}{L} = 0.10$); (c) ($\frac{L_{cx}}{L} = \frac{L_{cy}}{L} = 0.30$); (d) ($\frac{L_{cx}}{L} = \frac{L_{cy}}{L} = 0.50$).

Higher levels of concentration reduction efficiency, E_c , and mass removal rate, \dot{m} , were obtained for lower values of the correlation length (Fig. 5.9). This is due to the fact that higher correlation lengths are associated with the existence of preferential flow paths that allow contaminants to be transported along the less densely vegetated regions of the wetland. The short-circuiting effect induced by the heterogeneity of the spatial vegetation distributions decreases if the size of the patches is sufficiently small. Figure 5.9 shows that mass removal rate is sensitive to $\frac{l_c}{L}$ for the range $\frac{l_c}{L} = 0.01$ to 0.50 , but increasing l_c further had significantly less influence on mass removal rate. Findings are consistent to the results from previous studies where, (Wörman and Kronnäs) (2005) used a numerical model to show that increasing the correlation length of heterogeneity of the vegetation density affects the wetland's RTD, and consequently, reduces the removal rate of system.

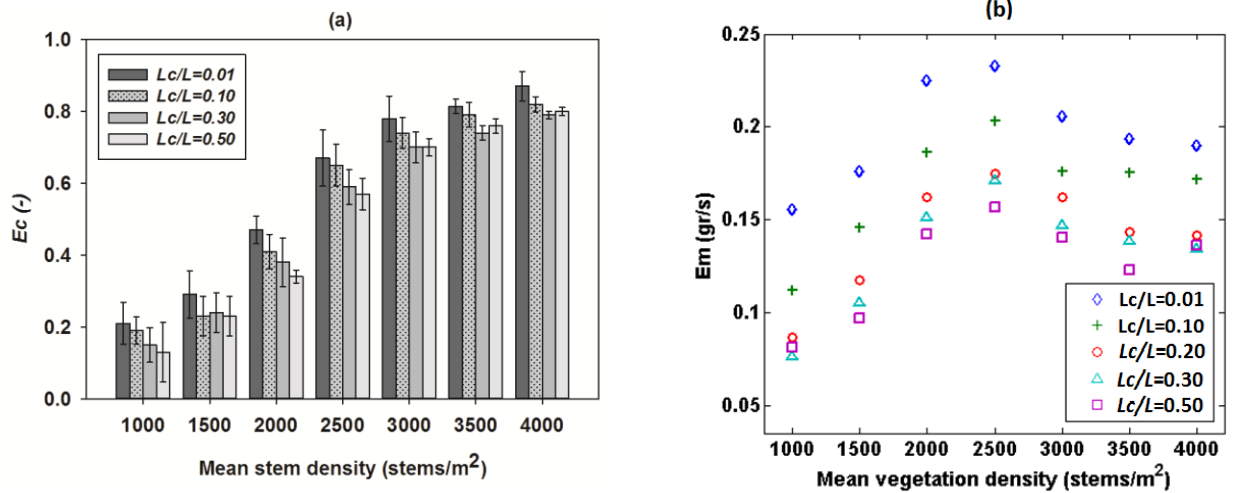


Figure 5.9 The concentration reduction efficiency, E_c , and mass removal rate, \bar{m} , as a function of mean stem density and relative correlation length, l_c .

5.6.2 Anisotropic vegetation patterns

The hydrodynamic and solute transport model was also applied to three different vegetation patterns with the same mean vegetation density and spatial variance, but different patterns of correlation length-scale, namely: an isotropic correlation length 30×30 ($m \times m$) (Fig. 5.10a); an anisotropic correlation length-scale 3×30 ($m \times m$) producing stripes parallel to the flow direction and correlation lengths (Fig. 5.10b); and an anisotropic correlation length-scale 30×3 ($m \times m$) producing stripes perpendicular to the flow direction (Fig. 5.10c). The resulting concentration efficiency and mass removal rate are shown in Figures 5.11 and 5.12, respectively. The graphs show that the spatial distribution of vegetation is a key factor affecting wetland performance. As the patterns considered have the same mean vegetation density and variance, the observed performance variation is merely due to the spatial structure of the random vegetation field. The bar chart in Fig. 5.11 shows mean and standard deviation of the concentration reduction efficiency, E_c , as a function of vegetation density and type of vegetation pattern. Each bar represents the ensemble average of E_c resulting from 10,000 random vegetation fields with the patterns shown in Fig. 5.10. The E_c increased with the average stem density from $E_c \approx 0.2$, for $\bar{n} = 1000$ stems m⁻², to approximately 0.8 for $\bar{n} = 4000$ stems m⁻². For all values of mean stem density the elongated patches perpendicular to the flow direction produced the greatest value of E_c , whereas the elongated patches parallel to the flow direction had the lowest value of E_c . The difference was most pronounced for the lowest mean stem density and almost

disappeared for the highest density, $\bar{n} = 4000$ stems m^{-2} . A similar trend was observed for mass removal (Fig. 5.12), which was lowest for the striped pattern parallel to the flow direction and highest for the striped pattern perpendicular to flow. For the parallel striped pattern (Fig. 5.10b) the average mass removal rate is 0.05 gr/s when the average vegetation density is $\bar{n} = 1000$ stems m^{-2} , and is almost 3 times higher for $\bar{n} = 2500$ stems m^{-2} , for which the curve shows a distinct peak. The type of vegetation pattern has a significant effect on mass removal, with an increase of approximately 10% and 30% for the dotted and perpendicular striped patterns, respectively, compared to parallel striped pattern.

These trends can be explained by the enhancing or diminishing effect of different vegetation patterns on flow short-circuiting. Vegetation bands parallel to the flow direction produce a higher variance of the residence time within the wetland, with short residence times associated with the transport along preferential flow paths, and longer residence times associated with transport in the more densely vegetated regions characterized by low velocities and small mixing rates. Conversely, vegetated stripes perpendicular to the flow direction can reduce short-circuiting by producing a more uniform velocity distribution across the wetland. However, it is interesting to note that the curves in Fig. 5.12 appear to converge to a common asymptote when the vegetation density is higher than 3500 stems m^{-2} , suggesting that the mass removal rate is independent of the spatial vegetation pattern for high vegetation densities.

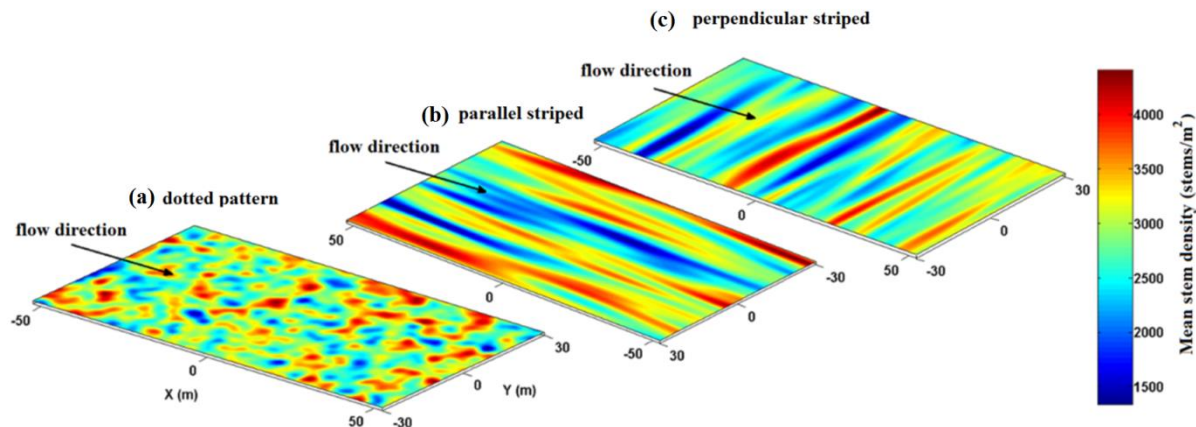


Figure 5.10 Types of vegetation patterns of the same mean stem density and the same variance considered in the simulations: (a) dotted pattern; (b) striped pattern aligned with the flow direction; (c) striped pattern perpendicular to the flow direction.

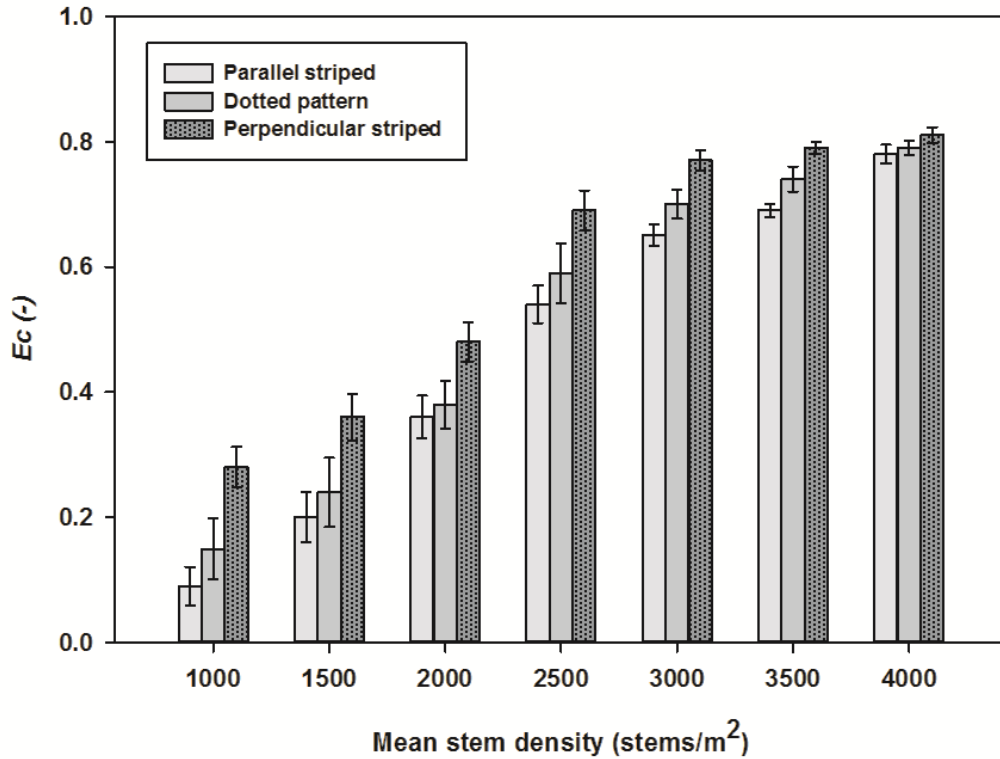


Figure 5.11 Concentration removal efficiency as a function of mean stem density for the different vegetation patterns presented in Figure 5.10.

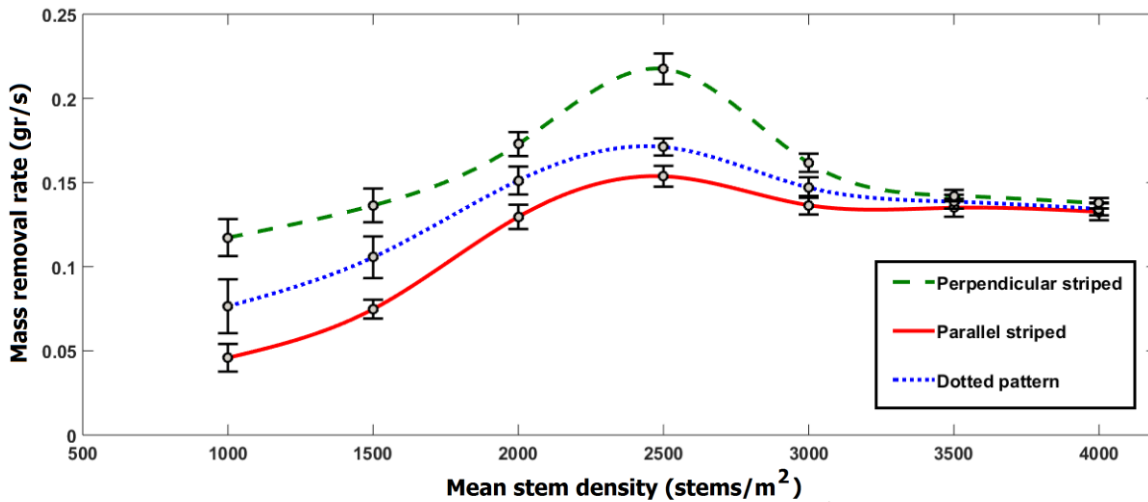


Figure 5.12 Mass removal rate versus vegetation density for the different vegetation patterns presented in Figure 5.10.

5.7 Effect of vegetation heterogeneity on wetland performance

This study has analyzed the influence of the statistical properties of a heterogeneous vegetation field on the treatment performance of a wetland. The results show that the average stem density,

the stem density variance and correlation length, all, are significant parameters, determining concentration reduction and mass removal fluxes through FWS wetlands. The maximum concentration reduction did not coincide with the maximum mass removal, because mass removal depended on both concentration reduction and flow rate. Whereas concentration reduction increased monotonically with increasing stem density, mass removal had a maximum value at less than the maximum stem density considered. This non-monotonic response resulted from the competing trends of reaction rate increasing but flow rate declining with increasing stem density. Although the average stem density is an important factor affecting total mass removal, another effect is associated to the vegetation distribution represented by the stem density variance and correlation length. In particular, the ensemble average of the total mass removal is shown to decrease when variance and correlation length of the vegetated field increase. The physical explanation for this effect is that high stem density variance and high correlation length are associated with extended, contiguous regions of low stem density that produce preferential flow paths. The validity of this statement is also supported by the graphical illustration of vegetation patterns of different statistical characteristics.

Wetland performance also varied in response anisotropic vegetation patterns. In particular, , the best performance was observed for a striped pattern with elongated vegetation patches perpendicular to the main flow direction (Figure 5.10.c). The observed improvement in removal performance was explained by the fact that potential effects of short-circuiting can be intercepted by vegetation bands perpendicular to the flow direction. The research suggests that such a pattern, can be utilized to provide a higher levels of treatment in constructed wetlands. Conversely, for the same mean vegetation density and standard deviation, mass removal was lowest when the vegetation was distributed in longitudinal stripes parallel to the flow direction. It can thus be concluded that the spatial distribution of vegetation can significantly affect the treatment performance of wetlands and should therefore be taken into account in the predictive evaluation of their treatment efficiency.

Chapter 6

6 Discussion and conclusions

6.1. Design recommendations

The previous sections have shown that low aspect ratio (wide basins) decreases the hydraulic efficiency metrics in FWS wetlands. Moreover, Results confirmed that sparse vegetation coverage causes more dispersion and larger dead zones and consequently decreases contaminant removal rates. The results also suggest that a higher contaminant rate can be archived by appropriately designing wetland shape. Ellipse-shaped wetlands improved treatment processes through increasing the detention time (higher e_v) and reducing dispersion (higher e_d) compared to rectangular wetlands. The better performance wetlands can be explained by the difference in flow pattern. Rectangular shape wetlands formed larger dead zones in the corners, implying that some parts of wetland was excluded from main flow surface. Whereas, elliptical cases had smaller or no dead zones on the corners. Moreover, The results from numerical model showed smaller level of dispersion for more efficient elliptical wetlands than rectangular basins. The results were consistent with the velocity fields maps, where the model produced a more uniform cross-sectional velocity profiles for elliptical wetlands. A smaller spatial variation in the velocity field is associated with smaller wetland scale dispersion. The numerical model shows that vegetation bands perpendicular to the flow

direction can improve wetland performance through two separate mechanisms. Fractions of water participating in short-circuiting is diluted, when the lateral mixing occurs within perpendicular vegetation bands. Therefore, retention time increases and dispersion index improves. In addition, vegetation bands intercept the high velocity flowpaths, and makes it less probable that fast flowpaths will align throughout the entire wetland. Therefore, even in absence of lateral mixing within perpendicular vegetation bands, there is a still a great probability that fractions of flow will be exposed to longer treatment processes, resulting in an increasing performance. Design recommendations based on these findings are presented below, as well as suggestions for further research.

Discussed numerical modeling efforts, which are based on realistic assumptions from field data, suggest the following recommendations for future wetland design. Wetland performance depends on many factors including basin aspect ratio and geometry, inlet-outlet configuration, and vegetation density and distribution, and it is impossible to predict wetland removal without knowing those variables. In addition, the model is not fully capable to predict the exact position of fast flowpaths in a particular wetland because the vegetation distribution is random pattern, and is the subject of constant change due to hydrodynamic processes. Even so, preliminary recommendations are provided in this chapter to highlight trends and relative tradeoffs between various design choices.

6.1.1 Wetland size

Results from numerical model confirm that the retention time is the key factor in treatment processes. The degree of biological, chemical functions necessary for pollutant removal are directly dependent on the time pollutants stay in wetland system. A higher retention time provides a longer time for reactions to take place in a basin, which consequently increases wetland efficiency. The retention time of FWS wetlands is function of wetland size. Even a complicated design cannot compensate for an under-sized wetland with too short retention time. As a result, despite the increasing usage of FWS wetlands as a secondary wastewater treatment solution and rainfall treatment ponds, they may not be the appropriate for highly urbanized areas where land costs limits projects with large footprints.

6.1.2 Aspect ratio

One important feature in designing wetlands is aspect ratio (length to width, L/W). Modeled results showed that the contaminant removal rate increases, when the basin is long and narrow. Moreover, it was confirmed when vegetation is not distributed uniformly and patches and canals are present, a higher length/width ratio decreases short-circuiting. However, it should be considered that that very high aspect ratios dramatically increase the head drop within the wetland, which can perversely increase the tendency to develop short-circuiting flow paths. The results from this study suggest that the length to width ratio (L/W) of vegetated wetlands should be appropriately high (at least 3/1) to maintain adequate retention time and provide desirable levels of contaminant removal.

6.1.3 Wetland shape

Most constructed treatment wetlands are rectangular, to minimize the construction costs that would be generated by a more sinuous shape. However, the modeled results of this study showed elliptical wetlands consistently had better performance than rectangular ones, i.e. produced higher values of volumetric, e_v , and dispersion indexes, e_d .

Unlike a rectangular wetland, in which prominent dead-zones formed in each corner of the wetland, an elliptical wetland produced a more uniform velocity distribution with fewer (or no) dead zones, increasing e_v , reducing RTD variance and thus increase the dispersion efficiency e_d . The reduction in dead-zone size and the more uniform velocity field of the elliptical wetland implies performance greater potential for pollutant removal. A wetland designer could use elliptical shape to improve the performance of a surface flow wetland in terms of both residence time duration and dispersion with the wetland.

6.1.4 Inlet-outlet configuration

Due to the laminar flows within FWS wetlands, the momentum created by inlets can have a important effect on flow patterns within the system. Numerical simulations of flow indicated that both parameters related to volumetric retention time and dispersion rate, e_v and e_d , are a function of inlet-outlet position. It was shown that, the minimum dead zone area (greatest effective area) and the lowest dispersion were achieved with the opposite corner-to-corner inlet-outlet configuration, which produced the maximum values of e_v and e_d , respectively. Similarly,

increasing the number of inlets from one to two increased the predicted volumetric and dispersion efficiencies within constructed; whereas, application of three inlets did not improve the efficiency metrics much, compared to two-inlet system. Wetland designers use an orthogonal inlet-out configuration and multiple inlets to promote the spreading of flow across a wetland.

6.1.5 Vegetation density and distribution

Vegetation in FWS wetlands within the deep zones provides contaminant removal, which drives wetland performance. The presence of vegetation may also inhibit air-water exchange of oxygen, control the wind effects, and aerate the water column through biological production during photosynthesis. In addition, floating and submerged serve to dissipate momentum, controlling residence time and dispersion levels within the wetland. Even though, higher vegetation density was associated with lower variances in the RTD and larger NTIS. However, above a threshold stem density of about 300 stems m^{-2} , the dispersion efficiency (e_d), and volumetric efficiency (e_v) remained almost constant, i.e. increasing vegetation density further did not significantly improve these efficiency metrics. From a design point of view, considering this threshold vegetation density can be useful for a cost-effective wetland design.

Considering the random distribution of vegetation within the wetland, designers should assume that short-circuiting will always be likely to occur, and take measures to prevent fast flowpaths, causing short-circuiting. The results from this study suggests vegetated stripes perpendicular to the flow direction can reduce short-circuiting by producing a more uniform velocity distribution across the wetland.

6.1.6 Wind effect

In a narrow wetland of high aspect ratio, an orientation perpendicular to wind direction is advisable, so that the risk of short-circuiting can be decreased due to the lateral mixing driven by wind. Wetland designers can take hydraulic benefits from combination of wind effect and replacing perpendicular vegetation bands to reduce the short-circuiting diverse effects. It should also be noted, however, in a wide wetland the wind can create a large setup that could cause sedimentation in corners and overtopping of berms.

Bibliography

- Abbas, H., Nasr, R., Seif, H., 2006. Study of waste stabilization pond geometry for the wastewater treatment efficiency. *Ecol. Eng.* 28, 25–34. doi:10.1016/j.ecoleng.2006.03.008
- Anderson, M.P., 2005. Heat as a Ground Water Tracer. *Ground Water* 43, 951–968. doi:10.1111/j.1745-6584.2005.00052.x
- Arega, F., Sanders, B.F., 2004. Dispersion model for tidal wetlands. *J. Hydraul. Eng.* 130, 739–754. doi:10.1061/(ASCE)0733-9429(2004)130:8(739)
- Arega, F., Sanders, B.F., 2004. Dispersion Model for Tidal Wetlands. *J. Hydraul. Eng.* 130, 739–754. doi:10.1061/(ASCE)0733-9429(2004)130:8(739)
- Arheimer, B., Wittgren, H.B., 2002. Modelling nitrogen removal in potential wetlands at the catchment scale. *Ecol. Eng.* 19, 63–80. doi:10.1016/S0925-8574(02)00034-4
- Arheimer, B., Wittgren, H.B., 1994. Modeling the effects of wetlands on regional Nitrogen removal. *Ambio* 23, 378–386.
- Atkinson, T.C., Davis, P.M., 2000. Longitudinal dispersion in natural channels: 1. Experimental results from the River Severn, U.K. *Hydrol. Earth Syst. Sci.* 4, 345–353. doi:10.5194/hess-4-345-2000
- Battin, T.J., Kaplan, L.A., Denis Newbold, J., Hansen, C.M.E., 2003. Contributions of microbial biofilms to ecosystem processes in stream mesocosms. *Nature* 426, 439–442. doi:10.1038/nature02152
- Batty, L.C., Younger, P.L., 2002. Critical role of macrophytes in achieving low iron concentrations in mine water treatment wetlands. *Environ. Sci. Technol.* 36, 3997–4002.
- Becker, M.W., Georgian, T., Ambrose, H., Siniscalchi, J., Fredrick, K., 2004. Estimating flow and flux of ground water discharge using water temperature and velocity. *J. Hydrol.* 296, 221–233. doi:10.1016/j.jhydrol.2004.03.025
- Bellin, A., Rubin, Y., 1996. HYDRO_GEN: A spatially distributed random field generator for correlated properties. *Stoch. Hydrol. Hydraul.* 10, 253–278. doi:10.1007/BF01581869
- Belyea, L.R., 2007. Climatic and topographic limits to the abundance of bog pools. *Hydrol. Process.* 21, 675–687. doi:10.1002/hyp.6275
- Bencala, K.E., 1984. Interactions of solutes and streambed sediment: 2. A dynamic analysis of coupled hydrologic and chemical processes that determine solute transport. *Water Resour. Res.* 20, 1804–1814. doi:10.1029/WR020i012p01804
- Bencala, K.E., Walters, R.A., 1983. Simulation of solute transport in a mountain pool-and-riffle stream: A transient storage model. *Water Resour. Res.* 19, 718–724. doi:10.1029/WR019i003p00718
- Bodin, H., Mietto, A., Ehde, P.M., Persson, J., Weisner, S.E.B., 2012. Tracer behaviour and analysis of hydraulics in experimental free water surface wetlands. *Ecol. Eng.* 49, 201–211. doi:10.1016/j.ecoleng.2012.07.009

- Bottacin-Busolin, A., Marion, A., 2010. Combined role of advective pumping and mechanical dispersion on time scales of bed form–induced hyporheic exchange. *Water Resour. Res.* 46, W08518. doi:10.1029/2009WR008892
- Bottacin-Busolin, A., Marion, A., Musner, T., Tregnaghi, M., Zaramella, M., 2011. Evidence of distinct contaminant transport patterns in rivers using tracer tests and a multiple domain retention model. *Adv. Water Resour.* 34, 737–746. doi:10.1016/j.advwatres.2011.03.005
- Bottacin-Busolin, A., Singer, G., Zaramella, M., Battin, T.J., Marion, A., 2009. Effects of Streambed Morphology and Biofilm Growth on the Transient Storage of Solutes. *Environ. Sci. Technol.* 43, 7337–7342. doi:10.1021/es900852w
- Bragato, C., Brix, H., Malagoli, M., 2006. Accumulation of nutrients and heavy metals in *Phragmites australis* (Cav.) Trin. ex Steudel and *Bolboschoenus maritimus* (L.) Palla in a constructed wetland of the Venice lagoon watershed. *Environ. Pollut.* 144, 967–975. doi:10.1016/j.envpol.2006.01.046
- Busenberg, E., Plummer, L.N., 1992. Use of chlorofluorocarbons (CCl_3F and CCl_2F_2) as hydrologic tracers and age-dating tools: The alluvium and terrace system of central Oklahoma. *Water Resour. Res.* 28, 2257–2283. doi:10.1029/92WR01263
- Cameron, K., Madramootoo, C., Crolla, A., Kinsley, C., 2003. Pollutant removal from municipal sewage lagoon effluents with a free-surface wetland. *Water Res.* 37, 2803–2812. doi:10.1016/S0043-1354(03)00135-0
- Cardenas, M.B., Wilson, J.L., Zlotnik, V.A., 2004. Impact of Heterogeneity, Bed Forms, and Stream Curvature on Subchannel Hyporheic Exchange. *Water Resour. Res.* 40. doi:10.1029/2004WR003008
- Carleton, J.N., Grizzard, T.J., Godrej, a. N., Post, H.E., 2001. Factors affecting the performance of stormwater treatment wetlands. *Water Res.* 35, 1552–1562. doi:10.1016/S0043-1354(00)00416-4
- Carleton, J.N., Montas, H.J., 2010. An analysis of performance models for free water surface wetlands. *Water Res.* 44, 3595–3606. doi:10.1016/j.watres.2010.04.008
- Chen, T.Y., Kao, C.M., Yeh, T.Y., Chien, H.Y., Chao, A.C., 2006. Application of a constructed wetland for industrial wastewater treatment: A pilot-scale study. *Chemosphere* 64, 497–502. doi:10.1016/j.chemosphere.2005.11.069
- Cheng, Y., Stieglitz, M., Turk, G., Engel, V., 2011. Effects of anisotropy on pattern formation in wetland ecosystems. *Geophys. Res. Lett.* 38, n/a-n/a. doi:10.1029/2010GL046091
- Comans, R.N.J., Hockley, D.E., 1992. Kinetics of cesium sorption on illite. *Geochim. Cosmochim. Acta* 56, 1157–1164. doi:10.1016/0016-7037(92)90053-L
- Conant, B., 2004. Delineating and Quantifying Ground Water Discharge Zones Using Streambed Temperatures. *Ground Water* 42, 243–257. doi:10.1111/j.1745-6584.2004.tb02671.x
- Constantz, J., 1998. Interaction between stream temperature, streamflow, and groundwater exchanges in alpine streams. *Water Resour. Res.* 34, 1609–1615. doi:10.1029/98WR00998

- Couwenberg, J., Joosten, H., 2005. Self-organization in raised bog patterning: the origin of microtopo zonation and mesotope diversity. *J. Ecol.* 93, 1238–1248. doi:10.1111/j.1365-2745.2005.01035.x
- Crites, R., Tchobanoglous, G., 1998. *Small and Decentralized Wastewater Management Systems*. McGraw-Hill, NY.
- D’Alpaos, A., Lanzoni, S., Mudd, S.M., Fagherazzi, S., 2006. Modeling the influence of hydroperiod and vegetation on the cross-sectional formation of tidal channels. *Estuar. Coast. Shelf Sci.* 69, 311–324. doi:10.1016/j.ecss.2006.05.002
- Davis, P.M., Atkinson, T.C., 2000. Longitudinal dispersion in natural channels: 3. An aggregated dead zone model applied to the River Severn, U.K. *Hydrol. Earth Syst. Sci.* 4, 373–381. doi:10.5194/hess-4-373-2000
- Dierberg, F.E., Juston, J.J., DeBusk, T. a., Pietro, K., Gu, B., 2005. Relationship between hydraulic efficiency and phosphorus removal in a submerged aquatic vegetation-dominated treatment wetland. *Ecol. Eng.* 25, 9–23. doi:10.1016/j.ecoleng.2004.12.018
- Duff, J.H., Triska, F.J., 1990. Denitrifications in Sediments from the Hyporheic Zone Adjacent to a Small Forested Stream. *Can. J. Fish. Aquat. Sci.* 47, 1140–1147. doi:10.1139/f90-133
- Ellery, W.N., McCarthy, T.S., Smith, N.D., 2003. Vegetation, hydrology, and sedimentation patterns on the major distributary system of the Okavango fan, Botswana. *Wetlands* 23, 357–375. doi:10.1672/11-20
- Ellins, K.K., Roman-Mas, A., Lee, R., 1990. Using ²²²Rn to examine groundwater/surface discharge interaction in the Rio Grande de Manati, Puerto Rico. *J. Hydrol.* 115, 319–341. doi:10.1016/0022-1694(90)90212-G
- Elliott, A.H., Brooks, N.H., 1997. Transfer of nonsorbing solutes to a streambed with bed forms: Theory. *Water Resour. Res.* 33, 123–136. doi:10.1029/96WR02784
- Elliott, R.J., Aggoun, L., 1996. Estimation for hidden Markov random fields. *J. Stat. Plan. Inference* 50, 343–351. doi:10.1016/0378-3758(95)00062-3
- EPA, 2000. *Manual Constructed Wetlands Treatment of Municipal Wastewaters*. Cincinnati, Ohio.
- Eppinga, M.B., de Ruiter, P.C., Wassen, M.J., Rietkerk, M., 2009. Nutrients and Hydrology Indicate the Driving Mechanisms of Peatland Surface Patterning. *Am. Nat.* 173, 803–818. doi:10.1086/598487
- Fernald, A.G., Wigington, P.J., Landers, D.H., 2001. Transient storage and hyporheic flow along the Willamette River, Oregon: Field measurements and model estimates. *Water Resour. Res.* 37, 1681–1694. doi:10.1029/2000WR900338
- Fick, A., 1855. Ueber Diffusion. *Ann. der Phys. und Chemie* 170, 59–86. doi:10.1002/andp.18551700105
- Fischer, H.B., 1975. Discussion of “Simple method for predicting dispersion in streams.” *J. Environ. Eng.* 101, 435–455.

- Fischer, H.B., List, E.J., Koh, R.C.Y., Imberger, J., Brooks, N.H., 1979. *Mixing in Inland and Coastal Waters*. Academic. Academic Press, New York.
- Fogler, H.S., 1992. *Elements of chemical reaction engineering*. Prentice-Hall, Englewood cliffs.
- Franken, R.J.M., Storey, R.G., Dudley Williams, D., 2001. Biological, chemical and physical characteristics of downwelling and upwelling zones in the hyporheic zone of a north-temperate stream. *Hydrobiologia* 444, 183–195. doi:10.1023/A:1017598005228
- Fuller, C.C., Harvey, J.W., 2000. Reactive Uptake of Trace Metals in the Hyporheic Zone of a Mining-Contaminated Stream, Pinal Creek, Arizona. *Environ. Sci. Technol.* 34, 1150–1155. doi:10.1021/es990714d
- Gill, L.W., Ring, P., Higgins, N.M.P., Johnston, P.M., 2014. Accumulation of heavy metals in a constructed wetland treating road runoff. *Ecol. Eng.* 70, 133–139. doi:10.1016/j.ecoleng.2014.03.056
- Haggerty, R., Martí, E., Argerich, A., von Schiller, D., Grimm, N.B., 2009. Resazurin as a “smart” tracer for quantifying metabolically active transient storage in stream ecosystems. *J. Geophys. Res.* 114, G03014. doi:10.1029/2008JG000942
- Hammer, D.A., Knight, R.L., 1994. *Designing Constructed Wetlands for Nitrogen Removal*. *Water Sci. Technol.* 29.
- Harvey, J.W., Bencala, K.E., 1993. The Effect of streambed topography on surface-subsurface water exchange in mountain catchments. *Water Resour. Res.* 29, 89–98. doi:10.1029/92WR01960
- Harvey, J.W., Saiers, J.E., Newlin, J.T., 2005. Solute transport and storage mechanisms in wetlands of the Everglades, south Florida. *Water Resour. Res.* 41. doi:10.1029/2004WR003507
- Hilbert, D.W., Roulet, N., Moore, T., 2000. Modelling and analysis of peatlands as dynamical systems. *J. Ecol.* 88, 230–242. doi:10.1046/j.1365-2745.2000.00438.x
- Holland, J.F., Martin, J.F., Granata, T., Bouchard, V., Quigley, M., Brown, L., 2004. Effects of wetland depth and flow rate on residence time distribution characteristics. *Ecol. Eng.* 23, 189–203. doi:10.1016/j.ecoleng.2004.09.003
- Hsueh, M.-L., Yang, L., Hsieh, L.-Y., Lin, H.-J., 2014. Nitrogen removal along the treatment cells of a free-water surface constructed wetland in subtropical Taiwan. *Ecol. Eng.* 73, 579–587. doi:10.1016/j.ecoleng.2014.09.100
- Jadhav, R.S., Buchberger, S.G., 1995. Effects of vegetation on flow through free water surface wetlands. *Ecol. Eng.* 5, 481–496. doi:10.1016/0925-8574(95)00039-9
- Jenkins, G. a., Greenway, M., 2005. The hydraulic efficiency of fringing versus banded vegetation in constructed wetlands. *Ecol. Eng.* 25, 61–72. doi:10.1016/j.ecoleng.2005.03.001
- Johansson, H., Jonsson, K., Forsman, K., Worman, A., 2001. Retention of conservative and sorptive solutes in streams — simultaneous tracer experiments. *Sci. Total Environ.* 266,

229–238. doi:10.1016/S0048-9697(00)00758-0

- Jonsson, K., Worman, A., 2001. Effect of sorption kinetics on the transport of solutes in streams. *Sci. Total Environ.* 266, 239–247. doi:10.1016/S0048-9697(00)00743-9
- Kadlec, R., Wallace, S., 2009. *Treatment Wetlands*, Second edition. CRC Press, Boca raton, Florida.
- Kadlec, R.H., 2007. The effects of deep zones on wetland nitrogen processing. *Water Sci. Technol.* 56, 101. doi:10.2166/wst.2007.492
- Karakashev, D., Galabova, D., Simeonov, I., 2003. A simple and rapid test for differentiation of aerobic from anaerobic bacteria. *World J. Microbiol. Biotechnol.* 19, 233–238. doi:10.1023/A:1023674315047
- Katsenovich, Y.P., Hummel-Batista, A., Ravinet, A.J., Miller, J.F., 2009. Performance evaluation of constructed wetlands in a tropical region. *Ecol. Eng.* 35, 1529–1537. doi:10.1016/j.ecoleng.2009.07.003
- Keefe, S.H., Daniels, J.S., Runkel, R.L., Wass, R.D., Stiles, E.A., Barber, L.B., 2010. Influence of hummocks and emergent vegetation on hydraulic performance in a surface flow wastewater treatment wetland. *Water Resour. Res.* 46, W11518. doi:10.1029/2010wr009512
- Kipasika, H.J., Buza, J., Lyimo, B., Miller, W.A., Njau, K.N., 2014. Efficiency of a constructed wetland in removing microbial contaminants from pre-treated municipal wastewater. *Phys. Chem. Earth, Parts A/B/C* 72–75, 68–72. doi:10.1016/j.pce.2014.09.003
- Koskiaho, J., 2003. Flow velocity retardation and sediment retention in two constructed wetland-ponds. *Ecol. Eng.* 19, 325–337.
- Kotti, I.P., Gikas, G.D., Tsihrintzis, V. a., 2010. Effect of operational and design parameters on removal efficiency of pilot-scale FWS constructed wetlands and comparison with HSF systems. *Ecol. Eng.* 36, 862–875. doi:10.1016/j.ecoleng.2010.03.002
- Larsen, L.G., Harvey, J.W., 2011. Modeling of hydroecological feedbacks predicts distinct classes of landscape pattern, process, and restoration potential in shallow aquatic ecosystems. *Geomorphology* 126, 279–296. doi:10.1016/j.geomorph.2010.03.015
- Larsen, L.G., Harvey, J.W., Maglio, M.M., 2014. Dynamic hyporheic exchange at intermediate timescales: Testing the relative importance of evapotranspiration and flood pulses. *Water Resour. Res.* 50, 318–335. doi:10.1002/2013WR014195
- Leonard, L.A., Reed, D., 2002. Hydrodynamics and Sediment Transport Through Tidal Marsh Canopies. *J. Coast. Res.* 36, 459–469.
- Lightbody, A.F., Avenier, M.E., Nepf, H.M., 2008. Observations of short-circuiting flow paths within a free-surface wetland in Augusta, Georgia, U.S.A. *Limnol. Oceanogr.* 53, 1040–1053. doi:10.4319/lo.2008.53.3.1040
- Lightbody, A.F., Nepf, H.M., 2006. Prediction of velocity profiles and longitudinal dispersion in emergent salt marsh vegetation 51, 218–228.

- Lightbody, A.F., Nepf, H.M., Bays, J.S., 2009. Modeling the hydraulic effect of transverse deep zones on the performance of short-circuiting constructed treatment wetlands. *Ecol. Eng.* 35, 754–768. doi:10.1016/j.ecoleng.2008.12.010
- Lightbody, A.F., Nepf, H.M., Bays, J.S., 2007. Mixing in deep zones within constructed treatment wetlands. *Ecol. Eng.* 29, 209–220. doi:10.1016/j.ecoleng.2006.11.001
- Lynn, a, Reed, D.J., Leonard, L. a, 2002. Hydrodynamics and sediment transport through tidal marsh canopies. *J. Coast. Res.*
- Mangangka, I.R., Liu, A., Egodawatta, P., Goonetilleke, A., 2015. Sectional analysis of stormwater treatment performance of a constructed wetland. *Ecol. Eng.* 77, 172–179. doi:http://dx.doi.org/10.1016/j.ecoleng.2015.01.028
- Marani, M., Silvestri, S., Belluco, E., Ursino, N., Comerlati, A., Tosatto, O., Putti, M., 2006. Spatial organization and ecohydrological interactions in oxygen-limited vegetation ecosystems. *Water Resour. Res.* 42, n/a-n/a. doi:10.1029/2005WR004582
- Mardia, K., 1988. Multi-dimensional multivariate Gaussian Markov random fields with application to image processing. *J. Multivar. Anal.* 24, 265–284. doi:10.1016/0047-259X(88)90040-1
- Marion, A., Bellinello, M., Guymer, I., Packman, A., 2002. Effect of bed form geometry on the penetration of nonreactive solutes into a streambed. *Water Resour. Res.* 38, 27-1-27–12. doi:10.1029/2001WR000264
- Marion, A., Nikora, V., Puijalon, S., Bouma, T., Koll, K., Ballio, F., Tait, S., Zaramella, M., Sukhodolov, A., O’Hare, M., Wharton, G., Aberle, J., Tregnaghi, M., Davies, P., Nepf, H., Parker, G., Statzner, B., 2014. Aquatic interfaces: a hydrodynamic and ecological perspective. *J. Hydraul. Res.* 52, 744–758. doi:10.1080/00221686.2014.968887
- Marion, A., Packman, A.I., Zaramella, M., Bottacin-Busolin, A., 2008. Hyporheic flows in stratified beds. *Water Resour. Res.* 44, W09433. doi:10.1029/2007WR006079
- Marion, A., Zaramella, M., 2005. A RESIDENCE TIME MODEL FOR STREAM-SUBSURFACE EXCHANGE OF CONTAMINANTS. *Acta Geophys. Pol.* 53, 527–538.
- Marion, A., Zaramella, M., Bottacin-Busolin, A., 2008. Solute transport in rivers with multiple storage zones: The STIR model. *Water Resour. Res.* 44, W10406. doi:10.1029/2008WR007037
- Martín, M., Oliver, N., Hernández-Crespo, C., Gargallo, S., Regidor, M.C., 2013. The use of free water surface constructed wetland to treat the eutrophicated waters of lake L’Albufera de Valencia (Spain). *Ecol. Eng.* 50, 52–61. doi:10.1016/j.ecoleng.2012.04.029
- Maucieri, C., Salvato, M., Tamiazzo, J., Borin, M., 2014. Biomass production and soil organic carbon accumulation in a free water surface constructed wetland treating agricultural wastewater in North Eastern Italy. *Ecol. Eng.* 70, 422–428. doi:10.1016/j.ecoleng.2014.06.020
- Meng, P., Pei, H., Hu, W., Shao, Y., Li, Z., 2014. How to increase microbial degradation in constructed wetlands: Influencing factors and improvement measures. *Bioresour. Technol.*

157, 316–326. doi:10.1016/j.biortech.2014.01.095

- Musner, T., Bottacin-Busolin, A., Zaramella, M., Marion, A., 2014. A contaminant transport model for wetlands accounting for distinct residence time bimodality. *J. Hydrol.* 515, 237–246. doi:10.1016/j.jhydrol.2014.04.043
- N.J. Comans, R., Haller, M., De Preter, P., 1991. Sorption of cesium on illite: Non-equilibrium behaviour and reversibility. *Geochim. Cosmochim. Acta* 55, 433–440. doi:10.1016/0016-7037(91)90002-M
- Nepf, H., Ghisalberti, M., White, B., Murphy, E., 2007. Retention time and dispersion associated with submerged aquatic canopies. *Water Resour. Res.* W04422. doi:10.1029/2006WR005362
- Nepf, H.M., 1999. Drag, turbulence, and diffusion in flow through emergent vegetation. *Water Resour. Res.* 35, 479–489. doi:10.1029/1998WR900069
- Nepf, H.M., Sullivan, J.A., Zavistoski, R.A., 1997. A model for diffusion within emergent vegetation. *Limnol. Oceanogr.* 42, 1735–1745. doi:10.4319/lo.1997.42.8.1735
- Nungesser, M.K., Chimney, M.J., 2006. A hydrologic assessment of the Everglades Nutrient Removal Project, a subtropical constructed wetland in South Florida (USA). *Ecol. Eng.* 27, 331–344. doi:10.1016/j.ecoleng.2006.08.007
- Nyffeler, U.P., Li, Y.-H., Santschi, P.H., 1984. A kinetic approach to describe trace-element distribution between particles and solution in natural aquatic systems. *Geochim. Cosmochim. Acta* 48, 1513–1522. doi:10.1016/0016-7037(84)90407-1
- Packman, A.I., Salehin, M., 2003. Relative roles of stream flow and sedimentary conditions in controlling hyporheic exchange. *Hydrobiologia* 494, 291–297. doi:10.1023/A:1025403424063
- Packman, A.I., Salehin, M., Zaramella, M., 2004. Hyporheic Exchange with Gravel Beds: Basic Hydrodynamic Interactions and Bedform-Induced Advective Flows. *J. Hydraul. Eng.* 130, 647–656. doi:10.1061/(ASCE)0733-9429(2004)130:7(647)
- Persson, J., Somes, N., Wong, T., 1999. Hydraulics efficiency of constructed wetlands and ponds. *Water Sci. Technol.* 40, 291–300. doi:10.1016/S0273-1223(99)00448-5
- Reed, S., Ronald, C., Middlebrooks, E., 1995. *Natural Systems for Waste Management and Treatment*. 2nd Ed. McGraw-Hill, NY.
- Reed, S.C., Crites, R.W., Middlebrooks, E.J., 1995. *Natural Systems for Waste Management and Treatment*. McGraw-Hill Professional.
- Rietkerk, M., Dekker, S.C., Wassen, M.J., Verkroost, A.W.M., Bierkens, M.F.P., 2004. A Putative Mechanism for Bog Patterning. *Am. Nat.* 163, 699–708. doi:10.1086/383065
- Sabokrouhiyeh, N., Bottacin-Busolin, A., Nepf, H., Marion, A., 2016. Effects of vegetation density and wetland aspect ratio variation on hydraulic efficiency of wetlands, *GeoPlanet: Earth and Planetary Sciences*. doi:10.1007/978-3-319-27750-9_9
- Sabokrouhiyeh, N., Bottacin-Busolin, A., Savickis, J., Nepf, H., Marion, A., 2017. A numerical

- study of the effect of wetland shape and inlet-outlet configuration on wetland performance. *Ecol. Eng.* 105, 170–179. doi:10.1016/j.ecoleng.2017.04.062
- Salehin, M., Packman, A.I., Wörman, A., 2003. Comparison of transient storage in vegetated and unvegetated reaches of a small agricultural stream in Sweden: seasonal variation and anthropogenic manipulation. *Adv. Water Resour.* 26, 951–964. doi:10.1016/S0309-1708(03)00084-8
- Savickis, J., Bottacin-Busolin, A., Zaramella, M., Sabokrouhiyeh, N., Marion, A., 2016. Effect of a meandering channel on wetland performance. *J. Hydrol.* 535. doi:10.1016/j.jhydrol.2016.01.082
- Serra, T., Fernando, H.J.S., Rodríguez, R. V., 2004. Effects of emergent vegetation on lateral diffusion in wetlands. *Water Res.* 38, 139–47. doi:10.1016/j.watres.2003.09.009
- Shucksmith, J.D., Boxall, J.B., Guymer, I., 2011. Determining longitudinal dispersion coefficients for submerged vegetated flow. *Water Resour. Res.* 47, n/a–n/a. doi:10.1029/2011WR010547
- Smith, J.T., Comans, R.N.J., 1996. Modelling the diffusive transport and remobilisation of ¹³⁷Cs in sediments: The effects of sorption kinetics and reversibility. *Geochim. Cosmochim. Acta* 60, 995–1004. doi:10.1016/0016-7037(96)00030-0
- Somes, N.L.G., Bishop, W.A., Wong, T.H.F., 1999. Numerical simulation of wetland hydrodynamics. *Environ. Int.* 25, 773–779. doi:10.1016/S0160-4120(99)00058-6
- Stoesser, T., Asce, M., Kim, S.J., Diplas, P., 2010. Turbulent Flow through Idealized Emergent Vegetation. *J. Hydraul. Eng.* 136, 1003–1017.
- Stone, B.M., Shen, H.T., 2002. Hydraulic Resistance of Flow in Channels with Cylindrical Roughness. *J. Hydraul. Eng.* 128, 500–506. doi:10.1061/(ASCE)0733-9429(2002)128:5(500)
- Storey, R.G., Howard, K.W.F., Williams, D.D., 2003. Factors controlling riffle-scale hyporheic exchange flows and their seasonal changes in a gaining stream: A three-dimensional groundwater flow model. *Water Resour. Res.* 39. doi:10.1029/2002WR001367
- Su, T.-M., Yang, S.-C., Shih, S.-S., Lee, H.-Y., 2009. Optimal design for hydraulic efficiency performance of free-water-surface constructed wetlands. *Ecol. Eng.* 35, 1200–1207. doi:10.1016/j.ecoleng.2009.03.024
- Suliman, F., Futsaether, C., Oxaal, U., Haugen, L.E., Jenssen, P., 2006. Effect of the inlet–outlet positions on the hydraulic performance of horizontal subsurface-flow wetlands constructed with heterogeneous porous media. *J. Contam. Hydrol.* 87, 22–36. doi:10.1016/j.jconhyd.2006.04.009
- Swanson, D.K., Grigal, D.F., 1988. A Simulation Model of Mire Patterning. *Oikos* 53, 309. doi:10.2307/3565529
- Tanino, Y., Nepf, H.M., 2008. Laboratory Investigation of Mean Drag in a Random Array of Rigid, Emergent Cylinders. *J. Hydraul. Eng.* 134, 34–41.

- Tao, W., Hall, K.J., Duff, S.J.B., 2006. Performance evaluation and effects of hydraulic retention time and mass loading rate on treatment of woodwaste leachate in surface-flow constructed wetlands. *Ecol. Eng.* 26, 252–265. doi:10.1016/j.ecoleng.2005.10.006
- Thackston, E.L., Shields, F.D., Schroeder, P.R., 1987. Residence Time Distributions of Shallow Basins. *J. Environ. Eng.* 113, 1319–1332. doi:10.1061/(ASCE)0733-9372(1987)113:6(1319)
- Thullen, J.S., Sartoris, J.J., Nelson, S.M., 2005. Managing vegetation in surface-flow wastewater-treatment wetlands for optimal treatment performance. *Ecol. Eng.* 25, 583–593. doi:10.1016/j.ecoleng.2005.07.013
- Toet, S., Logtestijn, R.S.P., Kampf, R., Schreijer, M., Verhoeven, J.T.A., 2005. The effect of hydraulic retention time on the removal of pollutants from sewage treatment plant effluent in a surface-flow wetland system. *Wetlands* 25, 375–391. doi:10.1672/13
- Triska, F.J., Duff, J.H., Avanzino, R.J., 1993. Patterns of hydrological exchange and nutrient transformation in the hyporheic zone of a gravel-bottom stream: examining terrestrial-aquatic linkages. *Freshw. Biol.* 29, 259–274. doi:10.1111/j.1365-2427.1993.tb00762.x
- Triska, F.J., Duff, J.H., Avanzino, R.J., 1990. Influence of Exchange Flow Between the Channel and Hyporheic Zone on Nitrate Production in a Small Mountain Stream. *Can. J. Fish. Aquat. Sci.* 47, 2099–2111. doi:10.1139/f90-235
- Triska, F.J., Kennedy, V.C., Avanzino, R.J., Zellweger, G.W., Bencala, K.E., 1989. Retention and Transport of Nutrients in a Third-Order Stream: Channel Processes. *Ecology* 70, 1877–1892. doi:10.2307/1938119
- Vymazal, J., 2014. Constructed wetlands for treatment of industrial wastewaters: A review. *Ecol. Eng.* 73, 724–751. doi:10.1016/j.ecoleng.2014.09.034
- Vymazal, J., 2013. Emergent plants used in free water surface constructed wetlands: A review. *Ecol. Eng.* 61, 582–592. doi:10.1016/j.ecoleng.2013.06.023
- Vymazal, J., Březinová, T., 2015. The use of constructed wetlands for removal of pesticides from agricultural runoff and drainage: A review. *Environ. Int.* 75, 11–20. doi:10.1016/j.envint.2014.10.026
- Ward, R.S., Williams, A.T., Barker, J.A., Brewerton, L.J., Gale, I.N., 1998. Groundwater tracer tests: a review and guidelines for their use in British aquifers. British Geological Survey, London.
- Werner, T.M., Kadlec, R.H., 1996. Application of residence time distributions to stormwater treatment systems. *Ecol. Eng.* 7, 213–234. doi:10.1016/0925-8574(96)00013-4
- White, F.M., 1991. *Viscous fluid flow*, 2nd ed. McGraw-Hill Professional, New York.
- Wilson, J., Cobb, E., Kilpatrick, FA, 1986. Fluorometric procedures for dye tracing. Department of the Interior, US Geological Survey.
- Wörman, A., Kronnäs, V., 2005. Effect of pond shape and vegetation heterogeneity on flow and treatment performance of constructed wetlands. *J. Hydrol.* 301, 123–138.

doi:10.1016/j.jhydrol.2004.06.038

- Wörman, A., Packman, A.I., Johansson, H., Jonsson, K., 2002. Effect of flow-induced exchange in hyporheic zones on longitudinal transport of solutes in streams and rivers. *Water Resour. Res.* 38, 2-1-2–15. doi:10.1029/2001WR000769
- Wu, S., Wallace, S., Brix, H., Kusch, P., Kirui, W.K., Masi, F., Dong, R., 2015. Treatment of industrial effluents in constructed wetlands: Challenges, operational strategies and overall performance. *Environ. Pollut.* 201, 107–120. doi:10.1016/j.envpol.2015.03.006
- Wu, W., 2007. *Computational River Dynamics*. CRC Press.
- Yang, L., Tsai, K.-Y., 2011. Treatment of landfill leachate with high levels of ammonia by constructed wetland systems. *J. Environ. Sci. Heal.* 46, 736–741. doi:10.1080/10934529.2011.571586
- Yoneda, M., Inoue, Y., Takine, N., 1991. Location of groundwater seepage points into a river by measurement of ²²²Rn concentration in water using activated charcoal passive collectors. *J. Hydrol.* 124, 307–316. doi:10.1016/0022-1694(91)90021-9
- Zhang, D., Jinadasa, K.B.S.N., Gersberg, R.M., Liu, Y., Tan, S.K., Ng, W.J., 2015. Application of constructed wetlands for wastewater treatment in tropical and subtropical regions (2000 – 2013) 0.
- Zheng, Y., Wang, X.C., Ge, Y., Dzakpasu, M., Zhao, Y., Xiong, J., 2015. Effects of annual harvesting on plants growth and nutrients removal in surface-flow constructed wetlands in northwestern China. *Ecol. Eng.* 83, 268–275. doi:10.1016/j.ecoleng.2015.06.035